國 立 交 通 大 學

光電工程研究所

博士論文

可重組態寬頻網路系統之新穎架構

Novel Architectures for Reconfigurable
Broadband Optical Networks

研 究 生 ：黃明芳
指導教授：祁 甡 教授
　　　　　陳智弘 副教授

中華民國 九十六 年 十二 月

可重組態寬頻網路系統之新穎架構

Novel Architectures for Reconfigurable Broadband Optical Networks

研 究 生 ：黃明芳　　　　　Student：Ming-Fang Huang

指導教授：祁　甡　　　　　Advisors：Sien Chi
　　　　　陳智弘　　　　　　　　　　Jyehong Chen

國立交通大學 電機學院
光電工程研究所
博士論文

A Dissertation
Submitted in Partial Fulfillment of the Requirements
for the Degree of Doctor of Philosophy in
The Institute of Electro-Optical Engineering
College of Electrical and Computer Engineering
National Chiao Tung University
Hsin-Chu, Taiwan, R.O.C.

中華民國 九十六 年 十二 月

可重組態寬頻網路系統之新穎架構

研究生：黃明芳　　　　　　　　　指導教授：祁　甡
　　　　　　　　　　　　　　　　　　　　　陳智弘

國立交通大學 電機學院

光電工程研究所

摘要

在本篇論文中提出利用光學延遲技術而準確達成新穎無色散的光學交錯器。擁有相同振幅響應但相反相位響應的一對光學交錯器成功的在模擬與量測結果相符合下實現，並且使用於雙向波分多工(WDM)傳輸系統當中。此外，將原本設計可用於單向放大功能的三通道光學交錯器進一步設計成四個通道，以用於雙向波分多工傳輸架構。在這個研究裡面，深入的探討並實驗論證此四通道光學交錯器在雙向傳輸系統裡的應用。在網路擷取信號方面，達成 ROADM 以及色散補償光學交錯器之應用，以解決網路中信號重組的問題；在網路中節省成本的問題下，雙向傳輸系統將是重要的解決方案，點對點的雙向直線傳輸，高速信號，以及利用迴路的長距離傳輸都在實驗上成功的實現。也進一步探討不同的調變信號（如 OOK，RZ-DPSK，NRZ-DPSK）與不同放大機制（如摻鉺光纖放大器與半導體光學放大器）在傳輸系統裡的影響。然而，在不久的將來，WDM-PON 將成為趨勢，在此論文中也更進一步討論 WDM-PON 的應用，主要分為三個方向：經濟且有效率的雙向傳輸架構，提供用戶有選擇性的服務以及利用簡單架構同時提供用戶聲音，影像，資料的三功能服務。實驗結果證實了所提出的方法皆為針對系統缺陷之經濟且有效率的解決方案，並對於未來光網路的發展有著廣闊的前景。

Novel Architectures for Reconfigurable Broadband Optical Networks

Student: Ming-Fang Huang

Advisor: Sien Chi
Jeyhong Chen

Institute of Electro-Optical Engineering
College of Electrical and Computer Engineering
National Chiao Tung University

ABSTRACT

In this dissertation, a novel dispersion-free interleaver using optical delay lines by accurately locating the zeros in the transfer function has been proposed. It has been implemented with the design of interleaver pairs with the same amplitude responses but opposite phase responses for bidirectional DWDM transmission systems. The measured results are consistent with device simulation. The original three-port design using unidirectional amplification has been further modified, and a four-port interleaver has been built and demonstrated to achieve bidirectional DWDM transmission. This investigate fully studied and verified the applications of our four-port interleavers in bidirectional transmission. A re-circulating loop has been setup for metro add/drop applications using an ROADM and dispersion-compensated interleaver pairs to solve the problem of re-configuration. To unravel the fiber shortage issue in metro link, a bidirectional straight-line system, a re-circulating loop and high bit rate transmission had been proposed and experimentally demonstrated. The comparison of different modulation formats, such as OOK, RZ-DPSK and NRZ-DPSK, with different amplification functions, e.g. SOA and EDFA, are also illustrated. Furthermore, WDM-PON is an ultimate solution

for ever increasing bandwidth requirement in the near future. Therefore, a cost-effective bidirectional WDM-PON using novel four-port interleaver, select-cast WDM-PON based on simultaneously generated OOK and DPSK downstream traffic and a simple architecture for WDM-PON to provide triple play services with centralize lightsources have been also established. The experimental results have clearly manifested that the proposed architectures can provide significant improvement on both cost-effective and system reliability.

誌 謝

(ACKNOWLEDGEMENTS)

TABLE OF CONTENTS

LIST OF TABLES

LIST OF FIGURES

LIST OF ACRONYMS

ADSL	asymmetric digital subscriber line
ASE	amplified spontaneous emission
ATM	asynchronous transfer mode
AO	acousto-optic
AWG	array waveguide grating
BPON	broadband PON
BS	band separators
CBR	constant-bit-rate
CDR	clock and data recovery
CO	central office
DAM	dual-arm modulator
DBA	dynamic bandwidth allocation
DCF	dispersion compensated fiber
DFB	distributed feedback
DPSK	differential phase-shift keying
DQPSK	differential quaternary phase shift keying
DSL	digital subscriber line
DWDM	dense wavelength-division-multiplexing
DXC	digital cross-connects
EDFA	erbium-doped fiber amplifier
EO	electro-optical
EPON	Ethernet PON
FEC	forward error correction
FP	Fabry-Perot
FTTB	fiber-to-the-building
FTTH	fiber-to-the-home
GPON	Gigabit PON
GTI	Gires-Tournois interferometer
GTR	Gires-Tournois resonator
HDTV	high-definition TV
HFC	hybrid fiber-coax
HWP	half-wave plates
IP	Internet protocol
ITU	International Telecommunication Union
IL	Interleaver
IM	intensity modulator

LO	local oscillator
LOA	linear optical amplifier
MAN	metro area networks
MCA	media access controller
MI	Michelson interferometer
MZ-DI	Mach-Zehnder delay-line
NF	noise figure
NRZ-DPSK	non-return-to-zero differential phase-shift keying
OCSS	optical carrier suppression and separation
OLT	optical line terminal
ONU	optical network unit
OOK	ON-OFF keying
OSA	optical spectrum analyzer
OSNR	optical signal to noise ratio
PBS	polarization beam splitter
PBS	proxy base stations
PC	polarization controller
PDG	polarization dependent gain
PDL	polarization dependent loss
PLC	Plana r lightwave circuit
PM	phase modulator
PON	passive optical networks
PRBS	pseudo random binary sequence
QoS	quality of service
QPS	quadruple play services
RB	Rayleigh backscattering
RDCC	Railway WiMAX/RoF Distribution and Control Center
ROADM	reconfigurable optical add/drop multiplexer
ROF	radio over fiber
RSOA	reflective semiconductor optical amplifier
RZ-DPSK	return-to-zero differential phase-shift keying
SCM	sub-carriers multiplexing
SDH	synchronous digital hierarchy
SOA	semiconductor optical amplifier
SSMF	standard single-mode fibers
TDM-PON	time-division-multiplexing passive optical networks
TAP	train access point
TPS	triple play services

VDSL	very high speed digital subscriber line
WDM	wavelength division multiplexing
WDM-PON	wavelength division multiplexing passive optical network
WiFi	wireless fidelity
WiMax	World interoperability for microwave access
XGM	cross-gain modulation
YWC	YVO walk-off crystal

LIST OF SYMBOLS

Δn	group index difference between ordinary and extraordinary axes
c	speed of light
FSR	free spectral range
L	length of the crystal
λ_{center}	center wavelength of the operation wavelength range
m	the order of the birefringent wave plate
β	normalized variation in the wavelength with temperature
$\hat{x}(f_n)$	target amplitude response
$x(f_n)$	real transmission function
f_c	central frequency

CHAPTER 1

INTRODUCTION

1.1   Network Evolution

Over the past few years, the evolution of the Internet has proved that wavelength-division multiplexed (WDM) is the most flexible and robust solution for the present and future dynamic network traffic. As the Internet transitions from a best-effort network to a strategic global Internet protocol (IP) infrastructure, demands will not only be for higher bandwidth, but also for a wider range of integrated services demanding high reliability [1–5]. The broadband access network connects the service provider at a central office (CO) to the subscribers, which include businesses and homes. Recently, subscribers have been demanding high bandwidth services such as video-on-demand and high-speed internet for both downloading and uploading information. Current access technologies such as hybrid fiber-coax (HFC), digital subscriber line (DSL), and wireless networks have severe limitations in transporting symmetric traffic or high bandwidth information. However, the nature of the traffic that is sent through the Internet is changing. New applications require higher bandwidths, support for constant-bit-rate (CBR) streaming media, symmetric data rates for peer-to-peer file transfer, low delay for interactive applications and security. The internet will need many architectural upgrades to accommodate these new demands. The common used methods are included:

1) IP — the Internet Protocol. It started life as protocol which was used for communication over the Internet. IP was optimized for data service and was packet

based, rather than circuit switched and also well suited to streamed audio and video broadcast.

2) ATM— Asynchronous Transfer Mode. It was probably the first serious contender for providing broadband multi-service network. ATM is a packet based system, using fixed length packets, and is designed to support a wide range of services such as voice, video and frame relay.

3) ADSL— Asymmetric Digital Subscriber Line. It was first developed to enable a broadband always-on connection to be provided over a copper pair. ADSL is asymmetric and supplies a greater downstream capacity than the upstream, typically of 1.5 Mbps downstream and 128 Kbps upstream bandwidth.

4) VDSL— Very high speed Digital Subscriber Line. An increased downstream of 50 Mbps can be achieved using VDSL, but this comes at the expense of shorter distance, typically less than 1500 ft (457.2 km).

5) PON — Passive Optical Network. It provides fiber communications without expensive electronics. PON are well studied to enhancing existing networks by replacing the copper between the local exchange and a flexibility point.

6) HFC— Hybrid-fiber Coax. HFC systems substitute most of co-axial cable between the cable TV head-end and the customer with fiber. It is used to transmit both broadcast video and high-speed data services.

Figure 1.1 shows the possible evolution skeleton for the network. On the access side, the first evolution will include the development of optical fiber in the feeder network that close to the customer by ADSL technology, allowing the last relatively short copper. Similarly, the fiber in HFC networks will come closer to the customer, serving the small
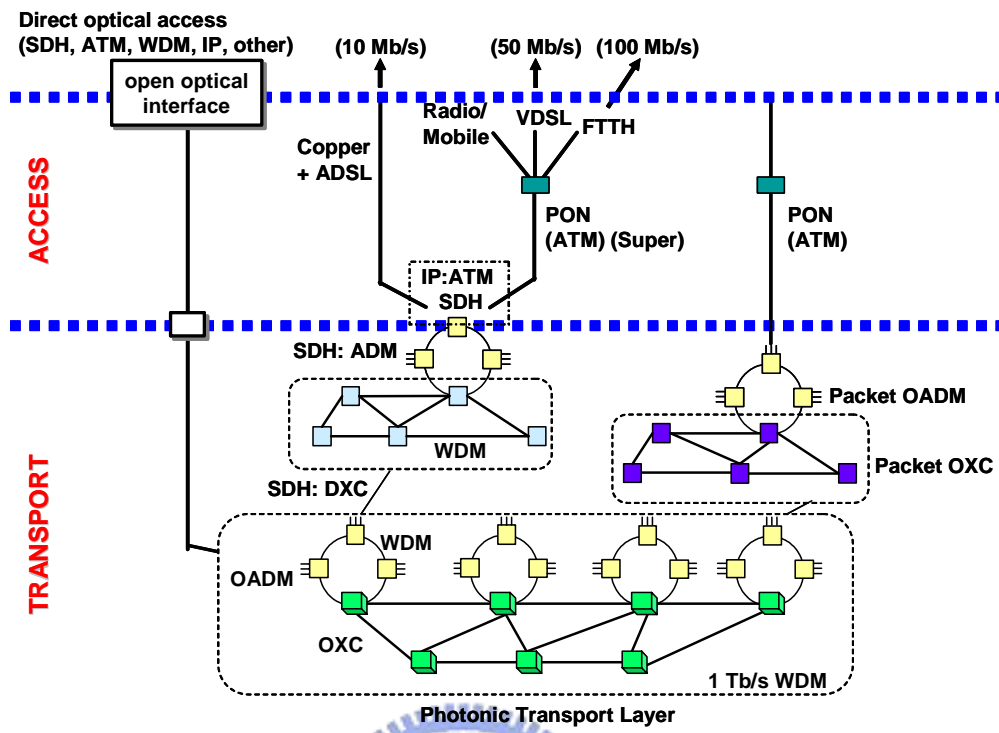
Figure 1.1: Network evolution options.

number of businesses and homes with the coax tree. This will support bit rate up to 10 Mbps downstream and meet the capacity requirement of small offices and homes. The copper based access, such as VDSL technology that support up to 50 Mbps downstream bandwidth, will gradually migrate to fiber access. The fiber link can be based on passive optical network technology (PON) and SuperPON using optical amplifiers. Ultimately, the bandwidth of 100 Mbps per subscriber will meet the demands of fiber-to-the-home (FTTH).

The transport network supports the accumulated traffic generated in the access network and the link capacities on the order of 1 Tbps will be necessary in the near future. Currently, many networks are progressing to synchronous digital hierarchy (SDH) architecture, with a transport comprising a mesh of digital cross-connects (DXCs)

3

interconnecting rings. Fiber link in the long-haul networks is currently being upgraded to use WDM technique, which has similar functions to the electrical SDH network. The optical transport layer is a key evolutionary development because of its effectively transparent to bit rate and signal format. Furthermore, it also can support different types of access, such as WDM, IP and so on. Unlike HFC and DSL technologies, wireless networks such as wireless fidelity (WiFi) and world interoperability for microwave access (WiMax) do not require any optical fiber or cable for the transmission of information from the central office to the subscribers. Wireless networks allow users to be mobile but have limited bandwidth and security issues.

1.2 Motivation

Next generation broadband optical network will likely require a considerable increase in total spectral efficiency. The emergency of broadband communications has increased the need for bulk transport of high capacity signals and services. Optical WDM networks have been widely recognized as the dominant transport infrastructure for future Internet backbone networks with its potential of providing virtually unlimited bandwidth [5]. The reconfigurability of WDM networks has the following features: the network's configuration can be increased by bypassing, adding or dropping the traffic and the capacity throughput enlarges when the traffic is multiplexed on the fiber by WDM. However, in metro area networks (MAN) that encounter fiber shortages problem, bidirectional transmission is an appealing means of increasing the bandwidth utilization in a single optical fiber and, at the same time, reducing the operation and maintenance cost [6–8]. One of the core technologies in bidirectional transmission system is realizing

of bidirectional amplification, which typically requires high gain, low noise and the elimination of Rayleigh backscattering (RB) [9]. One of the efficient methods in bidirectional transmission is using wavelength interleaving scheme. As an optical filter, an interleaver combines or separates a comb of dense wavelength-division multiplexed (DWDM) signals [10–12]. Although interleaver has been widely used in multiplexing and demultiplexing of DWDM optical signals, its applications in bidirectional transmissions have not been fully studied and verified. As a result, the motivation of this dissertation lies in the investigation of a reliable solution for bidirectional transmission in WDM network by using a new designed four-port interleaver.

Among several choices of modulation and demodulation formats in optical access networks, ON-OFF keying (OOK) format [13, 14] is the most popular for its simple generation. Recently, special attention has been given to differential phase-shift keying (DPSK), which was proving to be superior [15] relative to the traditional OOK in optical fiber communication system. This is due to its larger tolerance to fiber nonlinearity and noise from amplified spontaneous emission (ASE). The phenomenon of different modulation formats, such as OOK, return-to-zero DPSK (RZ-DPSK) and non-return-to-zero DPSK (NRZ-DPSK) with dissimilar amplification schemes, i.e. erbium-doped fiber amplifier (EDFA) and semiconductor optical amplifier (SOA) in bidirectional transmission systems would be investigated.

Since the downstream data is shared among several subscribers in HFC systems, the available bandwidth per user depends on the number of subscribers connected to the internet. Additionally, the upstream bandwidth is limited because of ingress noise generated from appliances at the subscribers end. Therefore, highly efficient, next

generation, broadband optical networks providing symmetric upstream and downstream information would be difficult to develop using HFC and DSL infrastructures. However, PON technology is a considered an ultimate solution. Network carriers have begun to deploy time-division-multiplexing passive optical networks (TDM-PONs) such as broadband PON (BPON), Ethernet PON (EPON) and Gigabit PON (GPON) and wavelength-division multiplexing passive optical networks (WDM-PON) in response to the current trend of data- and image-based services resulting from the rapid growth of all kinds of multimedia Internet applications. In addition, WDM-PON is a promising approach for gigabit optical access network [16].

How to reduce the cost is always the most important issue in WDM-PON system. The first subject of WDM-PON is to design and implement a cost-effective scheme for bidirectional WDM-PON using the four-port interleaver. The second subject is to design a new method to provide select-cast services in WDM-PON system. The proposed WDM-PON has been implemented using optical carrier suppression and separation (OCSS) technology to generate a wavelength pair from a single laser source at the central office and deliver downstream signals in different modulation formats, i.e. OOK and DPSK. This method enables the co-location of both upstream and downstream WDM transmission in the central office. Additionally, the complexity, cost and maintenance of the optical network unit are reduced by enabling wavelength-independent operation. Since radio/mobile access is continuously growing and placing increasing demands on the network. The third subject is to devise a simple and cost-effective configuration in WDM-PON to supply triple play service (TPS). Only one single-arm intensity modulator is needed in this proposed scheme to provide significant improvement on both power

budget and system reliability.

1.3 Organization of the Dissertation

In Chapter I, a brief introduction of WDM networks and the motivation to overcome the limitation in bidirectional WDM transmission in different modulation formats are introduced. In Chapter II, an overview of bidirectional transmission system and the technique of the interleaver are studied. Four different types of interleaver by using Michelson-Gires-Tournois interferometers, Fabry-Perot resonator arrays, planar optical waveguides, and Lattice Filters are prsented, respectively. In Chapter III, the design, simulation and experiment of the four-port interleaver is illustrated.

In Chapter IV, a re-circulating loop to simulate long distance transmission has been introduced and experimentally demonstrated. Two experiments, using reconfigurable optical add/drop multiplexer (ROADM) and cascaded dispersion-compensated interleaver, are demonstrated. Novel bidirectional transmission using four-port interleaver to enable unidirectional amplification scheme is presented in Chapter V. The characteristics of the four-port interleaver and three experiments are shown in this chapter: straight-line bidirectional transmission, long-distance transmission using a re-circulating loop, comparison between bidirectional DPSK and OOK signals, and high bit rate transmission. New bidirectional WDM-PON, select-cast services in WDM-PON and triple-play services WDM-PON configuration are discussed and realized in Chapter VI. The future work will be presented in Chapter VII as novel hybrid 10G/1G coexisted TDM-PON and mobile WiMAX /Radio over fiber for broadband Internet access in high-speed railway system. Finally, the conclusions are summarized in Chapter VIII.

CHAPTER 2

OVERVIEW OF BIDIRECTIONAL SYSTEMS AND INTERLEAVER

2.1 Overview of Bidirectional Systems

For any multispan DWDM system, optical components such as transmission fiber and optical amplifiers represent substantial cost. In the past few years, the traditional unidirectional transmission, as shown in Figure 2.1(a), had been realized in the market. Nonetheless, more network links are needed for different directional transmission. However, bidirectional transmission has many obvious advantages over unidirectional transmission. Bidirectional transmission through one fiber, shown in Figure 2.1(b), is an attractive method for simultaneously reducing operating and maintenance costs by sharing the optical transmission fiber and the inline amplifiers [9, 17]. In addition, it can increase the spectral efficiencies of the conventional unidirectional WDM transmission system [18].
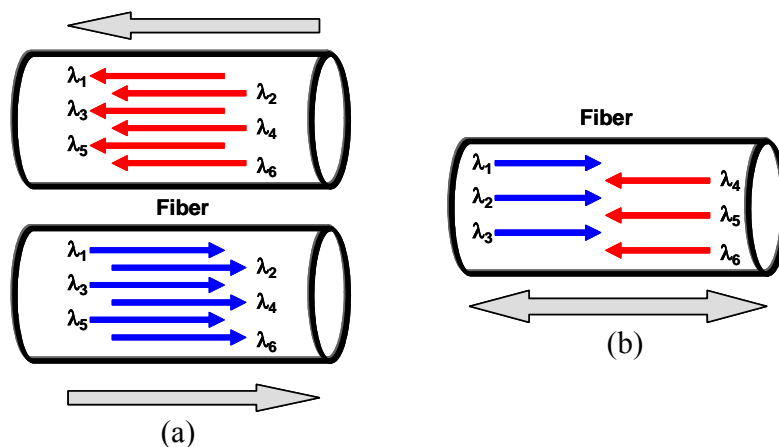
Figure 2.1: Sketch of (a) unidirectional and (b) bidirectional transmission

Possible approaches for bidirectional amplification are band splitting or channel interleaving [6, 8, 19], the use of arrayed waveguide gratings (AWGs), Mach-Zehnder WDM coupling, the use of circulators or the use of a gain-clamping semiconductor optical amplifier (SOA), called a linear optical amplifier (LOA) [9]. However, these approaches require the use of two or more EDFAs to achieve bidirectional transmission.

2.1.1 Bidirectional interleaved scheme

Basically, the counter-propagating signals on the same transmission fiber using suitable components are presented in Figure 2.2 [20]. Figure 2.2(a) shows the first approach for band separation by using band separators (BS). The transmitted signals are divided in two groups as red-band and blue-band, traveling in opposite directions. Bands are separated and combined by optical devices inserted in line along transmission medium. In order to prevent the adjacent bands from opposite direction, a band gap is needed between two bands. Figure 2.2(b) displays the second method to achieve bidirectional transmission and alleviates the band separation problem by using two interleavers (IL) to interleave channels in the two directions of transmission. This means that even channels will travel east to west, whereas odd channels will travel west to east. As the consequence, channel spacing for wavelength traveling in the same direction has to be doubled. There is another scheme to transmit the same wavelength in both directions, as Figure 2.2(c). Optical circulators (Cir) are used to separate transmitted eastbound and westbound traffic. However, in these technologies, traffic from each direction is then individually amplified using a corresponding erbium-doped fiber amplifier (EDFA). The gain of EDFAs are typically limited to avoid the RB self-

oscillation [21, 22], these limitations will significantly shorten the amplification span and reduce optical signal to noise ratio (OSNR) [23], thus increase the operational cost and degrade the transmission quality. One of the important issues in bidirectional transmission system is RB. In this wavelength interleaving scheme, the RB induced from eastbound traffic would be amplified in eastbound direction. Therefore, the performance of bidirectional transmission is severely impaired by this kind of nonlinearity. Furthermore, this scheme needs more optical components and more EDFAs; therefore, it is not a cost-effective solution.

From: Cisco Systems, Inc. White Paper, 2001.
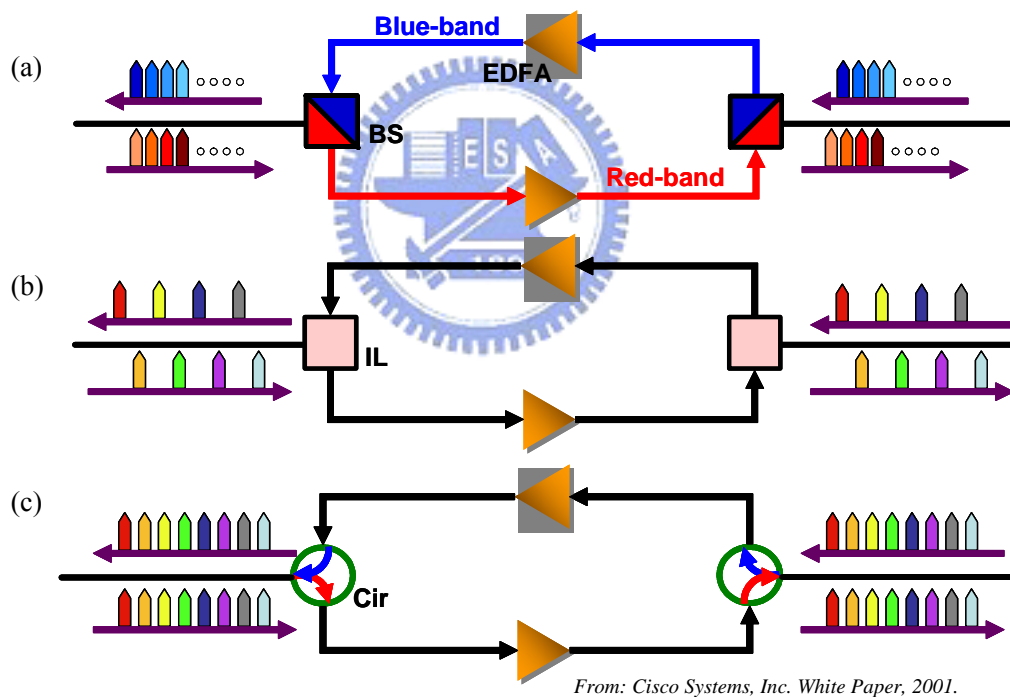
Figure 2.2: Wavelength interleaved scheme. (a) Separate bands, (b) interleaved channels, and (c) same wavelength using circulators.

2.1.2 Bidirectional amplification scheme

Another approach scheme is using bidirectional amplification as shown in Figure 2.3.

Two amplifiers in opposite direction [24], one inline amplifier, LOA [9], and one SOA [10] had been proposed and published. The first manner can not use any isolator within amplification section; therefore, the RB would be amplified and impaired the quality of the networks. In Ref. [9], the characteristics of the gain-clamping effect limit the gain of LOA to less than 20 dB and a high noise figure (NF) is inevitable. Although SOA can simplify the bidirectional transmission, it needs to be operated above the saturation level to obtain the required optical signal-to-noise ratio (OSNR) at the receiver. The waveform distortion and cross-gain modulation (XGM) poses severe challenges to operate SOAs in the saturation region.
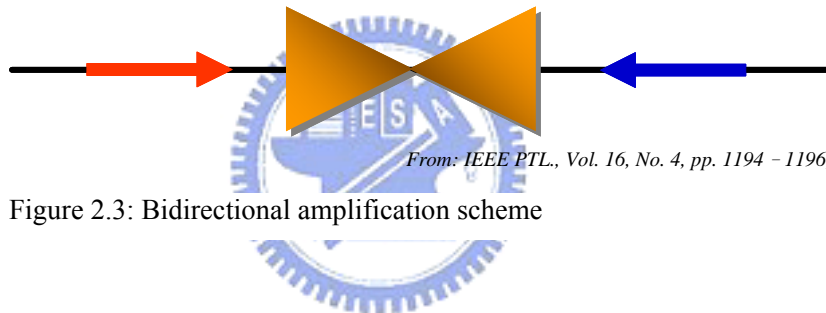
From: IEEE PTL., Vol. 16, No. 4, pp. 1194–1196, 2004.

Figure 2.3: Bidirectional amplification scheme

2.2 Overview of Interleavers

In an optical communication system using WDM, information is transmitted over several channels, each at different optical wavelength or optical carrier frequency. An interleaver is an optical filter having at least one input port and two complementary output ports, with an optical transfer functions that is periodic in frequency. In this way, even-numbered channels can be routed to one output port while the odd-channels will merge from the other output port, as depicted in Figure 2.4(a). Meanwhile, the device can be used in a reverse direction that combines two sets of DWDM channels (odd and even channels) into a composite signal stream in an interleaving way [13–15] as shown in
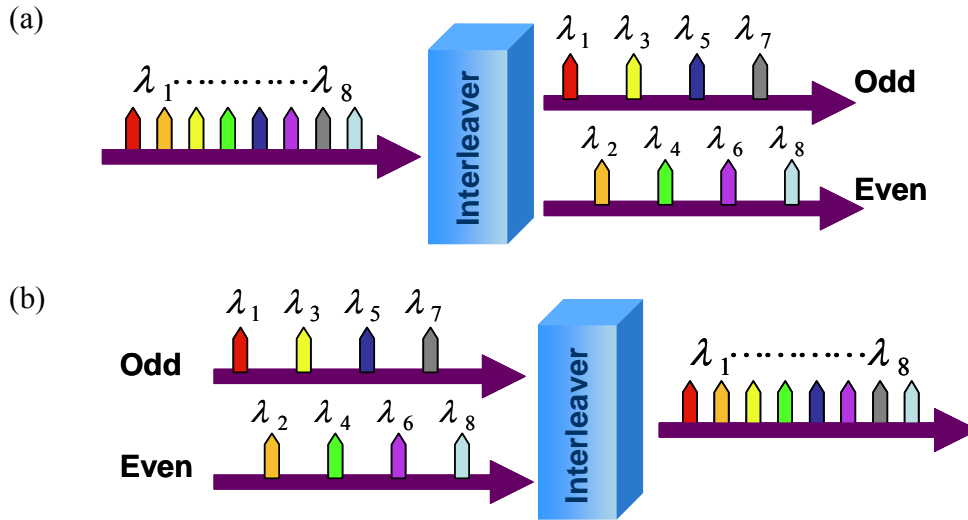
Figure 2.4: Illustration of the function of an (a) optical interleaver and (b) de-interleaver

Figure 2.4(b). There are different types of interleavers exhibited in Figure 2.5 [11]. The original 1:2 design is presented in Figure 2.4. The periodic separation of one in every 2^N input wavelengths is achieved using the 1:4 interleaver is shown in Figure 2.5(a). The last interleaver design (4:8) used to separate a band of even and odd wavelengths is indicated in Figure 2.5(b). Commercial interleavers are available separating DWDM combs with channel spacing of 25 GHz, 50 GHz, 100 GHz and 200 GHz. The period of the interelaver is determined by the FSR of the components used to make the device. As stated before, interleavers can be built from any type of wavelength filter having a periodic frequency response. In principle, any optical (de)multiplexer having a periodic response with frequency may be used as an interleaver. Currently, there are some approaches to building optical interleaver based on different operating principles and using different technologies: 1) Michelson-Gires-Tournois interferometers [28, 29], 2) Fabry-Perot resonator arrays [30], 3) planar optical waveguide interleavers [31], 4) Lattice Filters [32] and so on.

12
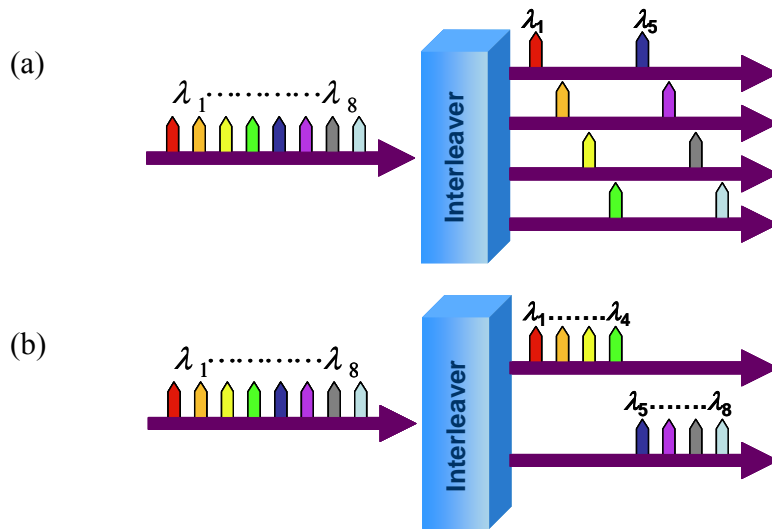
Figure 2.5: Different types of interleavers. (a) Seperation of channels out to 1:4, and (b) seperates even and odd bands of channels.

2.2.1 Michelson–Gires–Tournois Interferometers

The Michelson interferometer (MI) is the bulk equivalent of the Mach-Zender interferometer with a ring resonator coupled to one of its branches. It operates on the periodic of a Gires-Tournois interferometer (GTI). One or two mirrors of the MI are replaced by a Gires–Tournois resonator (GTR), a Fabry-Perot (FP) resonator with 100% mirror and can be used in reflection, so-called a Michelson-Gires-Tournois interferometer as displayed in Figure 2.6. Michelson-Gires-Tournois interferometers operate on the phase return from the two Michelson arms. Although one of the interleaver output signals will be back reflected, it can be separated from the input signals by tilting some of the mirrors. The back reflected light has a frequency response that is complementary to that of the transmitted light, and the input signal will appear frequency interleaved at the reflection and transmission port of the device.
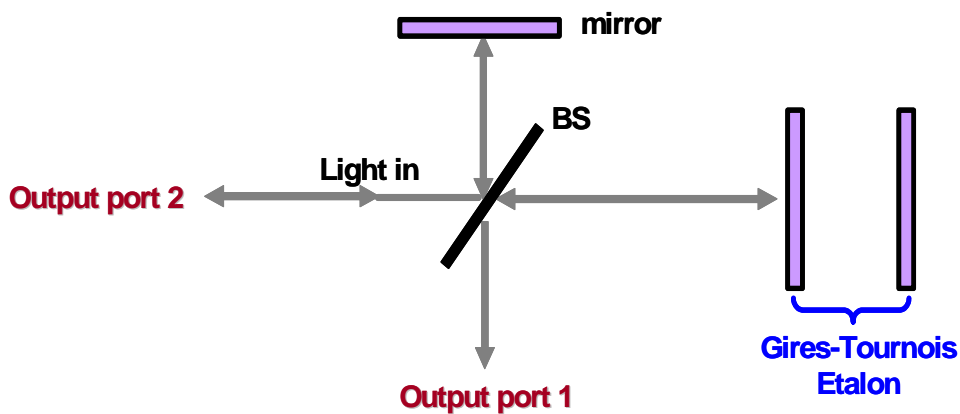
Figure 2.6: A Michelson–Gires–Tournois interferometer filter.

2.2.2 Fabry-Perot resonator arrays

Figure 2.7 illustrates the interleaver based on Fabry-Perot resonator arrays, a resonant cavity formed by two parallel reflecting mirrors separated by a medium, using a circulator for separating input and reflected output light. By arranging a number of resonators, while choosing the mirror reflectance carefully, the rectangular-shaped transfer function that is desirable for interleaver operation can be well approximated. Output 1 and output 2 are complementary that can produce frequency-interleaved signals.

From: Optics Communication, 233, pp. 113-117, 2004
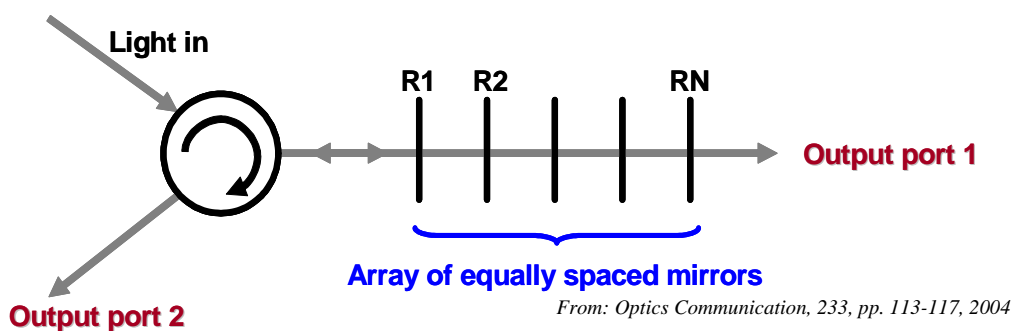
Figure 2.7: An Interleaver based on Fabry–Perot resonator arrays.

2.2.3 Planar Optical Waveguide Interleavers

Most of works on interleaver filters in planar technology have been done in silica-based waveguide systems by AT&T/Lucent [32], NTT [33], and others [34]. Polymers also can be used as the material because of their simple processing and hence possibly lower cost. However, this kind of material may have problems with long-term stability. Lithium niobate ($LiNbO_3$) is an attractive material because of its electro-optic properties and mature technology. Filters fabricated in this technology are often based on frequency-selective mode conversion. Electro-optically tunable interleaver based on this principle is shown in Figure 2.8 [30]. The strain-inducing strips produce an off-diagonal element in the refractive index tensor leading to different polarization mode conversion. The frequency at which the phase matching condition for efficient mode conversion is tuned by a voltage on the electrodes, changing the birefringence of the lithium niobate crystal.

From: J. Lightwave Technology, 21, pp. 837-847, 2003
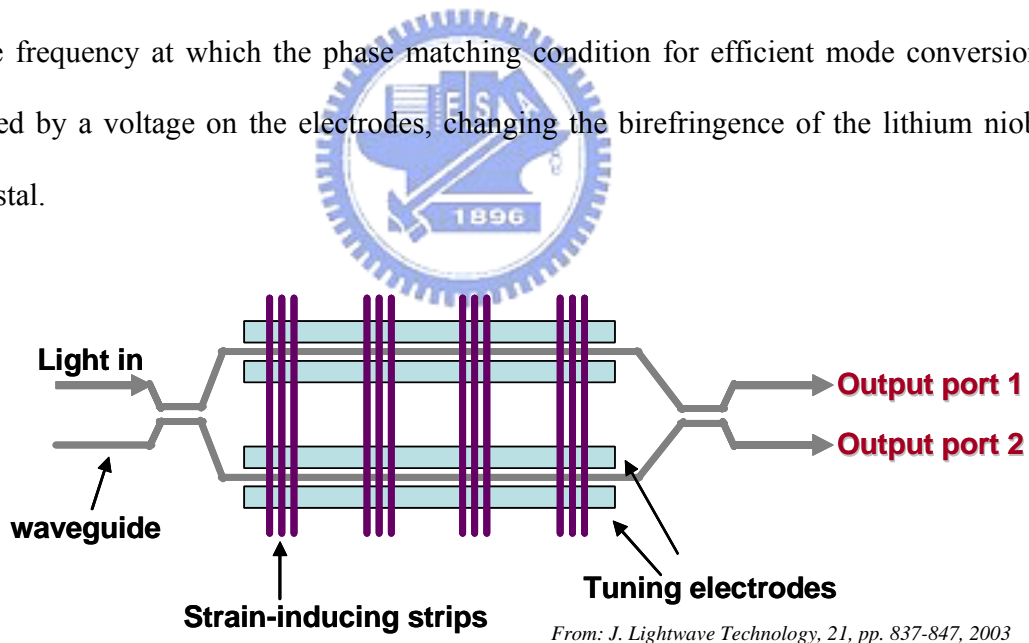
Figure 2.8: Electro-optically tunable lithium niobate ($LiNbO_3$) interleaver.

2.2.4 Lattice filters

Basically, lattice filters are made from many cascaded differential-delay elements

15

where one polarization is delayed along the slow axes of the crystal and the other polarization is not. The differential-delay of each element is an integral multiple of a unit delay and power is exchanged across paths between the elements. It is a huge topic in lattice filters and not limit to optical domain. Figure 2.9 only illustrated a simple and basic block structure of a lattice filter. Within the lattice filters, there is the birefrignent filters that adapted polarization insensitivity through polarization diversity. A polarization diversity scheme separates the input light into two orthogonally polarized rays. They take turns to pass through the waveplate cascaded. After that, the polarizations are re-combined onto two output ports. Consequently, the light that clipped by the output polarizer of the canonical birefringece filter is instead redirected to a complimentary port. In this dissertation, the design of our interleavers is based on the principles of lattice filter.
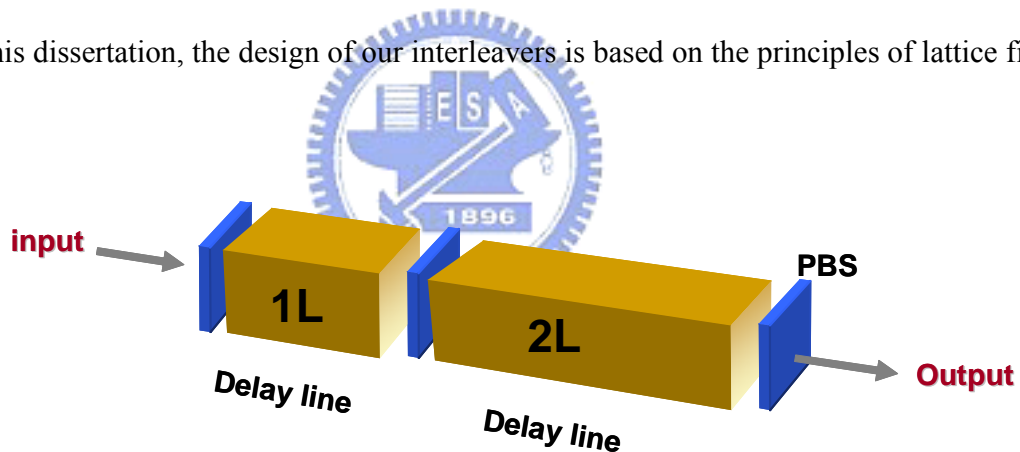
Figure 2.9: Lattice filters unit cell.

CHAPTER 3

DESIGN AND EXPERIMENT OF THE FOUR-PORT

INTERLEAVER

As an optical filter, an interleaver combines or separates a comb of dense wavelength-division multiplexed (DWDM) signals. The periodic nature of the interleaver filter reduces the number of Fourier components required for a flat passband and a high-isolation rejection band. This behavior is great contrasts to the single-channel add/drop filters that synthesize a single narrow-band filter over a wide rejection band. Because the interleaver requires fewer Fourier components than a single narrow band filter, the same flat top, sharp edge response of a higher-order narrow-band filter can be realized using a small number of sections [13]. The filter function of an interleaver and its period can be separated. Interleavers have been shown to resolve a comb of DWDM frequencies with channel spacing of 100, 50, 25, and 12.5 GHz. The period of the interleaver is governed by the free-spectral range of the core elements, in which a longer optical path achieves narrower channel spacing. Four-port interleaver has been proposed before [24] using fiber-based configuration. The device is sensitive to temperature variation and exhibiting Gaussian passband characteristics. This dissertation proposed and experimentally demonstrated a new four-port interleaver with temperature compensation, flat-top passband for dispersion-free transmission.

3.1 Considerations of Interleavers Design

Birefringent crystal has long been used in designing optical filters; which includes birefringent crystal plates and polarizers. The two major types of birefringent filters are Lyot-Öhman filters and Šolc filters [36–38]. Both types are based on interference between polarized light, and require phase retardation among the components of light polarized parallel to the slow and the fast axes of the crystal, as light passes through it. Consequently, birefringent crystal is served as an optical delay line, and a half-wave plate is used to alter the polarization between the delay stages. The rotation of the half-wave plates can also be considered to be designed to generate various required Fourier frequency components. Figure 3.1 shows the configuration of the three-port interleaver employed by the birefringent crystal. At the input and outputs of the interleaver, an YVO$_4$ walk-off crystal and a half-wave plate were used to ensure that the optical delay cells contained only a single polarization. Each delay cell includes two birefringent crystals, namely YVO$_4$ and Rutile (TiO$_2$), to compensate for the temperature variation. The lengths of YVO$_4$ and Rutile can be determined using (1) and (2).

$$\Delta n_1 L_1 - \Delta n_2 L_2 = m\lambda_{center} = \frac{c}{FSR} \qquad (1)$$

$$\frac{d}{dT}\left(\Delta n_1 L_1 - \Delta n_2 L_2\right) = 0 \Rightarrow \Delta n_1 L_1 \beta_1 - \Delta n_2 L_2 \beta_2 = 0 \qquad (2)$$

$$\text{with } \beta_i \equiv \frac{d\Delta n_i}{\Delta n_i dT} + \frac{dL_i}{L_i dT} = \frac{d\lambda_i}{\lambda_i dT}; \quad i = 1,2$$

In (1) and (2), Δn_1 and Δn_2 indicate, respectively, the group index difference between ordinary and extraordinary axes of YVO$_4$ and Rutile. Moreover, c denotes the speed of light, FSR represents the free spectral range, L_i represents the length of the crystal, λ_{center} denotes the center wavelength of the operation wavelength range, m
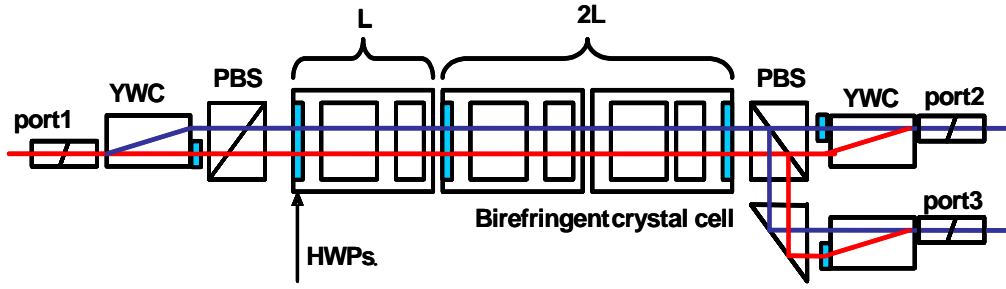
PBS: Polarization beam splitter; YWC: YVO₄ walk off crystal; HWP: Half wave plate

Figure 3.1: Possible configuration of a three-port L-2L interleaver.

represents the order of the birefringent wave plate and β_t is the normalized variation in the wavelength with temperature. Figure 3.2 shows the measurement setup used to determine β. Since for normal incident light, each crystal forms a Fabry-Perot Etalon cavity from the facets reflection and the transmission spectra will have null points with FSR determined by the cavity length. When the temperature of the crystal is changed, the cavity length will change and the null points will start to drift accordingly. β can then be determined by measuring the drifting of the null point with temperature in the optical spectrum analyzer. For YVO₄ and Rutile, the group index differences are 0.2139 and 0.2652, and the β are -26.54×10^{-6} 1/°C and -99.06×10^{-6} 1/°C, respectively. At the central frequency of 193.5 THz, the values of β correspond to 5.13 and 19.17 GHz/°C, respectively. For a 100-GHz interleaver, FSR equals to 200 GHz, solving (1) and (2) yields the lengths of the YVO₄ and Rutile crystals, which are 9.5697 and 2.0685 mm, respectively [39]. After temperature compensation, the temperature drift is reduced to approximately 0.056 GHz/°C. This corresponds to about 3.7 GHz drift in temperature variation from 0 °C to 65 °C. One difficulty that could not be fully compensated during the design process was the wavelength dependence of refractive index, namely dispersion.
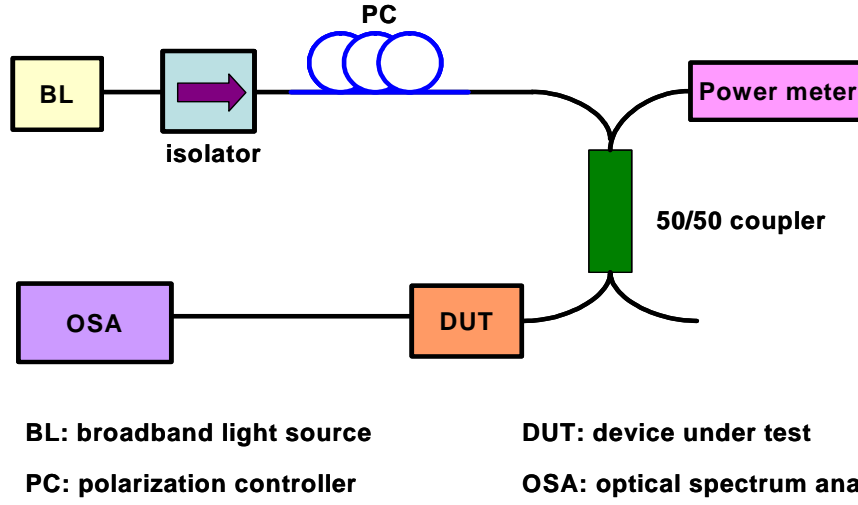
Figure 3.2: Measurement setup of birefringent crystal temperature sensitivity interleaver.

However, as shown in Appendix I, with proper selection of crystal lengths, for typical *C*-band application (with center frequency 193.5 THz and total bandwidth 4 THz), the refractive index dispersion introduces center frequency offset of only 2 to 2.5 GHz.

The optimized wave plate angles were determined using the "minimize the integral square error" method, as shown in (3).

$$\min\left\{\sum_{n=1}^{N}[\hat{x}(f_n) - x(f_n)]^2\right\} \tag{3}$$

$$\text{with } f_c - \frac{FSR}{2} \leq f_n \leq f_c + \frac{FSR}{2} \tag{4}$$

In (3), $\hat{x}(f_n)$ is the desired target amplitude response and $x(f_n)$ is the real transmission function. The transmission function is periodic, therefore, the errors can be summed over one FSR at the central frequency, f_c. By changing the position of the half-wave plate at the input walk-off crystal, the input polarization angle was shifted 90° and generates two delay responses. Minimizing (3) can yield the corresponding wave plate angles. Figure 3.3 presents the simulated amplitude and delay response of two types of

Dispersion Compensating Interelavers for Add/Drop Node
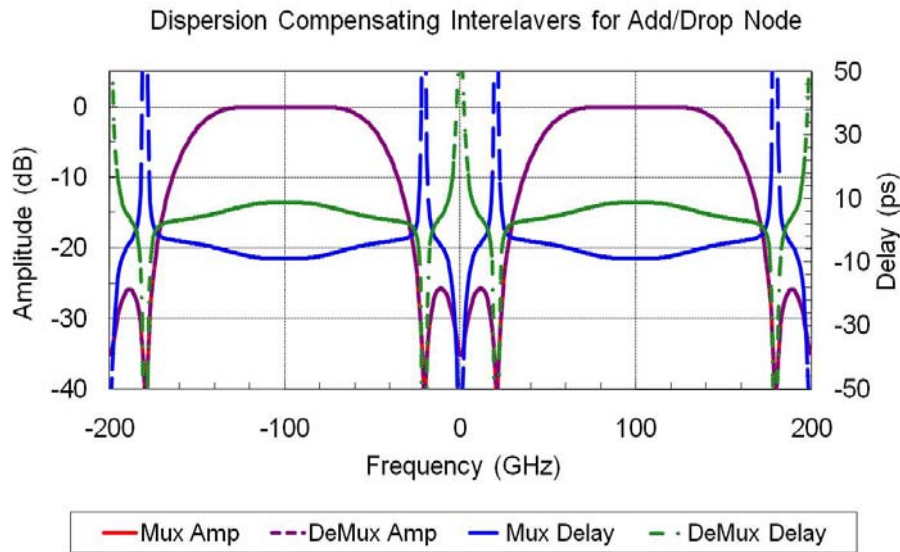
Figure 3.3: Two types of interleavers with same amplitude but opposite delay response.

interleavers. This figure shows that changing the input polarization yields two interleavers with the same amplitude responses but opposite delay responses. Therefore, the cascaded interleaver pair will have constant delay and therefore the dispersion will approach zero. To design an interleaver with sharp edge response, higher Fourier frequency components must be included. Additional delay line stages are required to increase the highest Fourier frequency, and pass band, insertion loss, size, reliability and cost are all traded off against one another. For a 100 GHz interleaver, L-2L-2L can meet the pass band and delay requirements for 40 Gb/s transmission without difficulty. If only a 10 Gb/s signal is transmitted, an L-2L design will suffice.

3.2 Experimental Results of 100 GHz L-2L-2L Interleavers

After design analysis, an L-2L-2L interlever was fabricated to verify the design. Figure 3.4(a) and (b) show the measurement results of the re-centered transmission

responses in a frequency range from 191.8 THz to 195.5 THz at 0 C°, 23 C° and 65 C°, respectively. The figures clearly demonstrate successfully mitigation of the temperature variation. Figure 3.4(c) shows the 0.5 dB passband of different channels at 0 C°, 23 C° and 65 C°. The average 0.5 dB passband is about 73 GHz. Figure 3.4(d) shows the polarization dependent loss (PDL) of different channels at 0 C°, 23 C° and 65 C°. The average PDL is below 0.15 dB meaning that there is good control of on the alignment
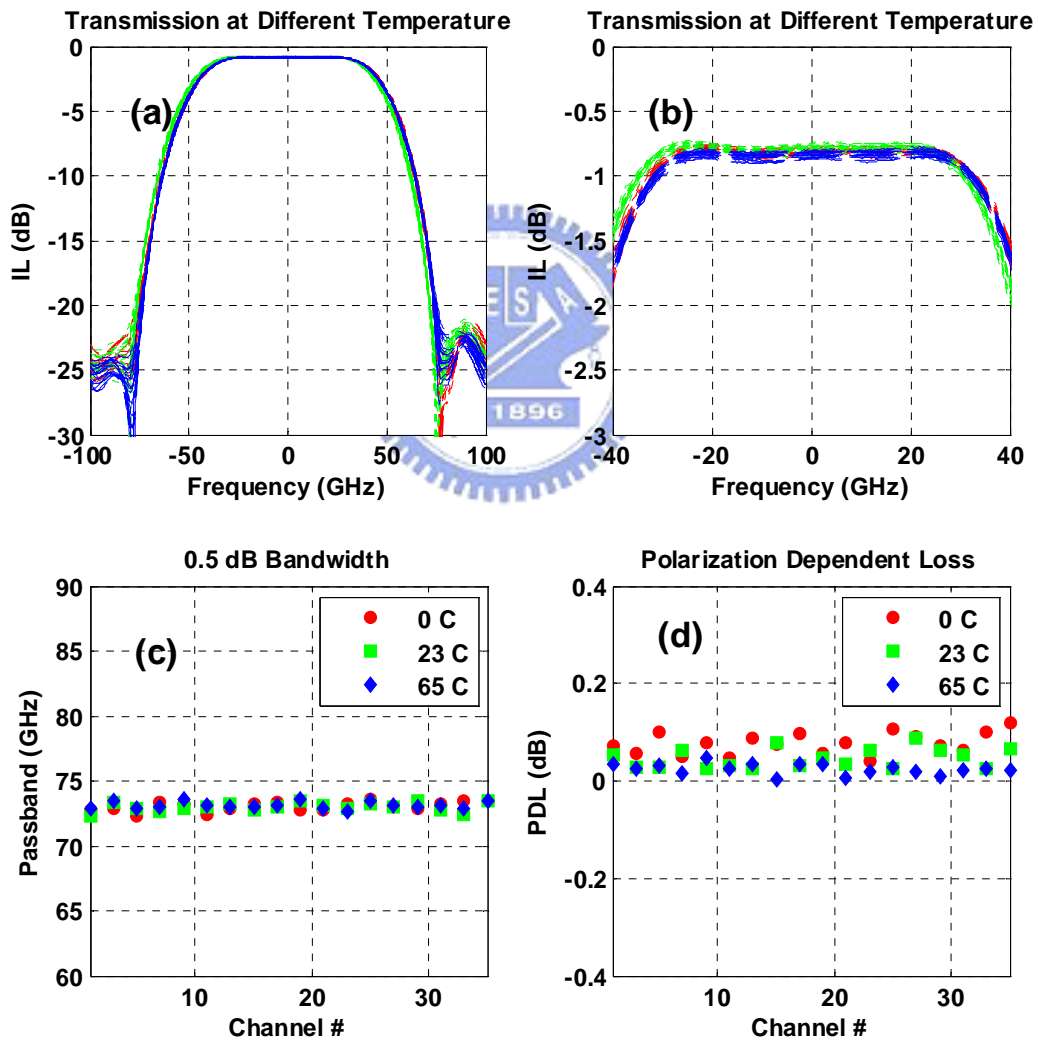
Figure 3.4: (a) Re-centered transmission at 0 °C, 23 °C and 65 °C. (b) Magnified Folded transmission at 0 °C, 23 °C and 65 °C. (c) 0.5 dB passband at 0 °C, 23 °C and 65 °C. (d) Polarization dependent loss 0 °C, 23 °C and 65 °C.

between the input fiber and the walk-off YVO$_4$ crystal. The fiber alignment is similar to typical micro-optic fiber devices such as isolator, circulator and switch. The alignment need to be very careful and active alignment is needed. Figure 3.5 plots the measured amplitude and the delay responses of two types of 100-GHz interleavers. Figure 3.5(a)–(d) illustrate type A and B interleavers that have identical transmission spectra but reversed delay responses. Meanwhile, type A and B interleavers can be cascaded to generate a linear phase interleaver pair with a total dispersion near zero, a feature that is desirable, particularly in metro add/drop applications and/or high bit rate transmission systems.
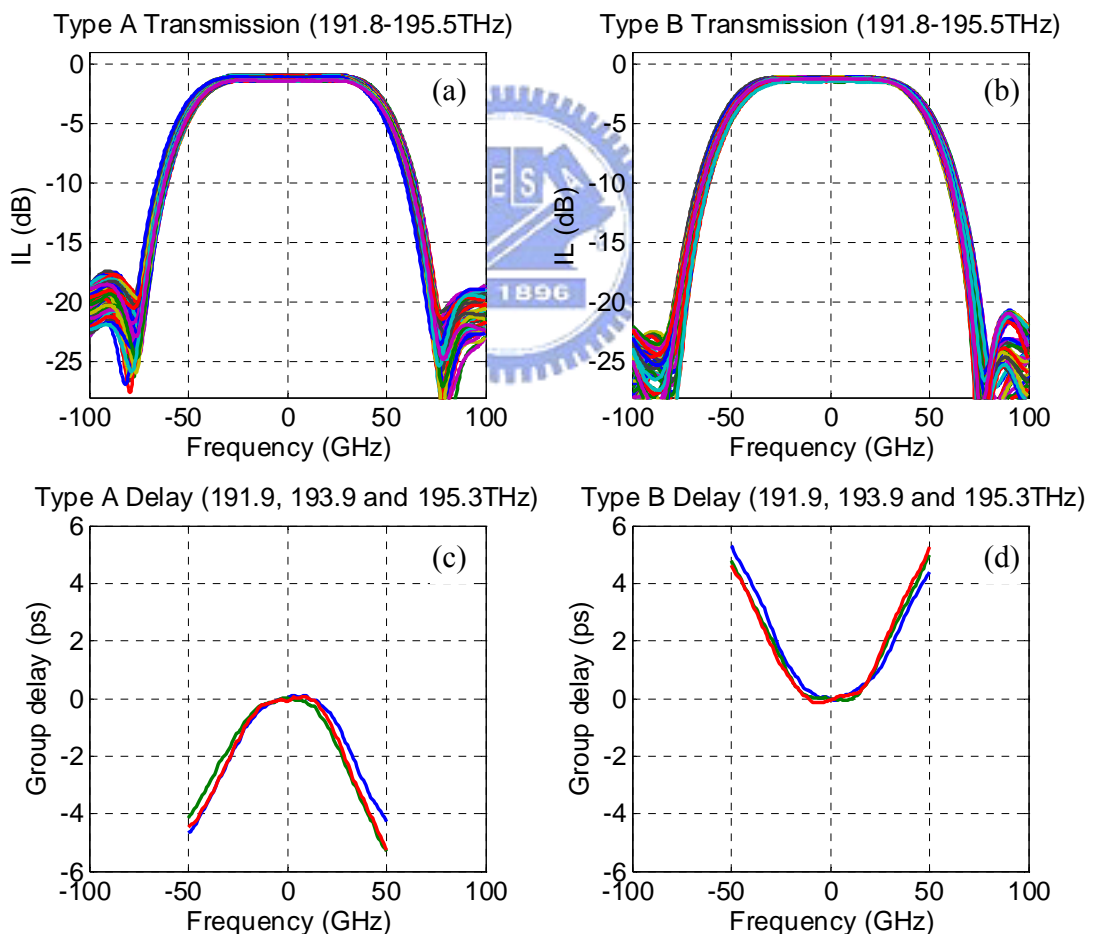
Figure 3.5: (a), (b): Measured re-centered amplitude of Mux and Demux; (c), (d) measured re-centered delay of Mux and DeMux.

23

Figure 3.6 depicts the measured results that relate to seven cascaded interleaver pairs. The figure shows that the total delay is below 1ps within the pass band. These figures clearly show that interleavers with same amplitude response and opposite delay response were successfully designed.

Average Group Delay of Cascaded Interlaever Pair in Different Frequency
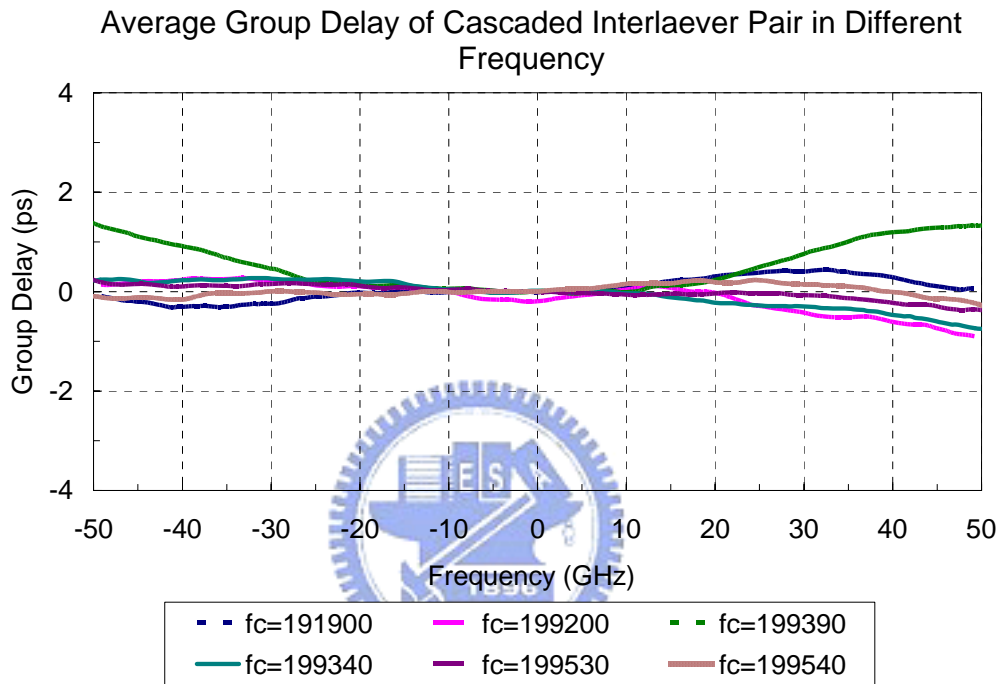
Figure 3.6: Measured cascaded delay response for different frequency.

CHAPTER 4

LONG DISTANCE TRANSMISSION BY USING A

RECIRCULATING-LOOP

As the Internet traffic is increasing rapidly and DWDM technologies in current optical communication systems is getting matured, the functionalities and configurations of DWDM networks must be rapidly evolving accordingly [40]. The reconfigurability of WDM networks has the following features: The network's configuration can be increased by bypassing, adding, or dropping the traffic and the capacity throughput enlarges when the traffic is multiplexed on the fiber by WDM. As a result, optical add-drop node will play an important role in high bite rate networks [41–43]. Two of experiments of optical add/drop technologies will be discussed and demonstrated in this chapter.
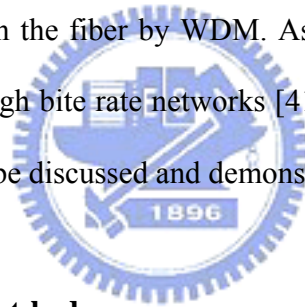
4.1 Recirculating Loop Test-bed

Modern optical fiber communication systems employ lots of components and hundreds or thousands of kilometers of optical fibers. In the lab environment, recirculationg optical loop tests-bed is a method for simulating long distance optical links to reduce the components, fiber span and the cost [6, 56]. Figure 4.1 illustrates the simple functions of the recirculating loop. Optical signals of limited duration are fed into an optical link as Figure 4.1(a). This optical link may consist of optical components, such as fiber coils, amplifiers, filters and so on. Then, in Figure 4.1(b), the source would be disconnected and allowed the signals to circulate within a closed optical loop. After a number of round-trips, loop would be opened by the loop switch and the circulating
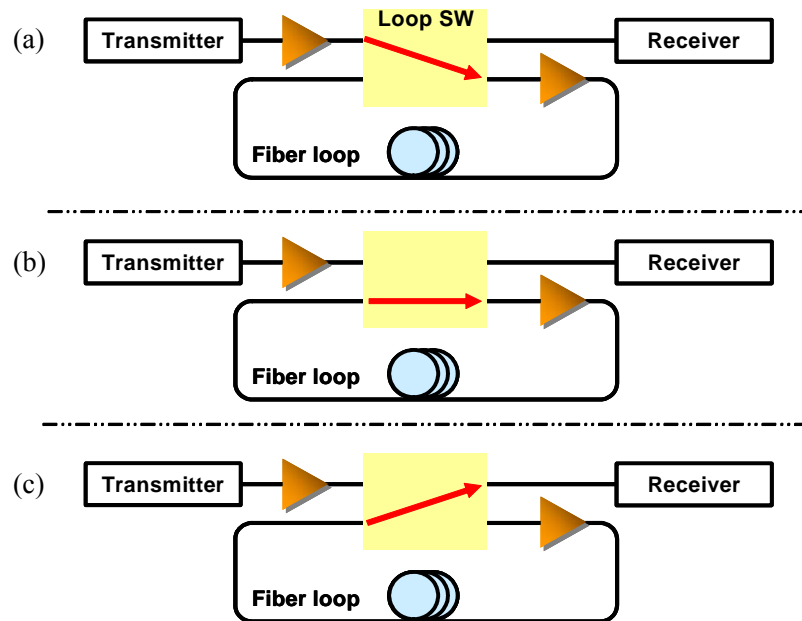
Figure 4.1: Phase of a recirculating loop. (a) Filling the loop, (b) circulating, and (c) emptying the loop.

signals are fed into the receiver, as displayed in Figure 4.1(c). Once the loop has been emptied, the signals are fed into the fiber loop by the switch again. Consequently, the optical loop switch is a core component that has to be precisely controlled. A simplified description of the operation of a recirculating loop by acousto-optic (AO) switches follows, as in Figure 4.2. The pulse duration defines the length of the fill cycle. The loop time is related to loop length by $Loop \ \ Time \ \ (\tau_{Loop}) = \dfrac{Loop \ \ length}{Velocity \ \ of \ \ light \ \ in \ \ fiber}$.

Closing the transmit switch loads the data stream into the optical loop. After the loop fills with data (Loop Time), the transmit switch opens (turn off) and the loop switch closes (turn on). The loaded bit stream then recirculates around the loop. A delay circuit (Error Gate) sets the distance range monitored and detected by the receiver after many times of circulations in the loop. After that, the loop can be emptied, refilled, and a new measurement cycle can begin.
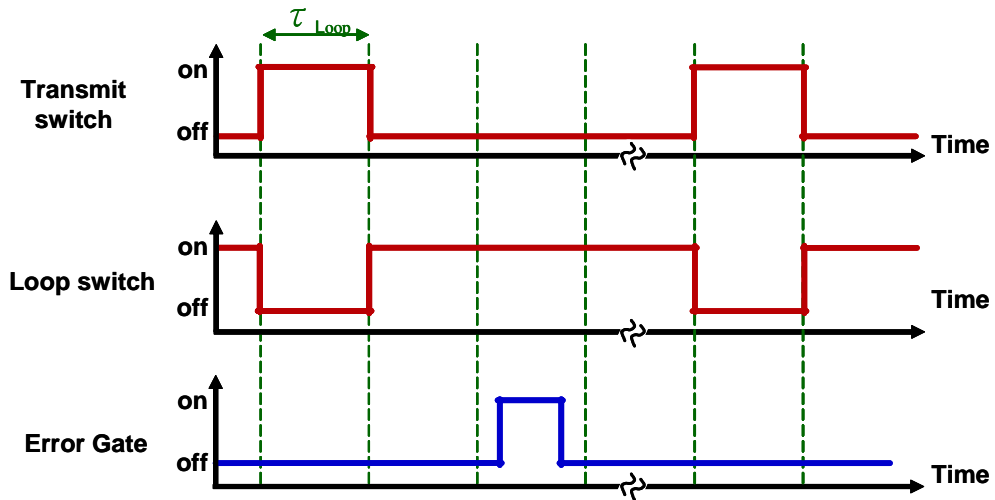
Figure 4.2: Timing diagram of the recirculating loop.

4.2 Add/Drop Applications in Fiber Ring Networks Based on A Reconfigurable Optical Add/Drop Multiplexer (ROADM)

The ultimate goal of high bit rate networks is to have a large traffic bandwidth capacity and a flexible and dynamic reconfigurability to provide diversified bandwidth management in the optical layers of future all optical networks. One of the key enabling elements is the reconfigurable optical add/drop multiplexer (ROADM) which can insert (add) and extract (drop) channels at specific wavelengths and provide various supervisions and reconfigurations that are required at the nodes of future DWDM networks [44]. Recently, different technologies have been utilized to ensure the functionality of ROADM, such as planar waveguide switches [45], MEMS switches [46], and liquid crystal switches [47]. It is highly desirable to have the flexibility of directing the dropped and added optical channel to any specific port in an ROADM to achieve a real dynamically reconfigurable network. Hence, a monolithic integrated silica-on-silicon

planar lightwave circuit (PLCs) with a cross-bar switch array is the most promising candidate as an ROADM [48]. Since the traffic pattern is highly diverse in metro optical networks, the wavelengths are frequently reconfigured. As a result, the cascadability and extinction ratios of add/drop functions of ROADMs are important limiting factors on the applications of ROADMs.

4.2.1 Characteristics of ROADM

The system-on-a-chip ROADM used in this experiment is based on the cross-bar switch design to add/drop arbitrarily four out of 32 input wavelengths, its mask as shown in Figure 4.3. This ROADM is the first time to use a large-scale PLC device, 85.3 mm × 119 mm. Figure 4.4(a) schematically depicts the function of this ROADM. The 32 input WDM wavelengths, with a channel spacing of 200 GHz, are first demultiplexed by an array waveguide grating (AWG), and then sent to a 32 × 4 switching fabric for add/drop operations. Such a 32 × 4 switching fabric is scaled up by as many 2 × 2 cross-bar dilated thermo optic switches, as shown in Figure 4.4(b), and is built in the ROADM.
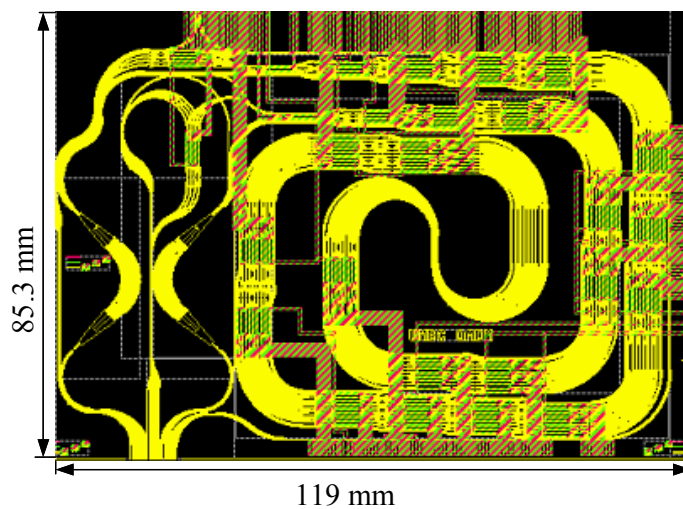
Figure 4.3: The mask of the ROADM.

For example, signals launched to the thermo optics switch from port 1 would be routed to output port, port 4. At the same time, the signals can be dropped from port 2 and be added from port 3. All the reconfigured output channels are subsequently optically multiplexed using a second AWG. The detailed design rules, the operation principles, the architectures and the device characteristics of this ROADM can be found in [48]. Figure 4.4(c) displays the optical spectrum when one of the 32 input wavelengths is dropped. The extinction ratio of the dropped channel is more than 40 dB and the adjacent channel isolation exceeds 25 dB. It also can be seen clearly that the channel spacing of this ROADM is 200 GHz. Nevertheless, the high extinction ratio and isolation of the ROADM provide the feasibility for fiber network. Due to the limitation of laser sources, eight DFB lasers have been used to demonstrate the features of this 32 × 4-channel

(a)   (b)

(c)
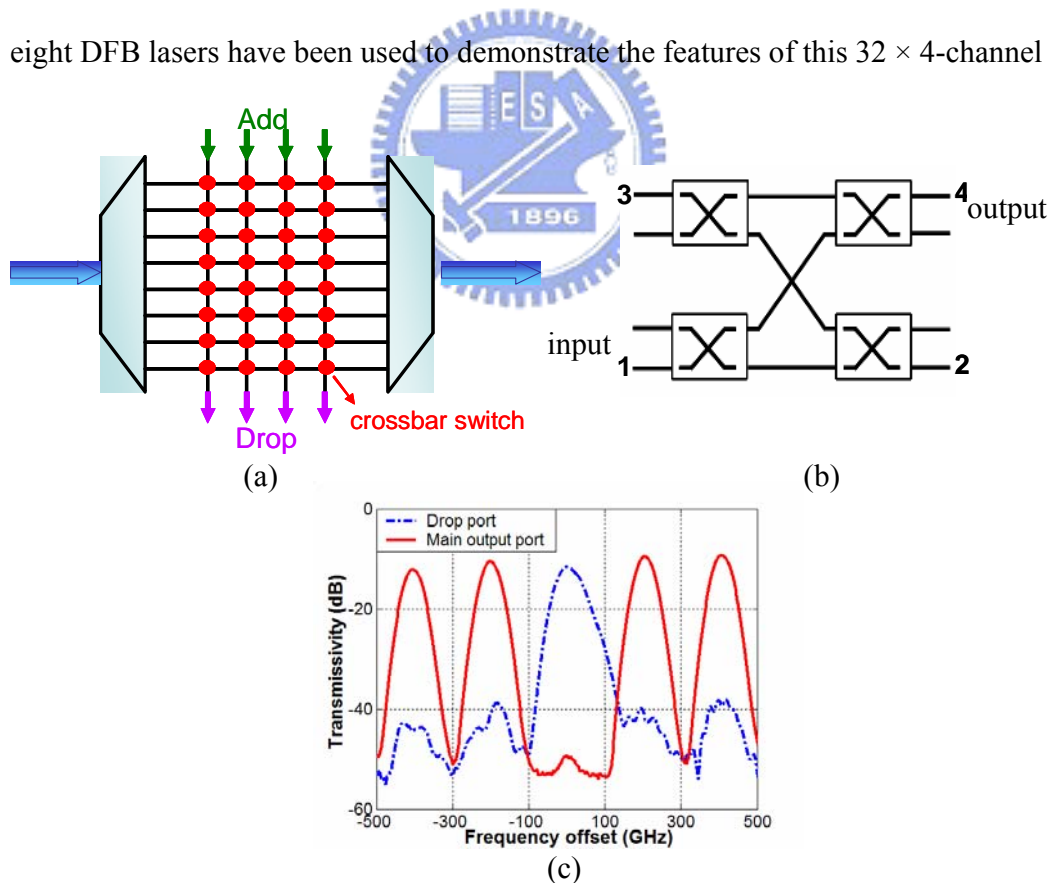
Figure 4.4: (a) Schematic diagram of the ROADM, (b) crossbar switch of the ROADM, and (c) optical spectra obtained at drop port and main output port when one channel is dropped.

ROADM for the passing through, adding and dropping channels that exhibited in Figure 4.4. Figure 4.5(a) and (c) schematically depict the measurements that yielded Figure 4.5 (b) and (d), respectively. As shown in Figure 4.5(a), the odd channels of the eight output wavelengths were added from the add-ports, and the even channels passed through the ROADM directly from the input-port to output-port. These eight channels were multiplexed by a second AWG and the corresponding adding and passing spectra are displayed in Figure 4.5(b). Owing to the heating characteristics of the thermo optic switches, the center wavelengths of the passing and adding channels are not accurately matched. The wavelength deviation from the International Telecommunication Union (ITU) grid, caused by the thermal effect, is approximately 8 GHz.
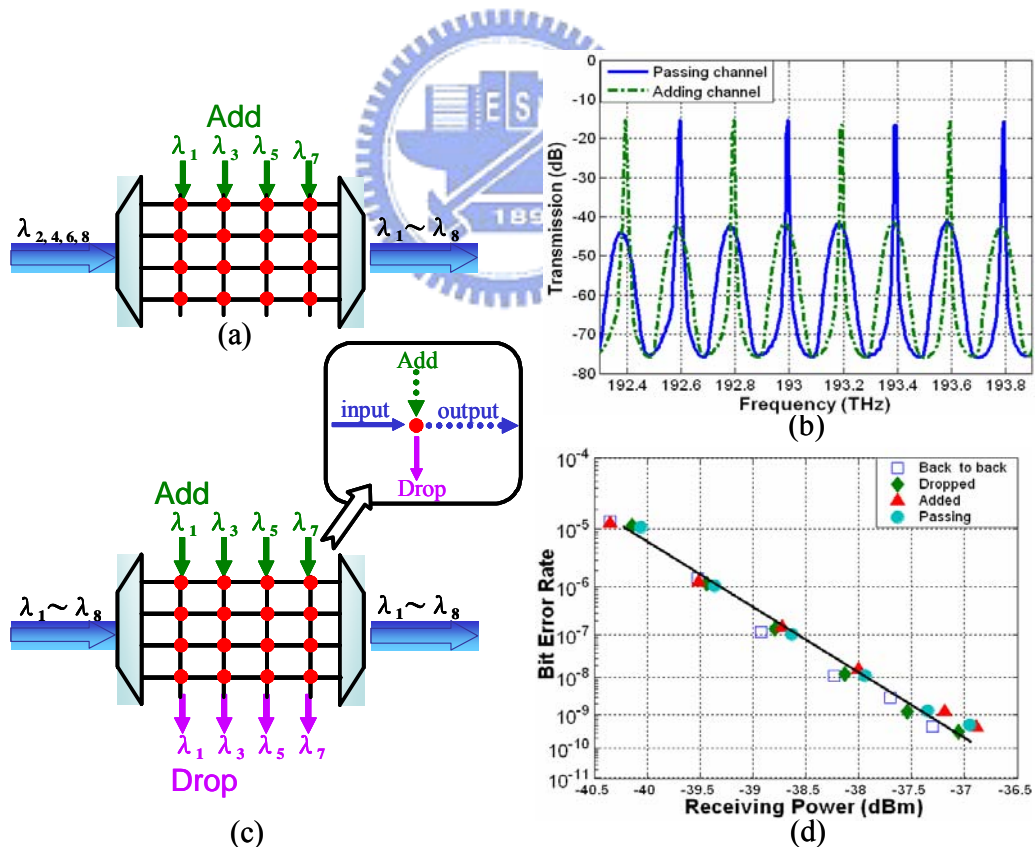
Figure 4.5: (a) Schematic diagram of simultaneous addition of odd channels and passing through of even channels at the ROADM, (b) optical spectra for passing (even) and adding (odd) channels, (c) schematic diagram for eight passing and four adding/dropping channels, and (d) the BER curves for these channels in (c).

Such a frequency deviation will degrade the BER performance as many of such ROADMS are cascaded. As a result, to investigate this degradation, we also performed the measurement to demonstrate the effects of passband frequency deviation on power penalty performance in Figure 4.7. To compensate this thermal drifting effect, simultaneous temperature compensation in thermal equilibrium to match the precise ITU grids is required in operating the Add/Drop functions of this ROADM. Moreover, the BER performance of the ROADM was measured under different operation conditions. Figure 4.5(c) schematically depicts the experimental setup and Figure 4.5(d) plots the corresponding BER curves. The dropped (diamond-symbol), added (triangle-symbol) and passing (circular-symbol) channels were measured from the "input" port to the "drop" port, from the "add" port to the "output" port and from the "input" port to the "output" port, respectively. This figure indicates a sensitivity variation of less than 0.3 dB under different operation modes in the ROADM. The variations were major due to different route paths in the cross-bar switching fabric under different operation conditions. The crosstalk-induced penalty was negligible, guaranteeing the strong performance of the ROADM device.

4.2.2 Periodic Add/Drop Ring Network System

In the system experiment, a re-circulating loop was employed to simulate multiple adds/drops in an add/drop ring network system and to demonstrate the attainable cascadability of the ROADMs. Figure 4.6 shows the experimental configuration of a periodic add/drop ring network [49]. The wavelengths of the eight-channel laser sources span from 192.4 THz to 193.8 THz with 200 GHz channel spacing.
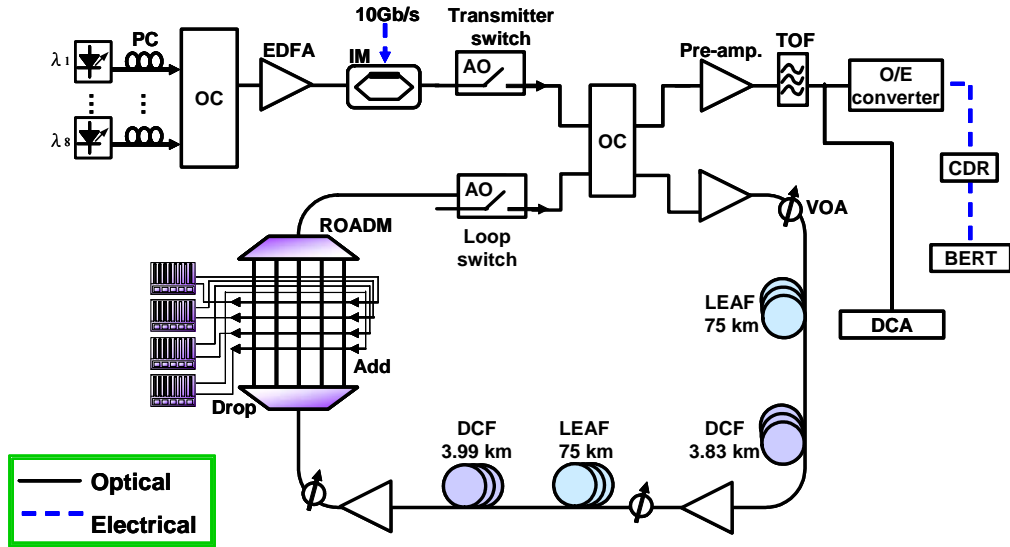
Figure 4.6: Experimental configuration of a recirculating loop based periodic add/drop ring network.

The optical channels were modulated by a LiNbO3 electro-optical (EO) modulator at 10 Gbps with a pseudo random binary sequence (PRBS) length of 2^{31}-1. Two types of fiber were used in this experiment. They were 150 km of Corning LEAF and 8 km of Corning dispersion compensation fiber (DCF), which was set to compensate accumulated chromatic dispersion in LEAF fiber, with -4 dBm launched power per channel into each fiber span. A 3R receiver, combined with an optical preamplifier, of –37-dBm receiving sensitivity at BER of 10^{-9} was used to evaluate the performance of signals after transmission. At every 150 km of transmission, an ROADM was installed to simulate periodic add/drop nodes in this fiber ring network.

4.2.3 Transmission Performances in Ring Network System

Since the pass bands of the ROADM are in Gaussian shapes, Figure 4.7 plots the power penalty variations at BER equals to 10^{-9}, with ± 11GHz frequency detuning,
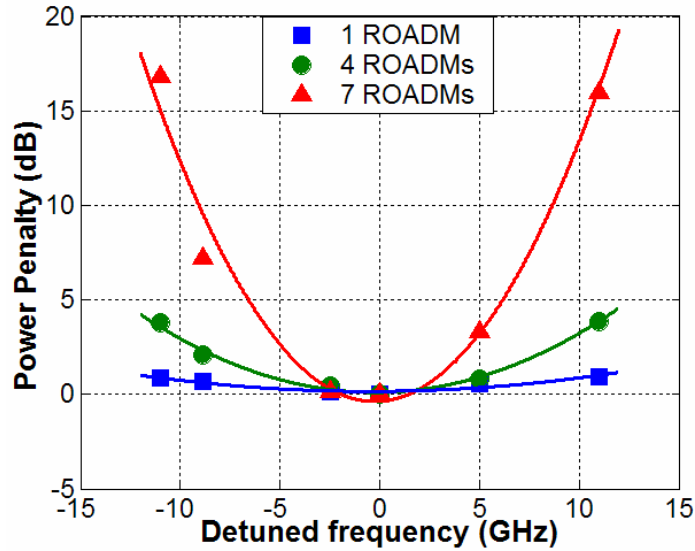
Figure 4.7: Power penalty variation at BER = 10^{-9}, with ±11 GHz frequency detuning, for cascading the ROADM for one, four and seven times.

after different numbers of cascaded ROADMs. This figure reveals power penalty variations of 1 dB, 3.9 dB and 16 dB, which are normalized to the corresponding receiving sensitivities at the ITU grid, following one, four and seven cascaded ROADMs, which correspond to 150, 600, and 1050 km of transmission, respectively. Non-flattened pass-band of the ROADM is responsible for the high sensitivity penalties at the offset frequencies. Optical signals pass through two AWGs at each ROADM, so the cascading filter narrowing effect results in a large penalty if the optical channels are not precisely aligned to the ITU grids. Therefore, a flat-top AWG passband is desirable in future design. Figure 4.8(a) presents the optical spectrum and the receiving sensitivity, measured at BER = 5×10^{-9}, for each of the eight channels after seven cascaded ROADMs and 1050 km of transmission. The sensitivity variations among all channels are less than 2 dB. Since the fully compensated channel was at 192.8 THz in the proposed re-circulating loop, the 2-dB sensitivity variation is caused mostly by the residual chromatic dispersion accumulation after 1050 km of transmission.
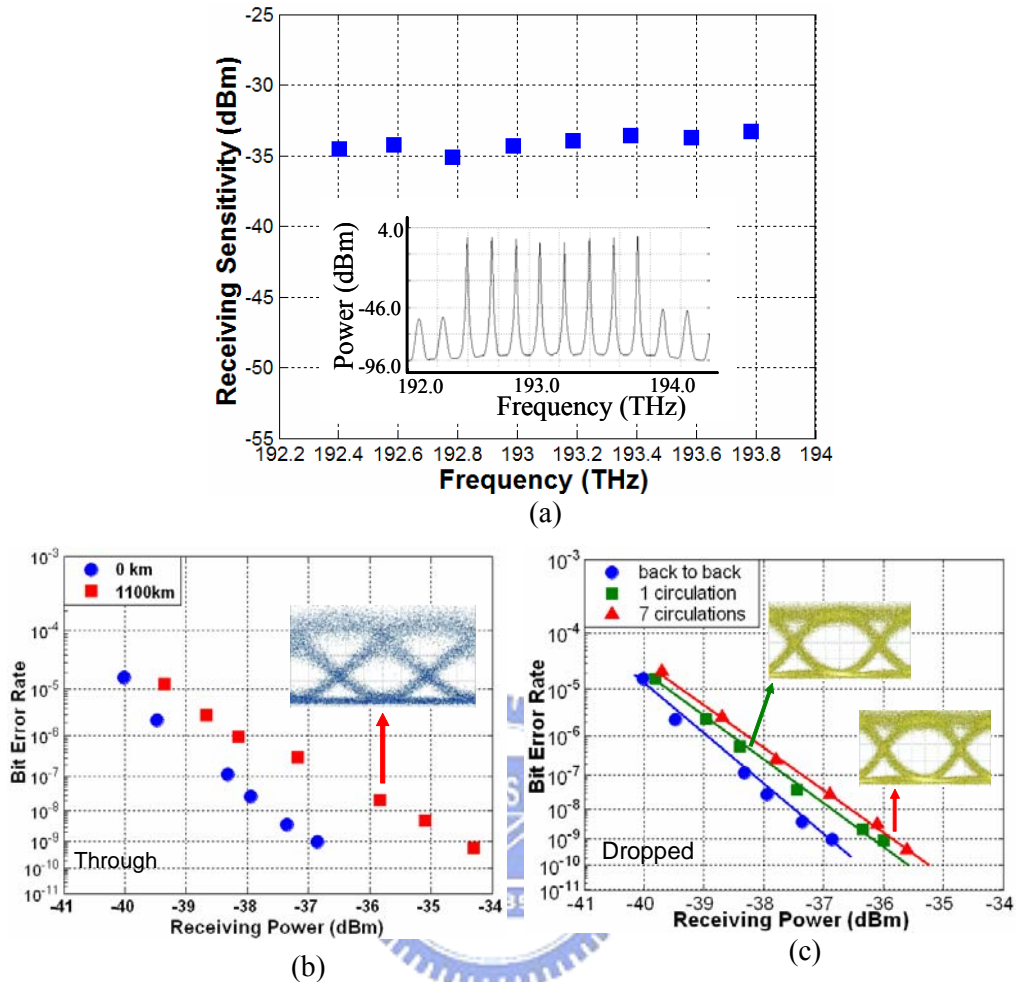
Figure 4.8: (a) Optical spectrum and receiving sensitivity for eight channels, and BER curves and corresponding eye diagrams at channel three for (b) pass-through function after 1050 km of transmission and (c) periodically added/dropped signals at every 150 km.

Figure 4.8(b) plots the BER curves and presents the corresponding eye diagrams at channel three (192.8 THz). BER curves obtained when all of the signals passed through the ROADM were measured. However, the add/drop function of the ROADM was turned off at this time. After seven cascaded ROADMs and 1050 km of transmission, a penalty of about 2.5 dB was observed. The chromatic dispersion is fully compensated for at this channel, so the accumulation of ASE noise from the EDFAs used in the loop are

responsible for most of this penalty. The periodic add/drop function was demonstrated by dropping and adding channel three (192.8 THz), while the remaining seven channels just passed through, at the ROADM in this re-circulating loop, which is identical to a periodic add and drop of channel three at every 150 km in an add/drop ring network. Consequently, after seven circulations, channel three had been added and dropped seven times, whereas the other seven channels had transmitted about 1050 km. Figure 4.8(c) shows the BER measurements and the corresponding eye diagrams at the "drop" port of the ROADM at every 150 km for back-to-back, after one circulation and seven circulations. The optical signal at channel three was refreshed every 150 km, so a very minor penalty, of less than 0.3 dB, between one circulation and seven circulations was observed. This minor penalty is attributable to the tiny wavelength deviation from the ITU grid due to the temperature effect of the optical thermo switches within the ROADM and the accumulation of the residual signals that had been dropped because of imperfect switching isolation. Because this ROADM is designed to cover the C band from 192 THz to 196 THz with 200 GHz channel spacing, this configuration can accommodate more optical channels within C band. The maximum number of channels is 32 with 4 adding and dropped functions simultaneously.

4.2.4 Summary

In this experiment, a periodic add/drop fiber ring network based on a 32-wavelength ROADM, which is a system-on-a-chip network subsystem and offers low loss and crosstalk performance, with a channel spacing of 200 GHz in a recirculating loop is proposed and experimentally demonstrated. The channel narrowing effect, caused by

non-flat-top pass bands, is critical as the number of cascaded ROADM nodes increases. After seven cascaded nodes and transmission for 1050 km through all passing channels, a 2.5-dB sensitivity penalty was observed. Furthermore, less than 0.3-dB penalty variation was obtained between one and seven circulations when one of the eight channels was periodically added and dropped at every 150 km and the remaining seven channels were just passed through. Such results indicate the feasibility of add/drop functions in dynamic fiber ring networks by using this silica-on silicon ROADM.

4.3 Metro Add–Drop Network Applications of Cascaded Dispersion-Compensated Interleaver

In a metro scheme, a pair of interleavers is utilized in add-drop applications to provide up to 50% adding and dropping of the total traffic while simultaneously reducing the insertion loss associated with the express channels. In such an application, the two factors that restrict the maximum number of cascadable nodes are the passbands' flatness (amplitude response) and group delay (phase response) [14, 50, 51]. As the data rate increases, the system becomes more sensitive to the dispersion variations within the signal bandwidth. Accordingly, the flattened phase response is a crucial parameter in determining the usable bandwidth of the passband in 40-Gb/s systems [39], [52].

4.3.1 Characteristics of the Interleaver

The interleaver designed and fabricated in this work is a symmetrical four-port interleaver with two input and two output ports. The details of the interleaver technologies, including principle of operation, architectures and design rules can be
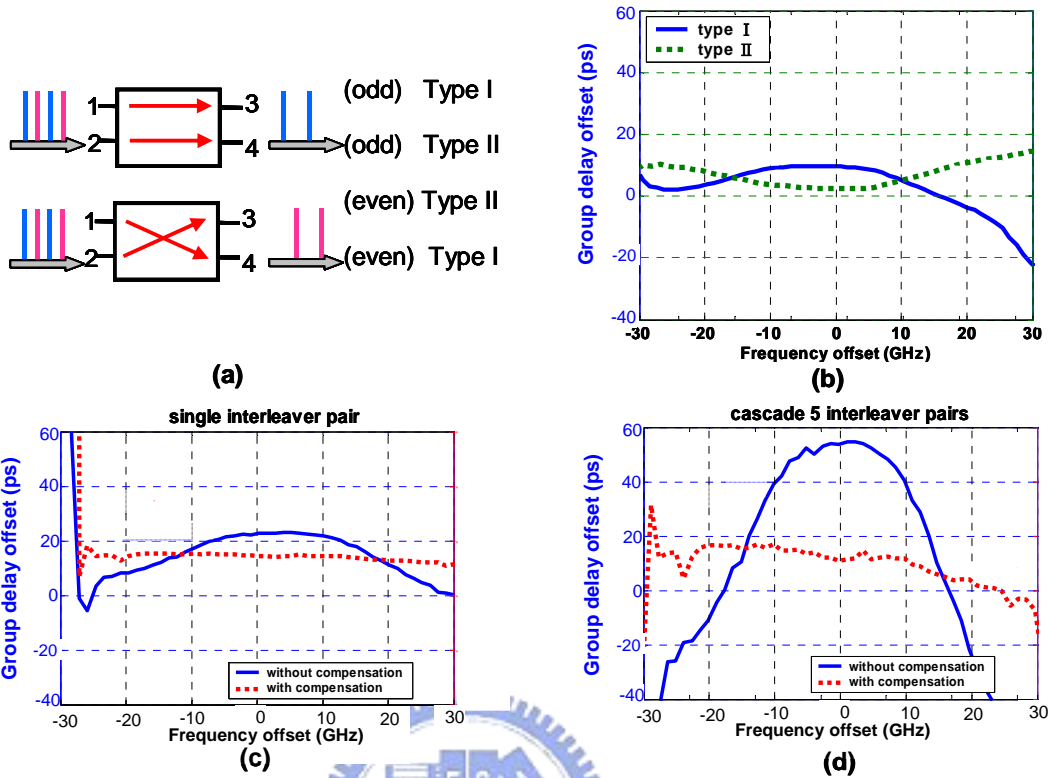
Figure 4.9: (a) Two operation connections for a four-port interleaver; (b) In-band group delays for two types of interleaver connection; (c) group delays of compensated and uncompensated interleaver-pair connections, and (d) group delays of two cases after five cascaded interleaver pairs.

found in Chapter III. Figure 4.9(a) shows two possible connections for such an interleaver. For Type I connection, the odd and even channels experience a convex group delay characteristic, while channels experience a concave group delay for Type II connection. Figure 4.9(b) illustrates the measured corresponding group delay curves for both connections in an interleaver's pass band. These two types of connections with two mirrored group delay can be cascaded to generate a linear phase interleaver pair that the total dispersion would be near zero. Figure 4.9(c) presents the group delay curves for the compensated and uncompensated interleaver pair connections. Clearly, for the compensated connection, the induced in-band dispersion is insignificant. However, when

the interleaver pair is connected without compensation, the dispersion, induced by each individual interleaver, accumulates. If such interleaver pairs are cascaded in a metro add-drop network, the interleaver-induced dispersion aggregates and limits the maximum cascadable nodes. Figure 4.9(d) displays the measured group delay curves accumulated after five cascaded interleaver pairs for the connections with and without dispersion compensation. The experimental results show that the wavelengths should precisely coincide with the ITU grids for the uncompensated case; otherwise significant interleaver induced dispersion accumulates. However, no noticeable interleaver induced dispersion was built up after five adds/drops for the compensated case.

4.3.2 Experimental Setup and Results

To demonstrate the feasibility of cascading interleaver pairs for add/drop application in metro networks, a re-circulating loop was employed to simulate multiple adds/drops in a ring network. Figure 4.10 shows the experimental setup of the re-circulating loop. The eight channel laser sources consisted of two groups: one from 193.2 THz to 193.35 THz and the other from 192.7 THz to 192.85 THz all with 50-GHz channel spacing. The odd and even channels were individually modulated by a $LiNbO_3$ electro-optical modulator at 10 Gb/s with a PRBS length of $2^{31}-1$ patterns. A polarization controller was employed to set the polarization state of the odd channels to be orthogonal to that of the even channels to reduce the deleterious nonlinear effects. Two types of fiber were used in the re-circulating loop: 100-km of Corning LEAF fiber and 4.8-km of Corning DCF, with -86.6231 ps/nm/km dispersion at 193.0 THz, to compensate the accumulated chromatic dispersion in LEAF fiber. The fully-compensated wavelength of this fiber loop was

38
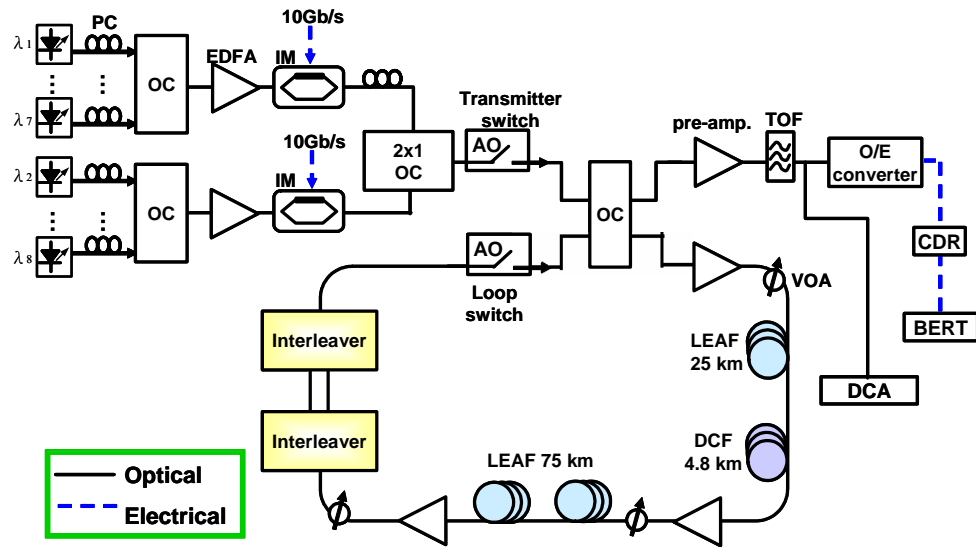
Figure 4.10: Experimental setup for metro add/drop applications

located at around 193.15 THz. After 105 km of fiber, the interleaver pair was inserted in

the fiber loop to simulate optical channel add-drop at every 105 km. A 3R receiver of

-33 dBm back-to-back sensitivity at BER equals to 10^{-9} was applied to obtain the signal's

performance after transmission. Figure 4.11(a) compares the receiving sensitivity at BER

level around 10^{-9} of each channel after five loops, i.e., 525 km of transmission and five

add-drop nodes, for both compensated and uncompensated cases. Since the two groups of

channels were deliberately selected to locate at the wavelength regions with opposite sign

of dispersion: one group with negative dispersion, and the other one with positive

dispersion, the experimental results for both cases indicate that the receiving sensitivities

of eight-channels exhibit a parabolic distribution centered at dispersion-zero wavelength.

The sensitivity difference for each channel is insignificant between the two cases because,

as the channel wavelengths are set at the center of the interleaver's pass band precisely,

very little dispersion is introduced by the interleaver, even for the uncompensated case.
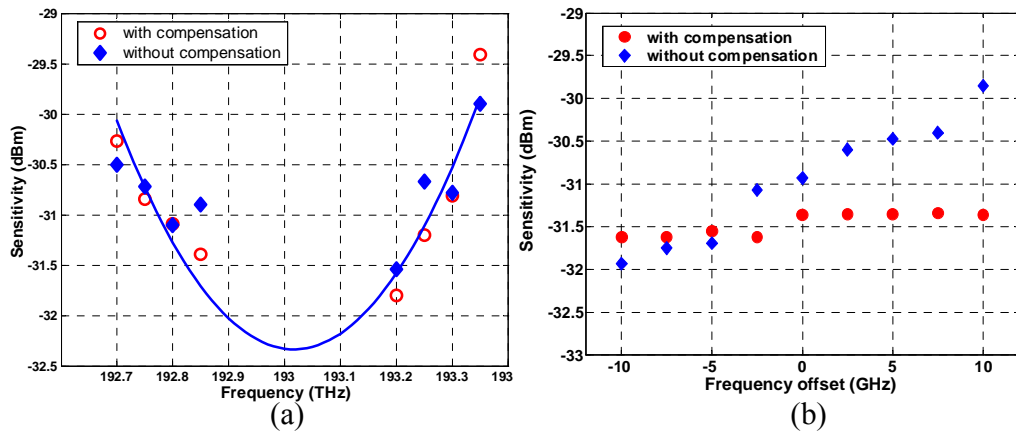
Figure 4.11: Receiving sensitivity variation. (a) compensated and uncompensated cases after five cascaded interleaver pairs, and (b) compensated and uncompensated configuration with ± 10 GHz wavelength detuning at BER = 10^{-9}

Thus the parabolic sensitivity distribution of the eight-channels for both cases mainly results from the residual dispersion accumulation after 525 km. Figure 4.11(b) compares the receiver sensitivity variations, with ±10GHz wavelength detuning, of the compensated and uncompensated configurations. This figure indicates that less than 0.4-dB sensitivity variation is observed within ±10GHz wavelength detuning for the compensated connection, while more than 2.5-dB sensitive variation is perceived for the uncompensated case at BER = 10^{-9}. Figure 4.12 shows the BER curves and the corresponding eye diagrams when the wavelength is either on the ITU grid or detuned from the ITU wavelength by ± 8 GHz at channel five. Both the eye diagrams and the BER curves indicate that the accumulated dispersion in the uncompensated connection will lead to pulse distortion and BER penalty. Figure 4.12 (a) showed that the sensitivity was improved more than 2.5 dB when the wavelength detuned ± 8 GHz from the center wavelength. It is because the dispersion from transmission fiber and the interleaver pairs would be opposite as the ITU wavelength detuned by − 8 GHz. In other words, the total dispersion decreased in this case. However, pulse distortion was shown when the

wavelength detuned +8 GHz. Conversely, if the interleaver pair is in the dispersion compensation connection, wavelength detuning up to ± 8 GHz does not introduce much sensitivity variation. Consequently, the dispersion compensated connection is less sensitive than uncompensated one to the wavelength deviation from ITU grids.
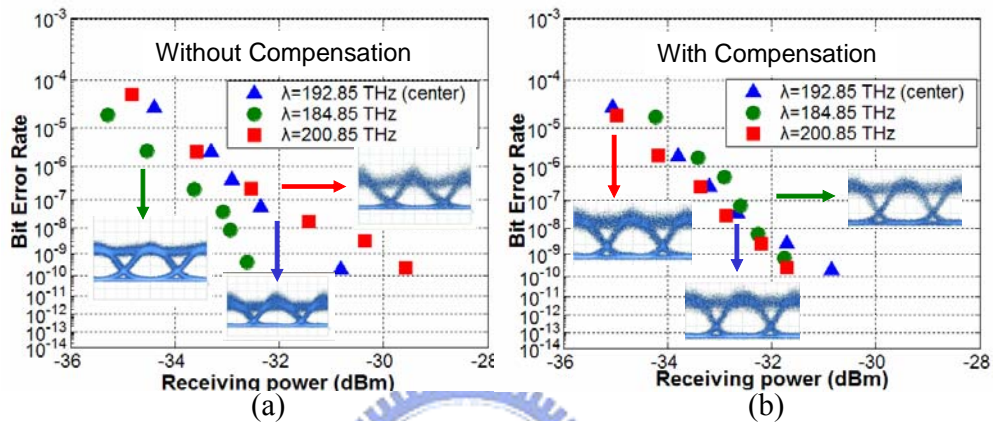
Figure 4.12: BER curves and corresponding eye diagrams at channel five when wavelength is detuned for ± 8 GHz (a) without compensation and (b) with compensation.

4.3.3 Summary

This investigation presents a cascadability study of a 50-GHz channel spacing dispersion-compensated interleaver pair using a re-circulating loop. After five cascaded nodes and 525 km of transmission, the interleaver-induced dispersion did not significantly degrade the system performance when wavelengths were exactly aligned to ITU grids. However, when the wavelength deviated from ITU grids, the sensitivity variation of the compensated case was much less than that of the uncompensated pair. Experimental results show that, with ± 10 GHz wavelength detuning, the sensitivity variations of these two configurations are less than 0.4 dB and more than 2.5 dB, for

compensated and uncompensated cases, respectively. Such results can lessen the

precision requirements in selecting DFB lasers for Metro add/drop network applications.

CHAPTER 5

NOVEL BIDIRECTIONAL TRANSMISSION U SING FOUR-PORT INTERLEAVER

In metro area networks (MAN) that encounter fiber shortages problems, bidirectional transmission is an appealing means of increasing the bandwidth utilization in a single-optical fiber and, at the same time, reducing the operation and maintenance cost. One of the main difficulties associated with a bidirectional transmission system is realizing bidirectional amplification, which typically requires high gain, low noise, and the elimination of Rayleigh backscattering (RB) [7]. The gains of EDFAs are typically limited to prevent RB-induced self-oscillation. In the LOA scheme [9], the characteristics of the gain-clamping effect limit the gain of LOA to less than 20 dB and a high NF is inevitable. These shortcomings significantly reduce the distance of amplification span and the OSNR [23], increasing the operation cost and the degradation in the quality of transmission. A four-port interleaver has been proposed before [24] using fiber-based configuration. The device is sensitive to temperature variation and exhibiting Gaussian passband characteristics. Through minor modification of the original three-port design in chapter III, a novel four-port interleaver that enables bidirectional transmission using unidirectional amplification was demonstrated. In this chapter, the novel four-port interleaver and three bidirectional transmission experiments would be discussed and demonstrated.

5.1 Characteristics of Four-Port Interleaver

The interleaver used in this study is a symmetrical four-port interleaver with two input and two output ports. The packaged interleaver I used in the lab is displayed in Figure 5.1(a). The size of this interleaver is 15 cm $\times$ 2 cm. The detail configuration of this four-port interleaver illustrates in Figure 5.1(b). It incorporates birefringent crystal cells, half-wave plates (HWP), YVO_4 walk-off crystal (YWC), and polarization beam splitters (PBS). At the input and outputs of interleaver, YWC and an HWP were used to ensure that light passed through optical delay cells, including two birefringent crystals, was polarized in only one direction. Each delay cell includes two birefringent crystals, namely YVO_4 and rutile (TiO_2), to compensate for any change in temperature. The detailed operating principles, architectures, and design rules associated with this interleaver are presented in [39, 52, 53].

(a)

(b)

PBS: Polarization beam splitter ; YWC: YVO_4 walk off crystal ; HWP: Half wave plate
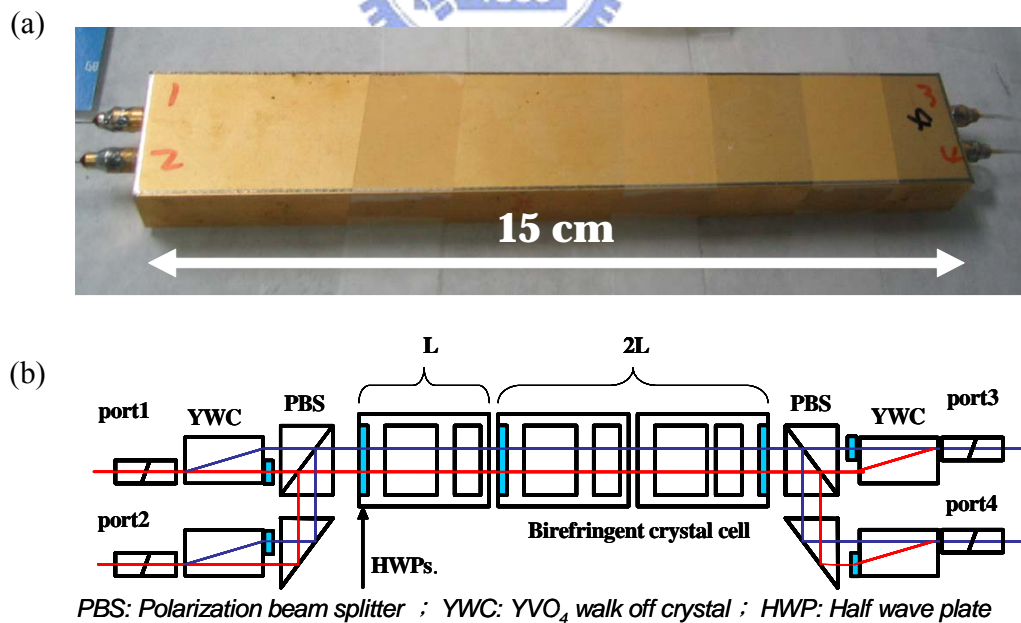
Figure 5.1: (a) Picture of the four-port interleaver; (b) Detail configuration of four-port L-2L interleaver.

44

In optical networks, one of important issues is polarization. The polarization dependence of the transmission properties of optical components has many sources, such as dichroism, fiber bending, angled optical interfaces and oblique reflection. The polarization state through one component is generally not the same as other components in the transmission link. Sine polarization dependent loss (PDL) effects build up in an uncontrolled manner; PDL can lead to a degradation of the transmission quality of the fiber-optic link, or even to a failure of the optical system. Therefore, modern fiber-optic communication systems require components with low PDL. Figure 5.2 shows the PDL measurement results of the four-port interleaver. The PDL at all the ITU channels in *C*-band can be measured by using a JDSU swept wavelength system. The PDL is defined as the maximum PDL within the bandwidth of ITU ± 12 GHz. This figure shows that the PDL of this four-port interleaver for all channels was less than 0.12 dB. This is a typical number for most of the optical devices used in current transmission system.
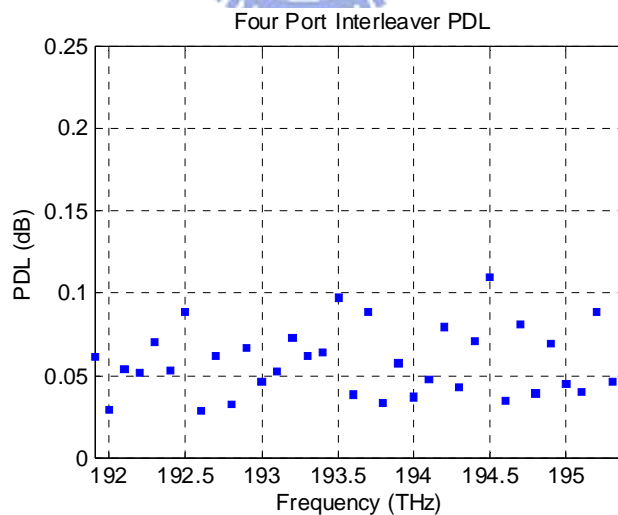
Figure 5.2: Measured PDL for the four-port interleaver.

Figure 5.3(a) and (b) illustrates the measured amplitude response of the interleaver for even and odd channels. It can bee seen clearly, the transmission spectrum of this interleaver covers the whole *C*-band from 193.8 to 195.4 THz. Figure 5.3(b) shows the amplitude response within 2-nm wavelength range. The channel spacing of this interleaver was 50 GHz, with insertion loss of 2.2 dB and a 0.5-dB passband of approximately 35 GHz, respectively. The interleaver was designed to have complementary wavelength dependent routing characteristics. For example, if λ_1 (odd channel) enters port 1, it is routed to port 4. However, when λ_2 (even channel) goes into port 2, it is also directed to port 4. By using this interleaver property, when east-even channels arrive at port 2 of the interleaver, they are sent to port 4.
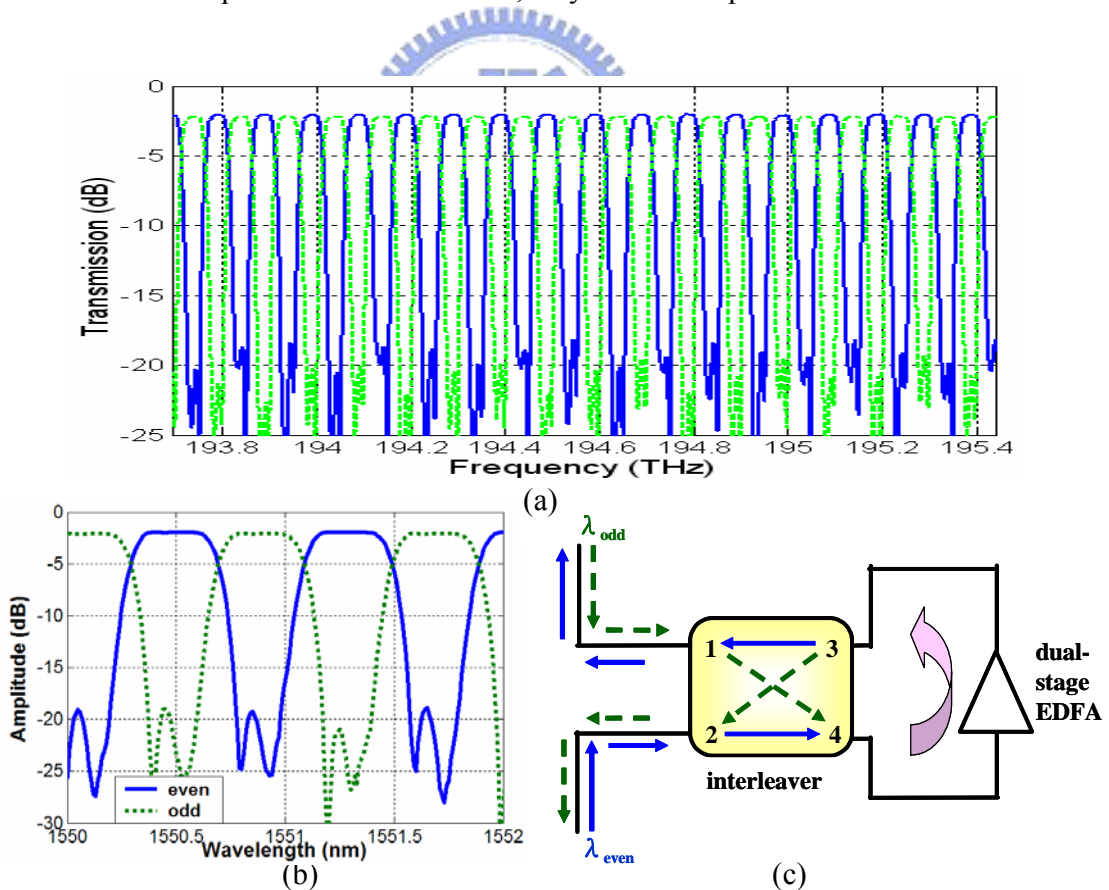
Figure 5.3: Transmission Spectrum of a four-port interleaver: (a) the whole *C*-band, (b) 2-nm wavelength range, and (c) illustration of working principle of a four-port interleaver.

On the other hand, when the west-odd channels enter port 1 of the interleaver, they are also routed to port 4. Therefore, a bidirectional transmission is routed into a unidirectional transmission and unidirectional amplification is achieved using a single EDFA, as shown in Figure 5.3(c).

5.2 Straight Line Bidirectional Transmission System

A new wavelength-sensitive routing experiment was conducted to confirm bidirectional transmission in unidirectional amplification using the proposed four-port interleaver. Figure 5.4 presents the experimental setup [54]. A dual-stage EDFA with a dispersion compensation module was employed in the midstage to compensate for the fiber loss and accumulated dispersion. The eight-channel laser sources are grouped into two categories, one with wavelengths between 1550.52 and 1551.72 nm and the other with wavelengths between 1554.54 and 1555.75 nm, all on standard ITU 50-GHz channel spacing grids. The east-even and west-odd channels were individually modulated by a LiNbO$_3$ EO modulator at 10 Gb/s with a 2^{31}-1 pseudorandom bit sequence pattern.
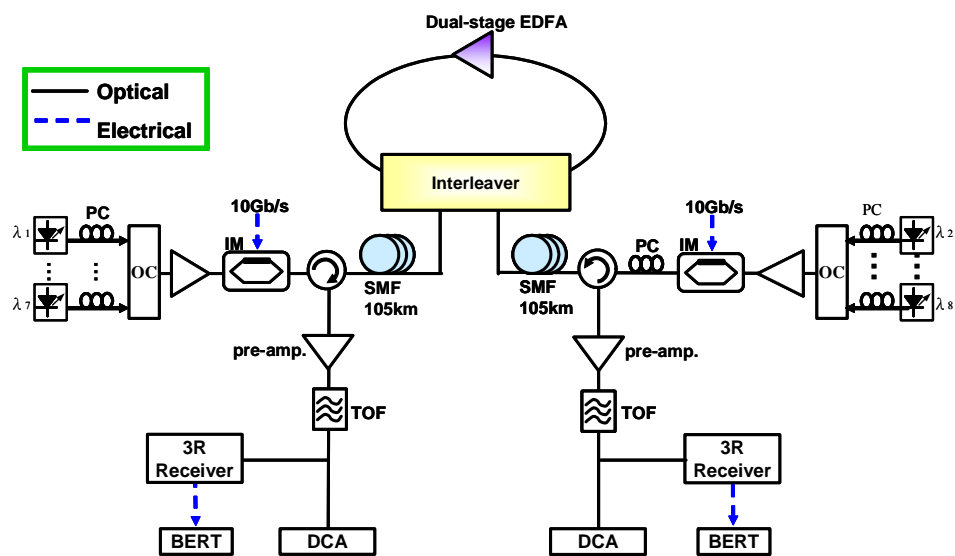
Figure 5.4: Experimental setup of a straight line bidirectional transmission system.

A polarization controller was used on the east-to-west traffic to ensure that the power between east-even and west-odd channels were maximum to reduce the crosstalk induced by the opposite traffics. The transmission fiber was 210 km of standard single-mode fibers (SSMF), with 13-dBm total launched power into each 105 km of SSMF. The 36 km of DCF was inserted in the dual-stage EDFA to compensate for the accumulated chromatic dispersion. A 3R receiver with a back-to-back sensitivity of 32 dBm at a BER of 10^{-9} was used to evaluate the system performance. The gains and NF of the dual-stage EDFA in all channels were around 23 dB and 5.5 dB, respectively.

5.2.1 System Performances on Straight Line Transmission

Figure 5.5(a) plots the BER curves and the corresponding eye diagrams at channel six. After transmission for 210 km, both the eye diagrams and the BER curves indicate that performance degradations caused by the accumulated ASE noise in the bidirectional and unidirectional transmission systems. Figure 5.5(b) presents the power penalties of all channels and compares them with the back-to-back results.
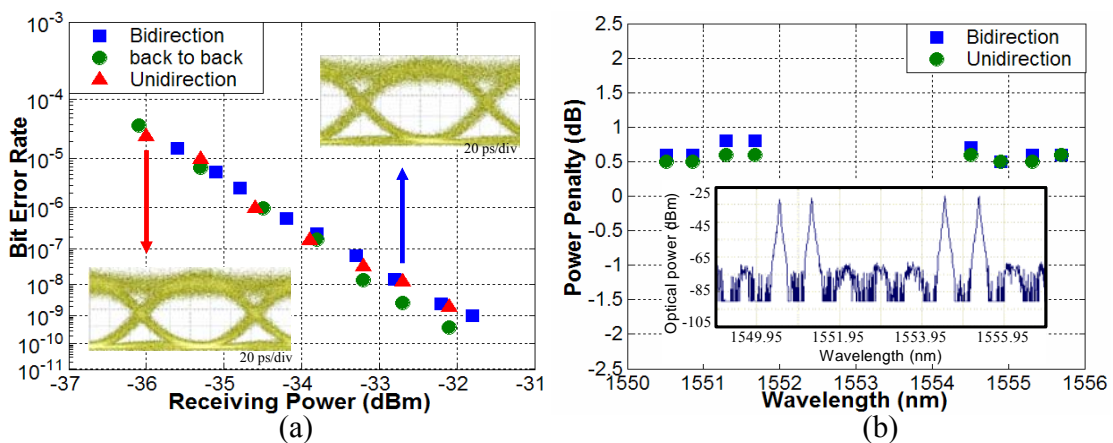
Figure 5.5: (a) BER curves and corresponding eye diagrams of the worse channel for unidirectional and bidirectional transmission. (b) Power penalty of bidirectional and unidirectional transmission and received optical spectrum for east-even channels after 210 km bidirectional transmission.

This figure clearly reads that the differences between the power penalty of the bidirectional and unidirectional transmissions were less than 0.2 dB in all channels. A comparison with back-to-back BER curves shows that the sensitivity penalties are less than 1 dB in both cases. The inset figure within Figure 5.5(b) is the received optical spectrum of the east-even channels (λ= 1550.92, 1551.72, 1554.94 and 1555.74 nm) after 210 km of transmission. It has been pointed out previously that the additive noise associated with RB limits the maximum gain of a linear amplifier with no isolator to around 19 dB [7]. Figure 5.5(b) reveals that RB can be ignored in this new proposed configuration. Moreover, an OSNR over 35 dB was achieved after 210 km of transmission in all channels due to the unidirectional, instead of bidirectional, amplification for the opposite transmission traffics. A residual crosstalk of 17 and 20 dB on the even and odd channels, respectively, as shown in Figure 5.3(a), was observed when the co-propagating channels were interleaved into bidirectional transmissions after amplification. The residual signals on the even/odd channels propagate in the opposite direction of the even/odd channels due to the rerouting characteristics of the interleaver, which will not interfere with the performance on both east-even and west-odd channels. In addition, the residual signals will also be blocked by the isolator, within the dual-stage EDFA, in the next amplification stage because of the rerouting nature by the interleaver. Therefore, a much longer distance and multiple spans transmission are achievable.

5.3 Long Distance Transmission Using a Bidirectional Re-circulating Loop

In order to simulate long distance transmission, a re-circulating loop had been set up as Figure 5.6 [55]. One of bidirectional loop has been proposed in Ref. [6]. However,
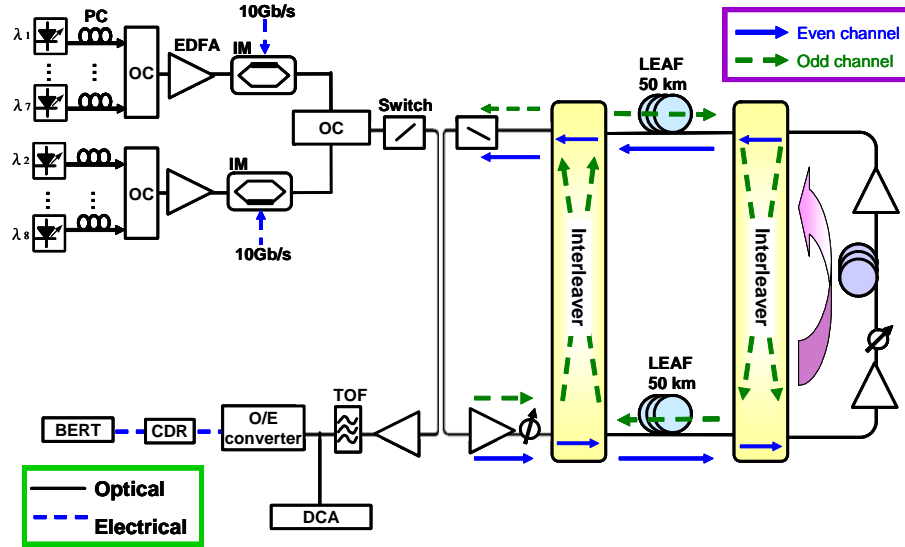
Figure 5.6: The recirculating loop setup for long distance bidirectional transmission experiment.

they need a dead zone in wavelength channels to prevent crosstalk in blue-red band splitting. Based on the new amplification scheme, no dead zone in allocated wavelengths is need in our re-circulating loop experiment. The same laser sources, as the setup in Figure 5.4, had been used in this configuration. Both eastbound and westbound traffic is driven by LiNbO$_3$ modulator with 10 Gb/s per channel and PRBS at 2^{31}-1. An interleaver was placed at the input of the re-circulating loop to split the east and west channels for bidirectional transmission and oppositely directed traffic was combined for unidirectional amplification. Two spools of 50-km Corning LEAF fiber were adopted in the re-circulating loop. A dual-stage EDFA with 5 km of Corning DCF was employed in the mid-stage of the loop to compensate for the transmission loss and accumulated dispersion in the LEAF fiber. The fully compensated wavelength of this fiber loop was located at approximately 1553.2 nm. The two interleavers in the loop were specially arranged to reduce chromatic dispersion caused by the flat-top transmission band design of the

interleaver [53]. A 3R receiver with a 32.5-dBm sensitivity at BER of was utilized to evaluate the quality of transmission.

5.3.1 System Performances on Loop Transmission

Figure 5.7(a) displays the received optical spectrum after 500 km with an OSNR of over 31 dB for all channels with a 0.02-nm resolution bandwidth on the optical spectrum analyzer. The configuration effectively blocks the RB using only one amplification section for two traffic directions. Figure 5.7(b) shows that the receiving power penalties of BER equals to 10^{-9} at all channels. All channels had power penalties of less than 2.5 dB and the penalty differential between them was less than 0.36 dB. Figure 5.7(c) plots the BER curves and the corresponding eye diagrams at channel seven, for back-to-back, 100 km, 300 km and 500 km transmissions. The measured power penalties were about 0.3 dB, 1 dB and 2 dB for 100, 300 and 500 km transmissions, respectively, at a BER of 10^{-9} under optimal polarization conditions. The polarization controller was used to minimize the polarization effects, such as polarization dependent gain (PDG) and PDL, in the recirculating loop. The penalties were attributed to ASE accumulation due to the SNR degradation results from high link loss between the amplifier span. Since in a recirculating loop experiment, if the optical data pattern length time is longer than the sampling window used to take the BER measurement, then pattern-dependent errors arise from time to time [56]. An accumulated error measurement can verify the stability and ensure that the proper sampling window is utilized in the recirculating loop experiment. The error counts accumulate almost continuously when the sampling window in the system is kept accurate [11]. Otherwise, the accumulated errors would be missed for long

periods, and then would be over-sampled for certain periods. Figure 5.7(d) plots the measured accumulated errors as a function of time (ten intervals) at a BER of 2.46×10^{-9} after 100 km and 500 km. This figure demonstrates the robustness in the transmission system for BER measurement.
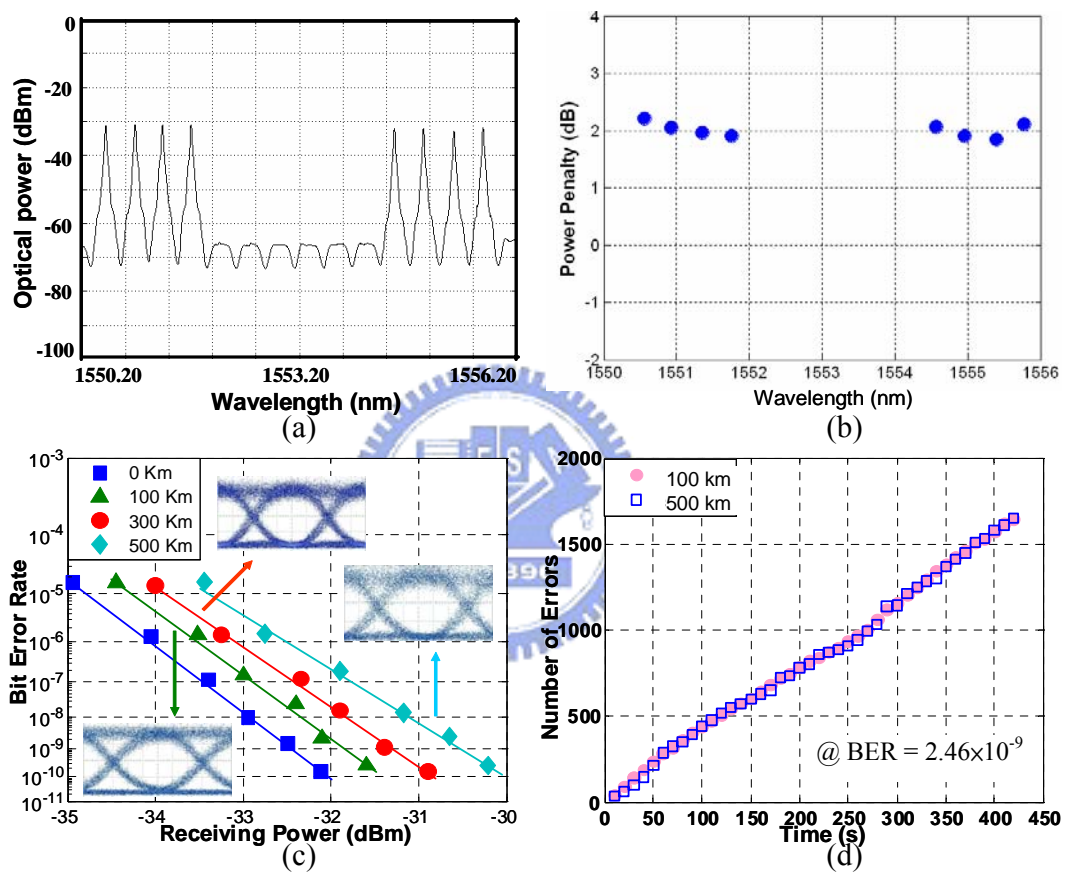
Figure 5.7: (a) Received optical spectrum; (b) received power penalties at BER equals to 10^{-9} of all channels after 500 km; (c) BER curves and corresponding eye diagrams at channel seven after transmission, and (d) accumulated errors measured as a function of time.

5.4 Comparison between Bidirectional DPSK and OOK Signals

In the previous work, the OOK modulation has been used in this bidirectional transmission system. However, there are lots of different modulation formats such as

DPSK and differential quaternary phase shift keying (DQPSK). In this section, the performance of RZ-DPSK would be compared experimentally with NRZ-DPSK and OOK modulation formats.

5.4.1 Bidirectional DPSK Transmission Configuration

The experimental setup for bi-directional DPSK transmission is shown in Figure 5.8. Eight distributed feedback (DFB) lasers producing continuous-wave lightwaves equally spaced by 50 GHz from 1556.56 nm to 1559.39 nm, all on standard ITU grid, were combined by an a multiplexer (MUX) and simultaneously modulated by a phase modulator (PM). The PM was driven by a 10 Gb/s electrical data with a PRBS with a sequence length of 2^{31}-1 to generate DPSK signals. The polarization controllers (PC) are attached to each DFB laser to achieve maximum output power and reduce the deleterious nonlinear effects. The transmission fiber was 230-km SSMF, with 3 dBm total launched power into each 115-km SSMF. The matched DCF were adopted in the configuration to compensate accumulated dispersion in the SSMF. A dual-stage EDFA, with a 24.45-dB
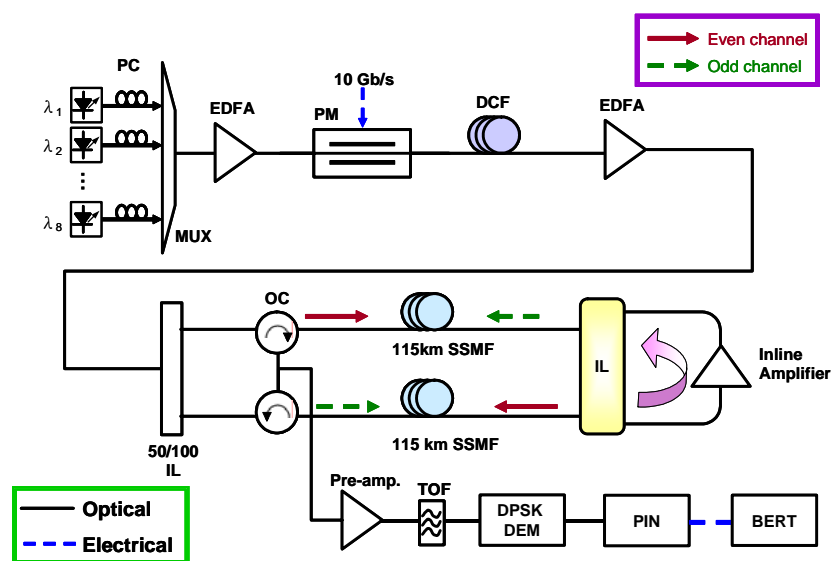
Figure 5.8: Bidirectional DPSK transmission experimental setup.

gain, was employed as the inline amplifier to compensate the transmission loss.

5.4.2 Results of Bidirectional DPSK Transmission

Figure 5.9(a) shows the BER curves and corresponding eye diagrams for three of eight RZ-DPSK signals as channel 1 (λ=1556.55 nm), 4 (λ=1557.77 nm) and 8 (λ=1559.39 nm). It can be seen that the penalty at a BER of 10^{-9} for channel 8 (λ=1559.39 nm) was less than 1.1 dB and the clear eye indicates the good quality of the signals after 230-km fiber. Figure 5.9(b) compares the RZ-DPSK and NRZ-DPSK modulation performance after 230 km at channel 4 (λ=1557.77 nm). RZ-DPSK signals improve a 2-dB penalty than NRZ-DPSK.
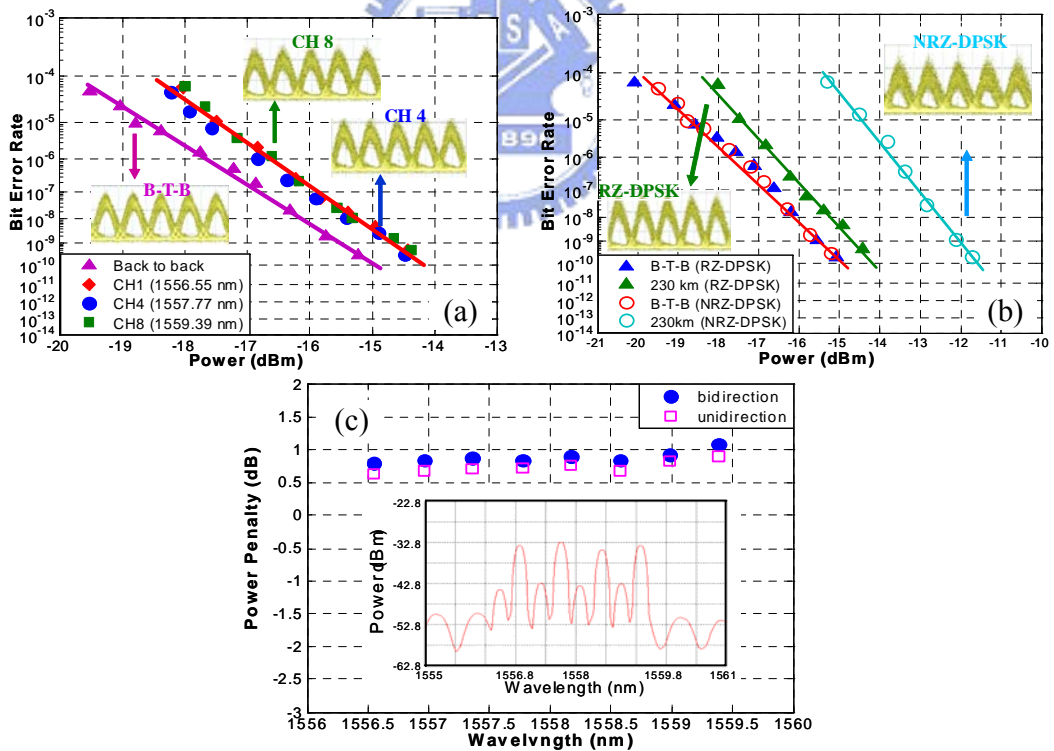
Figure 5.9: BER curves and corresponding eye diagrams of (a) RZ-DKSP at channel 1, 4, and 8, (b) comparison of RZ and NRZ-DPSK at channel 4, and (c) received power penalties for all channels for bi- and unidirectional transmission at BER = 10^{-9} and output optical spectrum of bidirectional RZ-DPSK transmission after 230 km for even channels.

It results from RZ-DPSK has a data-independent intensity profile and completely removes the pattern effects in the nonlinear fiber. Figure 5.9 (c) presents the power penalties for all channels and compares them with back to back results at BER = 10^{-9}. The inserted figure in Figure 5.9 (c) is the received optical spectrum of 230 km bidirectional RZ-DPSK transmission for even channels with a 0.2-nm resolution bandwidth on the optical spectrum analyzer. This figure clearly indicates that the power penalties for all channels are less than 1.1 dB and the differential between bidirection and unidirection are less than 0.2 dB. These power penalties are attributed to residual dispersion and ASE accumulation due to SNR degradation results from high link loss. These experimental results establish the feasibility of the bi-directional DPSK transmission using this four port interleaver to enable unidirectional amplification.

In order to compare the performance of different inline amplifiers in this bidirectional configuration, a SOA was employed to supersede the dual-stage EDFA. In contrast with [26], only one common SOA has been exercised to realize bi-directional transmission. Due to the gain limitation of SOA, an 80-km SSMF and the matching DCF were used in the transmission system. The SOA has a saturated power of 11 dBm, and it provides a gain of 14.3 dB to each wavelength channel. For comparison, an intensity modulator had replaced the phase modulator in our system in order to obtain OOK modulated signals, DPSK demodulator was removed at the receiver, and all other conditions were maintained. The measured BER curves and typical eye diagrams of channel 4 (λ =1557.77 nm) with RZ-DPSK, NRZ-DPSK and OOK modulation formats are depicted in Fig. 5.10. The power penalties of RZ-DPSK and OOK signals were about 0.2 dB and 1.6 dB, respectively. In this figure, the eye diagram of OOK signals was
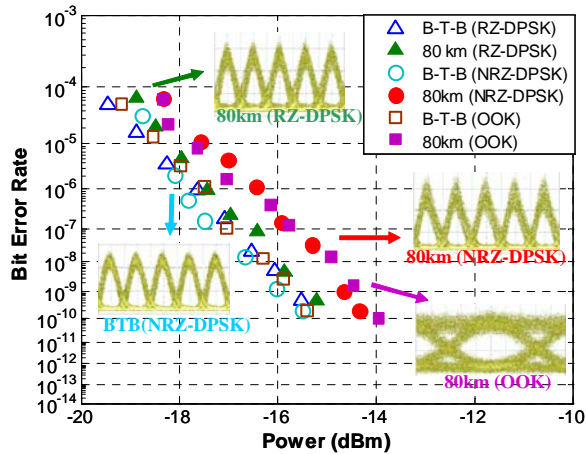
Figure 5.10: BER curves and corresponding eye diagrams after 80 km transmission by using a SOA as inline amplifier.

distorted. It is probably resulted from the pattern-dependent effect caused by the gain saturation and the cross-talk induced by XGM between WDM channels in the SOA.

5.5 Bidirectional Transmission 8×40 Gbit/s WDM Signals

Based on the experimental configuration of Figure 5.8, a 40-Gb/s transmission has been tested. A Mach-Zehnder intensity modulator was employed to supersede the phase modulator and driven by 40-Gb/s electrical signals. The 40-Gb/s electrical signals were generated by using a 4:1 electrical multiplexer with multiplexing four 10-Gb/s channels. The PRBS electrical signals at 10 Gb/s was 2^7-1. Two spoons of 103-km SSMF was used with total launched power into each spoon is 1.5 dBm. The SSMF has a dispersion of 17 ps/nm/km and a loss of 0.2 dB/km. The matched DCF was adopted in the configuration to compensate the accumulated dispersion in the transmission SSMF. After 206-km transmission, the 40-Gb/s electrical signals were demultiplexed into four-channels at 10 Gb/s before the BER measurement. Figure 5.11 exhibits the experimental results after 40-Gb/s WDM signals bidirectional transmission over 206 km.
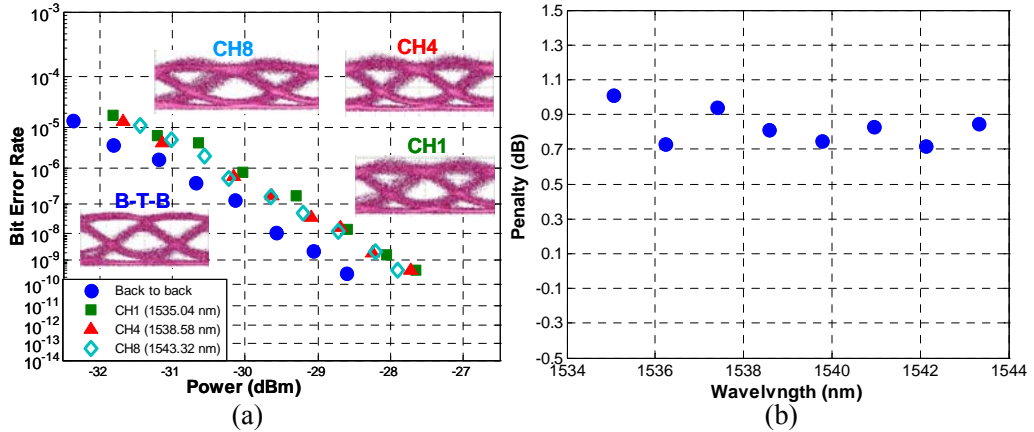
Figure 5.11: Experimental results. (a) BER curves and corresponding eye diagrams of Back-to-Back, ch1, ch4 and ch8 without transmission fiber and DCF; (b) received penalties at a BER of 10^{-9} of all channels.

Figure 5.11(a) is the BER curves and some typical eye diagrams of channel 1 at 1535.04 nm, 4 at 1538.58 nm and 8 at 1543.32 nm with and without transmission fiber and DCF (Back-to-Back). After bidirectional transmission over 206 km SSMF, the eye diagrams and the BER curves for all bidirectional transmission signals at different wavelength are identical. The power penalties at a BER of 10^{-9} for channel 1 (λ=1535.04 nm), 4 (λ=1538.58 nm) and 8 (λ=1543.32 nm) are 1, 0.8 and 0.8 dB, respectively. The clear eye indicates the good quality of the signals after transmission. Figure 5.11(b) presents the power penalties for all channels at a BER of 10^{-9}. The power penalty and penalty differentials of all channels are less than 1.1 dB and 0.4 dB, respectively. These power penalties are mainly caused by the OSNR degradation resulting in the large insertion loss of the transmission fiber. The experimental results establish the feasibility of bidirectional transmission high bit rate signals in this scheme.

5.6 Summary

This novel amplification scheme had been experimentally demonstrated in both straight line and recirculating loop transmission over 210 and 500 km with sensitivity penalty less than 0.8 and 2.5 dB, respectively. For comparison, 10-Gb/s DPSK signals were also transmitted over 230 km. In this bidirectional configuration, RZ-DPSK signals, with 1.1-dB sensitivity penalty, improved a 2-dB penalty than NRZ-DPSK. Furthermore, it has advantageous to use RZ-DPSK with dual-stage EDFA over SOA and other modulation formats in fiber-optics transmission. Not only 10-Gb/s signals, but 40-Gb/s data over 206-km SSMF had been demonstrated in this scheme. These experimental results establish the feasibility of the bidirectional transmission using the new four-port interleaver. Because the interleaver is designed to cover the whole *C*-band (i.e., 1525–1565 nm), the configurations we proposed can accommodate more optical channels within *C*-band, e.g., 16 or 32 channels. Nonetheless, due to the material dispersion of the birefringent crystal, the current design cannot cover both *C*-band and *L*-band at the same time. Therefore, it will need two types of interleavers, each with different lengths of the birefringent crystal cell, to achieve the task under the same configuration. In analyzing device performance, we also validated that the proposed interleaver design is capable of achieving DWDM spectral-efficient and crosstalk-tolerant signal transport for high capacity, bidirectional transmission systems.

CHAPTER 6

WAVELENGTH-DIVISION MULTIPLEXING PASSIVE OPTICAL NETWORKS

The current bottleneck for high data rate services from the service providers (or core network) to end users is believed to be in the access network. Fiber-to-the-home (FTTH) using passive optical networks (PONs) technology is considered an ultimate solution to meet ever increasing bandwidth requirements as well as provide Quadruple Play Services (QPS) in future access networks [57]. Network carriers have begun to deploy time-division-multiplexing passive optical networks (TDM-PONs) such as broadband PON (BPON), Ethernet PON (EPON) and Gigabit PON (GPON) in response to the current trend of data- and image-based services resulting from the rapid growth of all kinds of multimedia Internet applications [58] as shown in Figure 6.1. However, guaranteed bandwidth and quality of service (QoS) provided by these PONs might not be enough to satisfy the extensive bandwidth requirements of future video-centric services
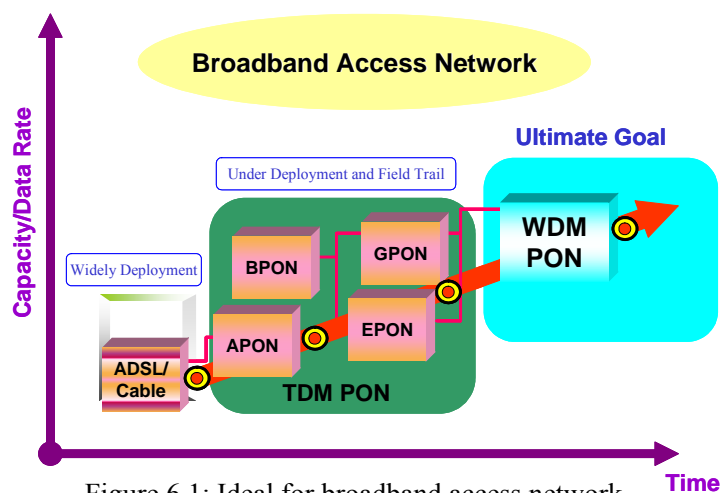
Figure 6.1: Ideal for broadband access network.

with high-definition TV (HDTV) quality, and thus present wavelength-division multiplexing passive optical networks (WDM-PON) should be upgraded in the near future. In this chapter, general architecture for WDM-PON system and three experiments would be discussed and demonstrated.

6.1 General Architecture for WDM-PON

Next generation optical access networks will need to provide broadband service to cater different customer needs, e.g. voice, video and internet access. PON have evolved to provide much higher bandwidth in the access network. However, there exists the need for further increasing the bandwidth of PON by employing WDM so that multiple wavelengths can be used in either upstream or downstream direction. Such a PON is known as WDM-PON, promising approach for gigabit optical access network [16, 59]. WDM-PON is a general purpose and extremely efficient future-proof optical transport technology for use in Access and Metro transport networks. It enables highly efficient use of the outside fiber plant by providing point-to-point optical connectivity to multiple remote locations through a single feeder fiber. Figure 6.2 illustrates the general architecture for a WDM-PON. As can be seen in the figure, this general-purpose architecture can serve multiple applications for both the business and residential customer such as fiber-to-the-home (FTTH) and fiber-to-the-building (FTTB). This functionality is possible since each end point is connected to the central office (CO) through a dedicated optical channel. This virtual point-to-point PON architecture enables large guaranteed bandwidths, bit rate independency, graceful upgradeability, high QoS and excellent security and privacy. The WDM-PON technique has the following advantages:

1) Large guaranteed bandwidth to support multiples services.

2) Point-to-point dedicated connectivity.

3) High security and privacy.

4) No need for dynamic range and signal equalization.

5) No need for high bit rate, expensive burst mode receiver in CO/OLT.

6) Compatible with DWDM Metro optical network for high bandwidth, symmetric, and end-to-end services.
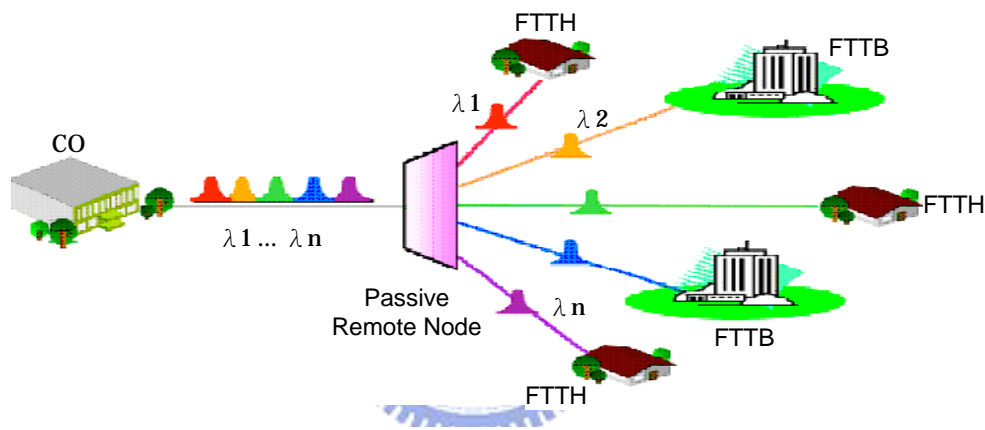
Figure 6.2: General architecture for a WDM-PON.

6.2 Cost-Effective Bidirectional WDM-PON Architecture

Many architectures incorporate WDM into access network have been proposed [16, 59, 60]. However, an amplification scheme of WDM-PON is required in a cost-effective manner to cover wider bandwidth and provide more power margin, especially in the form of single amplifier to support gain for bi-directional traffic at the same time. LOA had been proposed as a candidate for bidirectional amplifier [61]. However, LOA suffers smaller gain and larger cross-talk caused by cross gain modulation compared with

conventional EDFAs. Here a cost-effective bidirectional WDM-PON system using the four-port interleaver has been proposed.

6.2.1 Bidirectional WDM-PON Configuration Using Unidirectional Amplification Scheme

With our innovative interleaving configuration, only one unidirectional EDFA can be used to realize bidirectional signal amplification. The proposed bi-directional amplification WDM-PON scheme is shown in Figure 6.3 [62]. Our optical line terminal (OLT) design consists of N DFB laser sources. The downstream signals are generated in the C band with one DFB laser per user at the CO. They are multiplexed at CO and demultiplexed at the remote node to be distributed to the corresponding optical network unit (ONU). The novel bidirectional amplifier is located at the CO side to amplify both upstream data and downstream traffic simultaneously. The experimental setup for bidirectional WDM-PON is shown in Figure 6.4. Sixteen DFB lasers equally ITU 50-GHz channel spacing grids, were combined by an optical multiplexer (MUX). Due to the
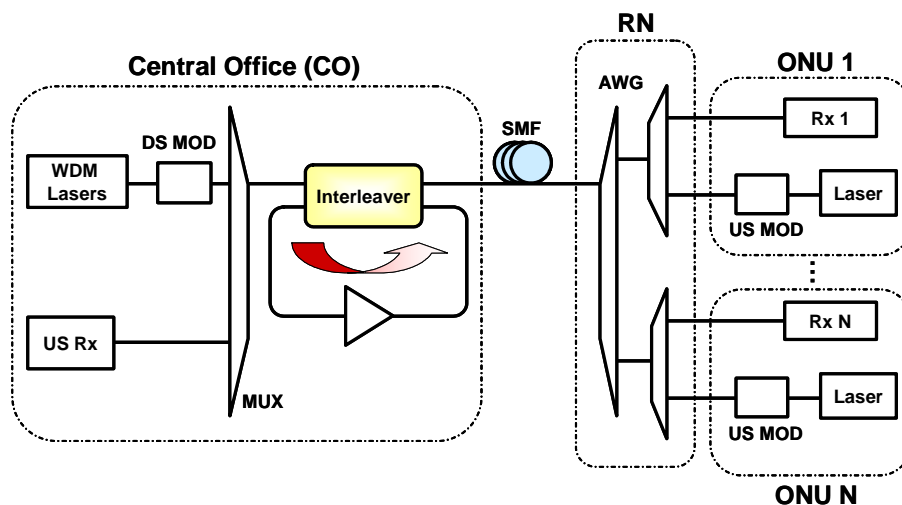
Figure 6.3: Proposed bidirectional WDM-PON system.
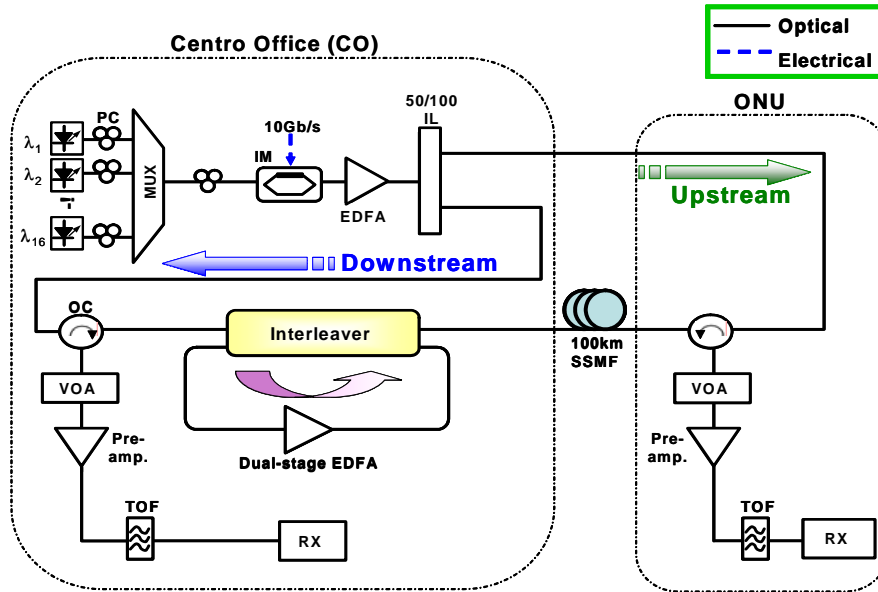
Figure 6.4: Experimental configuration for bidirectional WDM-PON system

limitation of the experimental components, sixteen channels were modulated by the same intensity modulator (IM) by 10 Gbit/s electrical signals with a PRBS length of $2^{31}-1$ and used a 50/100-GHz spaced interleaver to split even and odd channels as downstream and upstream traffic. This novel bidirectional amplifier located in CO to boost the downstream signals as a booster-amplifier and amplify the upstream signals as a pre-amplifier before receiver. The fiber length of the transmission SSMF is 100 km, and the total launched power into 100-km SSMF for downstream and upstream signals are 2 and 1.6 dBm, respectively. The SSMF has a dispersion of 17ps/nm/km and a loss of 0.2 dB/km. The matched DCF was adopted in the configuration within dual-stage EDFA to compensate the accumulated dispersion in the transmission SSMF. A dual-stage EDFA with a 24.5-dB gain per channel was employed as the inline amplifier to provide gain for all channels, partially compensating the transmission loss. A single channel was selected

63

by using a 0.5-nm optical tunable filter before the chosen channel was detected after a pre-amplifier.

6.2.2 Experimental Results

Figure 6.5(a) and (b) shows the received optical spectra of eight-upstream and eight-downstream signals after 100-km SSMF with 0.05-nm resolution bandwidth, respectively. Figure 6.6(a) is the BER curves and some typical eye diagrams of the upstream 1, 6 (channel 1 and 11) and the downstream 3, 8 (channel 6 and 16) with and without transmission fiber and DCF. After bi-directional transmission over 100-km SSMF, the eye diagrams and the BER curves for all bidirectional transmission signals at different wavelength are identical. The power penalties at a BER of 10^{-9} for upstream 1 (λ=1554.54 nm), upstream 6 (λ=1558.58 nm), downstream 3 (λ=1556.55 nm) and downstream 8 (λ=1560.61 nm) are 0.5 dB, 0.7 dB, 0.6 dB and 0.6 dB, respectively. The circle symbol is bidirectional transmission results when both upstream and downstream signals are turned on. The square and triangle symbol are upstream and downstream transmission results while downstream are turned off and upstream turned off,

(a)   (b)
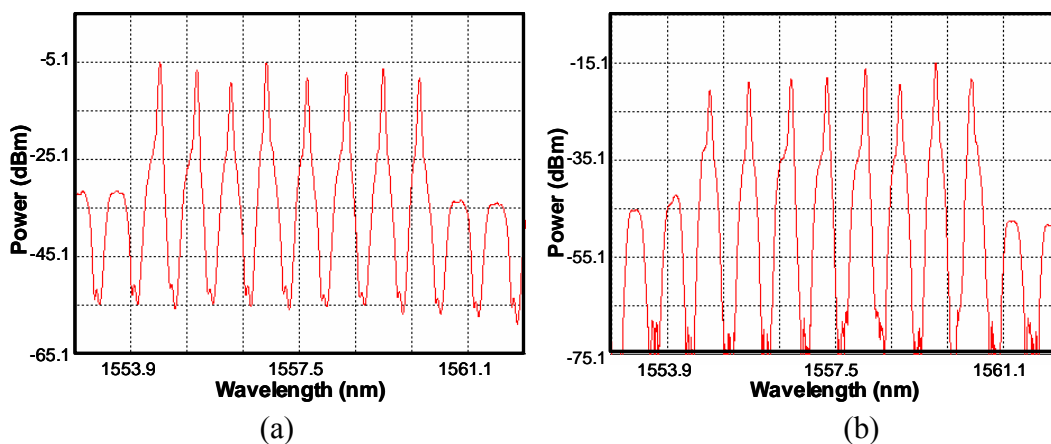
Figure 6.5: Received optical spectrum of (a) 8-upstream, and (b) 8-downstream signals after 100-km SSMF.

respectively. The power penalty and penalty differentials between bidirection and unidirection of all channels are less than 0.8 dB and 0.2 dB, respectively. These power penalties are mainly caused by the OSNR degradation resulting in the large insertion loss of the transmission fiber.
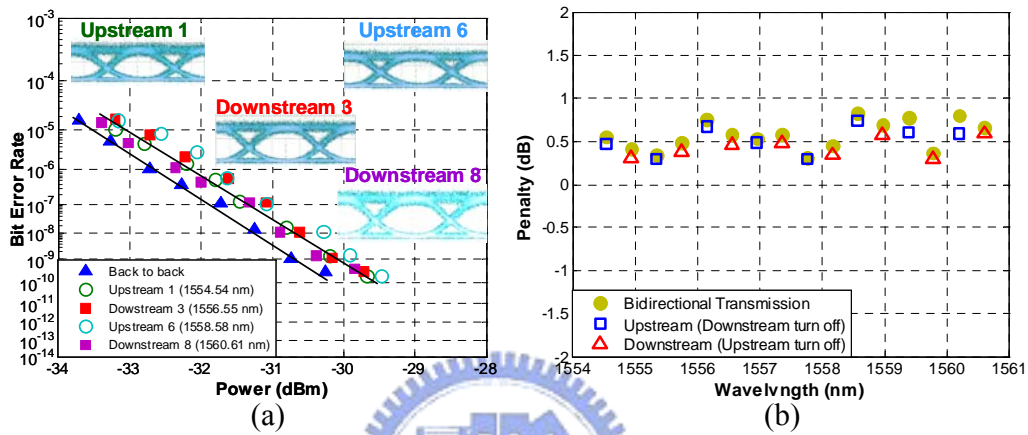
Figure 6.6: (a) BER curves at upstream 1, 6 and downstream 3, 8. Inset: Received eye diagrams. (b) Power penalties at BER = 10^{-9} of all channels with bi-directional transmission, upstream data only and downstream traffic only.

6.2.3 Summary

It is the first time, in our best knowledge, a bidirectional WDM-PON that used a novel four-port interleaver to enable unidirectional EDFA amplification. Given the creative complementary wavelength sensitive routing scheme, only one in-line unidirectional EDFA is needed to achieve bidirectional amplification. After bidirectional transmission over 100-km SSMF, the power penalties for all channels at a BER of 10^{-9} are less than 0.8 dB; this result indicates good amplification performance of the proposed innovative configuration. We believed that this bidirectional WDM-PON could be employed to transmit more channels because this four-port interleaver is designed to cover the whole C band.

6.3 Select-Cast Services in WDM-PON System

In WDM-PON system, one of the most critical issue is how to reduce the cost while to provide new services that require higher bandwidth. The best way to achieve this goal is to adopt wavelength reuse scheme and maintain source-free or colorless ONUs [63, 64]. Sub-carriers multiplexing (SCM) modulation techniques to deliver the downstream data by optical sub-carriers and wavelength reused have been reported in [60, 65]. In this scheme, non-modulated signal carriers were delivered to ONU directly. In this way, the optical power will be effectively utilized and highly efficient and low-cost operation can be realized if these non-modulated carriers can be accomplished. For wavelength reuse schemes, Fabry-Perot laser diodes (FP-LDs), SOAs and reflective SOAs (RSOAs) had been used to re-modulate downstream signals for upstream transmission. In a recent report, RSOA has been proposed as a low-cost optical network terminal [66] results from no need for extra optical amplifier within the system. In this section, a new colorless WDM-PON architecture for providing multi-services using centralized lightwave source to reduce the cost of the system with carrier suppression and separation (OCSS) technique had been proposed.

6.3.1 Principle of Optical Carrier Suppression and Separation

Figure 6.7 shows the principle of the proposed OCSS technique [67]. A sinusoid RF clock and its inverse (clock bar) are used to drive a dual-arm LiNbO$_3$ modulator (DAM) that biased at the minimum-intensity output point, as shown in Figure 6.7(a) and 6.7(b). The original carrier of the injected CW laser (ω_0) is suppressed and two symmetrical beat longitudinal sub-modes are generated ($\omega_0 - f_o$, $\omega_0 + f_o$) [68]. The spacing
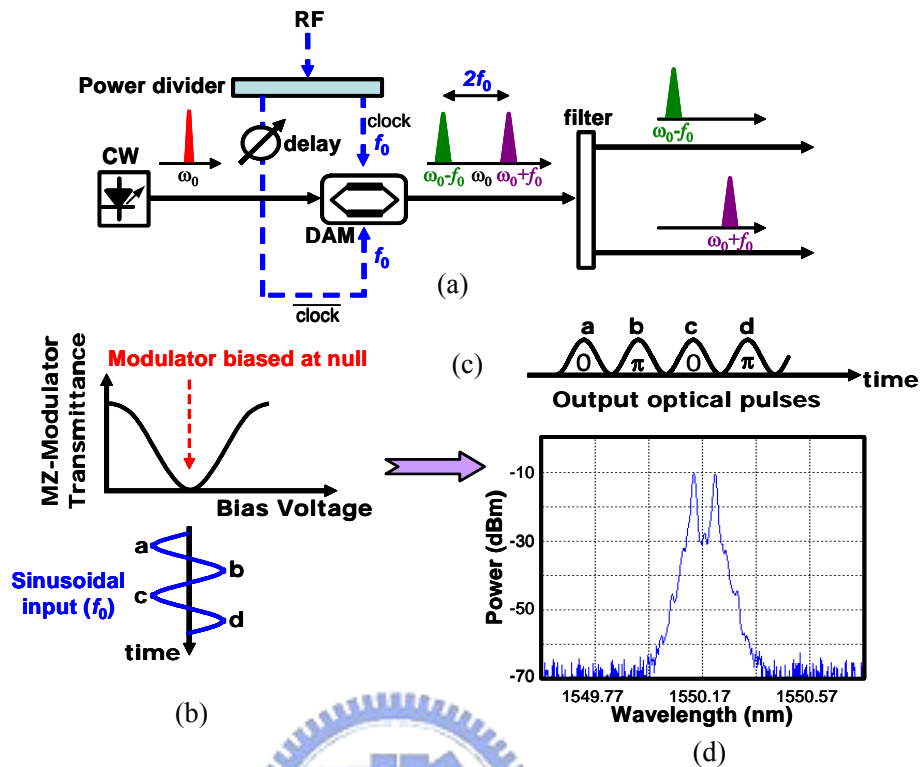
Figure 6.7: Principle of optical carrier suppression scheme. (a) experimental setup to generate OCSS technique; (b) the biased point of the modulator; (c) output optical pulse ; (d) optical spectrum after OCS with 5 GHz RF.

between two sub-carriers is always equal to twice the frequency of the sinusoidal modulation clock ($2f_o$). The output optical pulses are shown in Figure 6.7(d). In theory, the phase-encoding is alternate, as exhibited in Figure 6.7(c). As an example, the output optical spectrum shown in Figure 6.7(d) is for the case of a 5-GHz modulation frequency. From this optical spectrum, it can be seen that the wavelength spacing between two sub-carriers is 10 GHz, and the carrier is also suppressed. After DAM, an optical filter can be used to separate two sub-carriers. This result in two separate CW light with fixed wavelength spacing, and two of the CW light can be assigned to different applications. The OCSS technique has the following advantages:

1) OCSS suffers no extinction-ratio limitation for generation sub-carries; this is the main

drawback of orthogonal modulation technique [69].

2) The two sub-carries can be used in label swapping technology as payload and label. These two sub-carries can generate at different bit rate. For example, the payload can be chosen to operate at any bit rate, much higher than the bit rate of the label. The only requirement is that bit rate of the payload has to be less than or equal to twice the sinusoidal frequency that is used to generate the carrier suppression [70]. Therefore, two sub-carries are not overlapped in the frequency domain.

3) The OCSS technique can be easily used for high-speed generation. Due to the wide spacing between two modes, it is relatively easy to separate the two sub-carriers using optical filter [71].

4) Two sub-carriers can be separately generated and then combined by optical multiplexing, there is no crosstalk between two modes.

5) Narrow bandwidth for transporting two sub-carries is realized and thereby allowing better spectral efficiency [72].

6.3.2 Proposed WDM-PON with DPSK and OOK Centralized Lightwaves

Figure 6.8 shows the proposed novel colorless WDM-PON architecture to realize the centralized lightwaves for the upstream signals. Our CO consists of N DFB laser sources. Using a dual-arm modulator, two wavelengths (a total of $2N$ wavelengths) from each DFB laser source can be generated by using OCS technique as carriers and sub-cariers. An optical interleaver (IL) is employed to separate the generated $2N$ wavelengths into N odd channels for OOK and N even channels for DPSK modulation. The downstream OOK data and DPSK signals are delivered to the ONU by optical fiber. At the remote node, an interleaver is used to separate the intensity and phase modulated

68
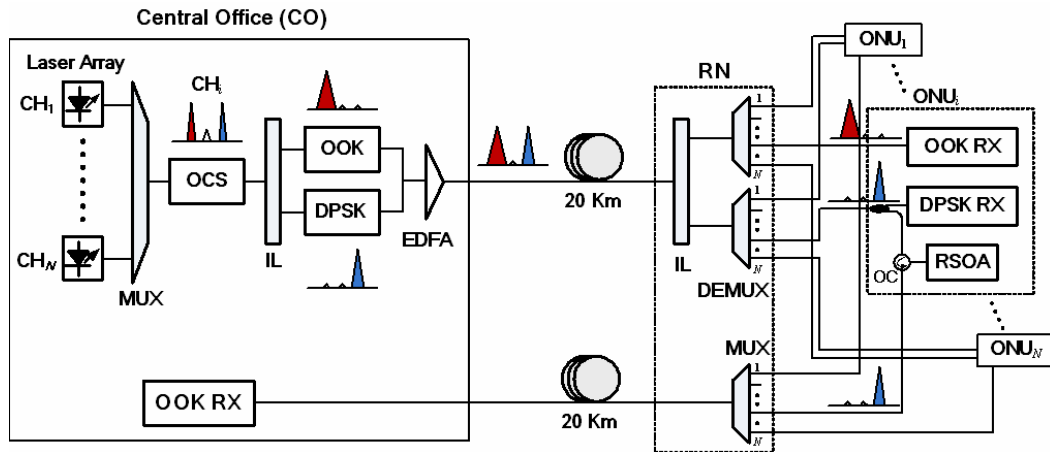
Figure 6.8: Proposed novel WDM-PON architecture with DPSK and OOK centralized lightwaves.

data. By using two DeMuxs, intensity and phase modulated signals are routed to each ONU. Here, a multi-service environment has been realized. In the ONU, a 3R receiver will detect OOK data directly. The phase modulated downstream signals are sent to two different paths after demultiplexing: one was converted into the intensity signals by using a Mach-Zehnder delay-lined (MZ-DI) interferometer and the other was re-modulated by an RSOA and sent back to the CO. Therefore, the centralized lightwaves in the OLT can be realized.

6.3.3 Experimental Setup and Results

The experimental configuration is illustrated in Figure 6.9 [73]. It includes four DFB lasers as the transmitter from 1556.55 nm to 1558.98 nm with 100-GHz channel spacing and they were combined by a coupler. The combined output was fed into a dual-arm Lithium Niobate modulator to realized optical carrier suppression. The clock modulation frequency for the DAM was set to 25 GHz. Therefore, the spacing between two new signals is equal to twice the frequency of the clock.
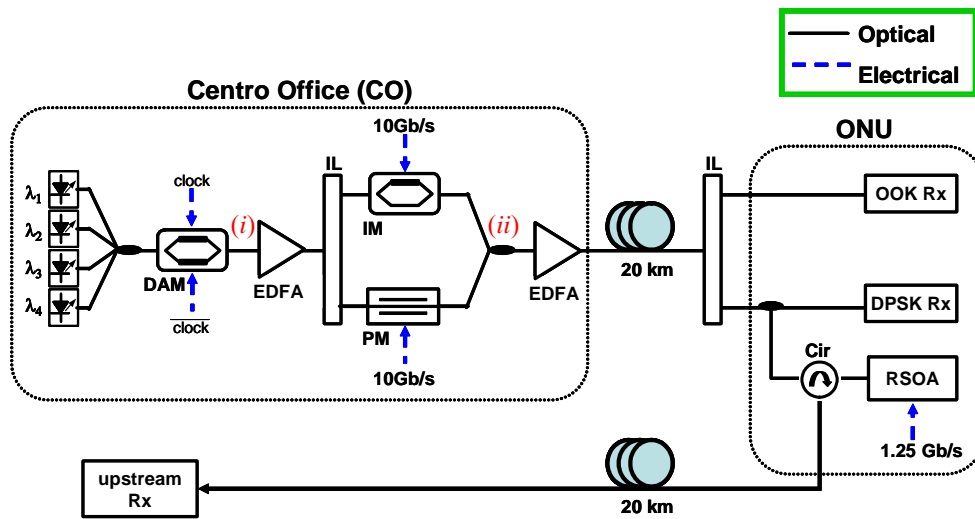
Figure 6.9: Experimental setup with centralized lightwaves in WDM-PON.

Thus, using OCS, eight wavelengths with 50-GHz spacing were generated at the output of the DAM as shown in Figure 6.10(a). It can be seen that good optical carrier suppression had been attained with the optical carrier more than 20 dB below the two generated the first sideband modes. A 100-GHz spaced IL was used to separate 8 channels into intensity modulator (IM) to generate OOK signals and phase modulator (PM) to obtain DPSK data. Figure 6.10(b) presents the combined OOK and DPSK signals as inset (ii) in Figure 6.9, respectively. After an optical coupler in OLT, the combined OOK and DPSK signals had been sent to the ONU over 20-km SMF-28 fiber. Both IM and PM were driven by a 10 Gb/s electrical data with a PRBS with a sequence length of 2^{31}-1. The downstream signals were separated by using an IL to support OOK and DPSK services. The separated DPSK downstream traffic was divided into two parts by a 3 dB coupler. The measured BER result for one of four OOK and DPSK signals for downstream is shown in Figure 6.11(a). The DPSK signals were detected by using a balance receiver; therefore, there is 2-dB margin in receiver sensitivity compared to OOK
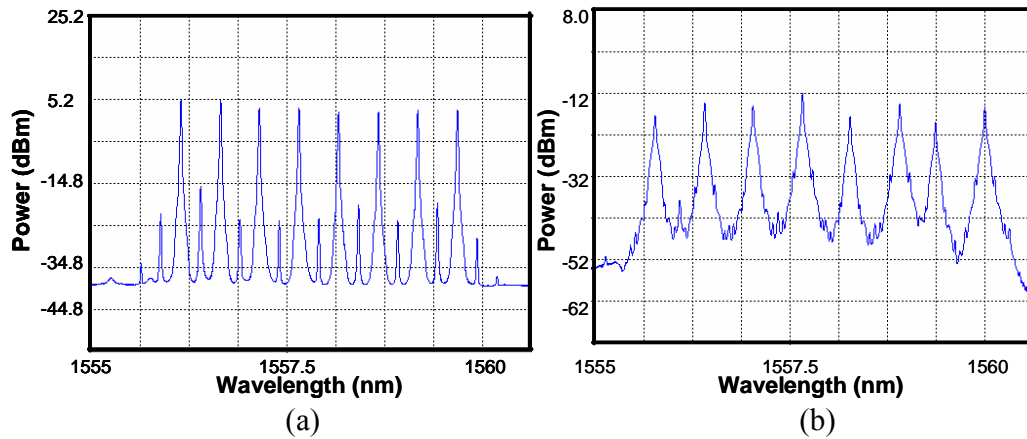
Figure 6.10: Received optical spectra (RB = 0.01 nm). (a) After DAM showing 8 channels as inset (*i*) in Fig. 6.9; (b) After IM and PM as inset (*ii*) in Figure 6.9

signals [11]. All channels for OOK and DPSK signals were measured; the BER performance is almost identical. Therefore, in Figure 6.11(a), only show BER performance of one channel has been sown. The power penalty caused by downstream transmission fiber is negligible for both OOK and DPSK. The other part from downstream DPSK was sent to an RSOA and re-modulated at 1.25 Gb/s with a PRBS length of 2^{31}-1 as an upstream where the modulation condition of RSOA was set to maximize the extinction ration (ER) of modulated upstream signals.

Figure 6.11: Measured BER curves and the corresponding eye diagrams. (a) Downstream B-T-B and after 20-km transmission for OOK and DPSK; (b) Upstream B-T-B and after 20 km SMF.

The operation bias current of the RSOA is 80 mA with 17-dB gain and the polarization dependent gain (PDG) is smaller than 1dB. The re-modulated at ONU provides upstream service over 20-km SMF-28 fiber and detected in OLT as shown in Figure 6.11(b). The power penalty caused by upstream transmission fiber is less than 0.5 dB at a BER of 10^{-9}.

6.3.4 Summary

Novel WDM-PON architecture with simultaneously generated DPSK and OOK centralized lightwaves in the OLT to provide downstream multi-services have been proposed and experimentally demonstrated. These two downstream signals were modulated as OOK and DPSK at 10 Gb/s. The phase modulated signals were re-modulated by a colorless transmitter using an RSOA in ONU with 1.25 Gb/s for upstream traffic. The receiver power penalty is very small, less than 0.5 dB, for both 10 Gb/s downstream and 1.25 Gb/s upstream signals after transmission over 20-km SMF-28. In the future, these two downstream signals can provide a dedicated select-cast service on OOK and a data channel at 10 Gb/s DPSK modulation format.

6.4 WDM-PON to Provide Triple Play Services

The capacity and speed requirements for Internet have been evolving in recent years to adapt emerging bandwidth-hungry, multi media applications. Therefore, next generation optical access network is desirable to support new broadband services for triple play services (TPS). It presents a great challenge in the ever-increasing demand of large capacity, low latency, and high security for triple-play service delivery and real time applications. Several proposed schemes used an additional set of wavelengths

separated by the arrayed waveguide grating (AWG) or time-multiplexing method to share the same wavelength and provided independent services in WDM-PON [74]. Nevertheless, these techniques can be complex and costly to implement. Consequently, the most critical issues to provide TPS in WDM-PON networks are to reduce the cost, increase transmission power margin, and improve system reliability.

6.4.1 Proposed TPS Scheme in WDM-PON System

In previous proposed schemes, source-free ONU, sub-carriers multiplexing (SCM) modulation technique and wavelength reuse have been demonstrated [60, 63, 73, 75]. However, in these schemes, more than two modulators are required to provide TPS. Compared to some proposed schemes, this proposed scheme does not require extra optical components such as interleavers and modulators to separate carrier and sub-carrier for realizing cascaded modulation, which improves system power budget and enhances network reliability. The principle of the proposed WDM-PON to provide TPS is illustrated in Figure 6.12. The OLT designed consists of *N* distributed DFB lasers.
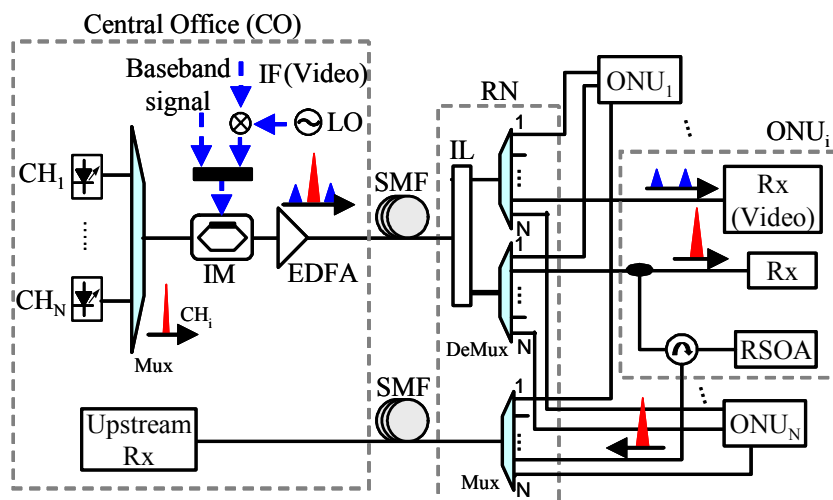
Figure 6.12: Proposed simple WDM-PON architecture simultaneously provides triple-play service.

By using one intensity modulator, three sub-channels can be generated from each DFB laser, as total 3N sub-channels. In the CO, video signals are up-converted in a mixer by local oscillator (LO) and carried by using sub-carrier multiplexing while baseband data are imposed on the original optical carrier. Therefore, the repetitive frequency of the SCM signals is double of the LO. The converted signals and baseband data are combined by an electrical power coupler before they are launched to drive one single-arm intensity modulator. At the remote node (RN), and optical interleaver (IL) is used to separate the baseband data and SCM signals. By using two DEMUX, baseband and SCM data are routed to each ONU. In the ONU, 3R receivers will detect SCM signals directly. The baseband downstream signals are sent to two paths after demultiplexing. One part is fed to a standard baseband receiver and the other part is re-modulated by an RSOA and sent back to the CO. Consequently, in this architecture, not only the numbers of lasers and external modulators have been reduced, but centralized lightwave has been realized in the OLT.
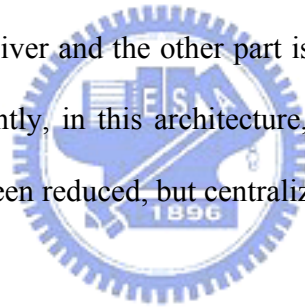
6.4.2 Experimental Setup and Results

The experimental configuration is depicted in Figure 6.13. In CO, the continuous wave (CW) lightwaves were generated by four DFB lasers from 1557.4 nm to 1559.8 nm with 100 GHz channel spacing and they were combined by an optical coupler. The combined output was fed into a single-arm LiNbO$_3$ intensity modulator to realize optical carrier suppression. The bansband signals are set to 10 Gb/s data with a pseudorandom binary (PRBS) word length of 2^{31} -1. 2.5 Gb/s signals with the same pattern format are mixed with a 20 GHz sinusoidal wave by a mixer to accomplish SCM for digital video
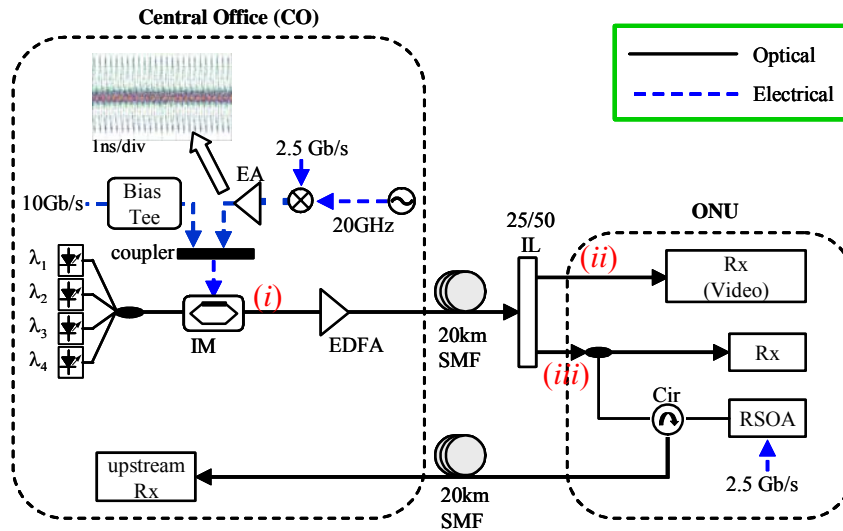
Figure 6.13: Experimental configuration for WDM-PON network.

data. 10 Gb/s baseband and 2.5 Gb/s SCM signals are combined by an electrical coupler

and used to drive the electrode of LiNbO$_3$ IM. The electrical eye diagram of the mixed

signals is shown in Fig. 6.13. The driving amplitude of mixed signals is 6.5 V and the

modulator is biased at 8.18 V, in the linear region but close to null point. In this bias

point, the baseband carried 2.5-Gb/s signals would be suppressed. Another DC bias at

4.1 V is used for 10 Gb/s baseband data to generate another working point of the IM.

Therefore, 10 Gb/s baseband data and 2.5 Gb/s SCM signals are realized by one single-

arm IM. The optical spectrum of the four modulated signals is shown in Figure 6.14(a) as

inset (*i*) in Figure 6.13. Figure 6.14(b) depicts the single modulated signal. It is clearly to

see that the spacing between two SCM signals is 40 GHz, double of the 20-GHz LO

frequency. One 25/50-GHz spaced interleaver with 30 dB channel isolation and two

outputs was set to separate optical carriers and sub-carriers to support TPS after over 20-

km SMF-28 fiber downstream transmission with 10.5-dBm total launched power. The

optical spectra of the separated carriers and sub-carriers with resolution equals to 0.01 nm
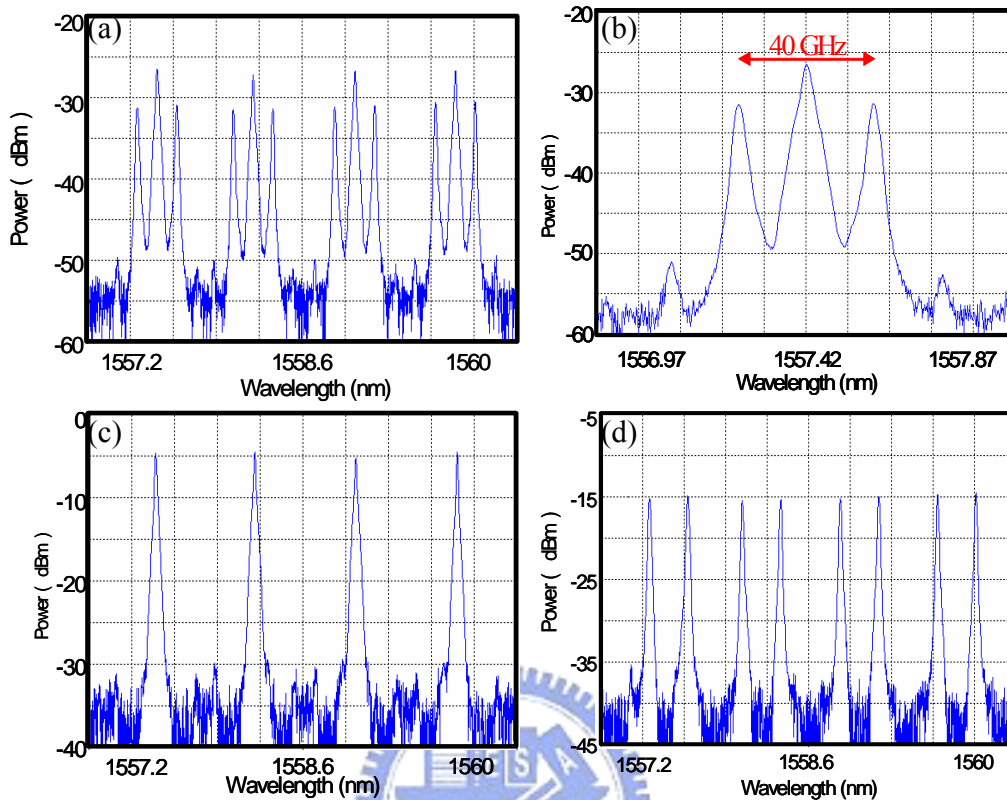
Figure 6.14: Received optical spectrum (RB = 0.01nm). (a) after intensity modulator showing 4 channels as inset (*i*) in Figure 6.13; (b) one of the four modulated signal; (c) separated optical carrier and (d) separated SCM signals as inset (*ii*) and (*iii*) in Figure 6.13

are shown in Figure 6.14(b) and (c) as inset (*ii*) and (*iii*) in Figure 6.13, respectively. A 3R receiver is set to detect 2.5 Gb/s sub-carriers directly. The separated 10 Gb/s downstream traffic was divided into two parts by a 3 dB coupler. The measured BER results for one of four 10 Gb/s data and 2.5 Gb/s digital video downstream transmission as shown in Figure 6.15(a). All channels of downstream and upstream were measured, the BER performance is identical. Therefore, in Figure 6.15, only BER performance and the corresponding eye diagrams of one channel with back-to-back and after over 20 km transmission has been displayed. The power penalty for both 10 Gb/s baseband and 2.5 Gb/s sub-carriers are less than 0.5 dB at BER equals 10^{-9}. This power penalty results
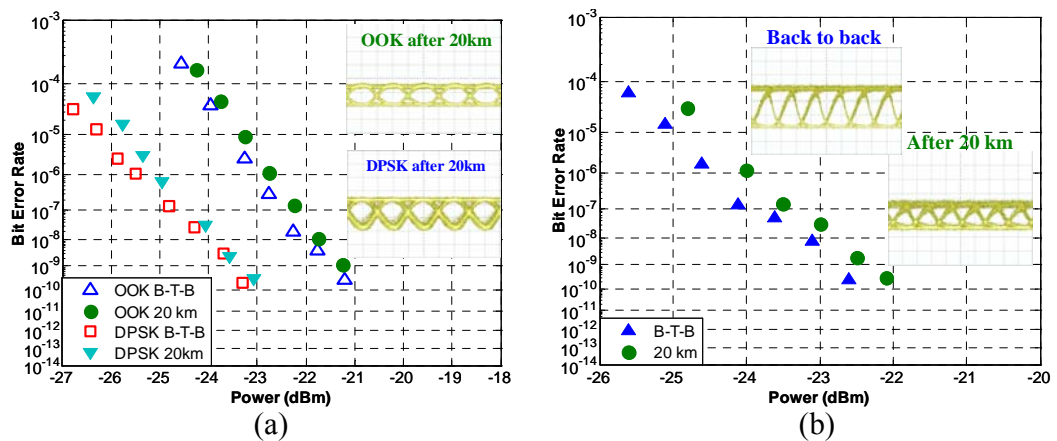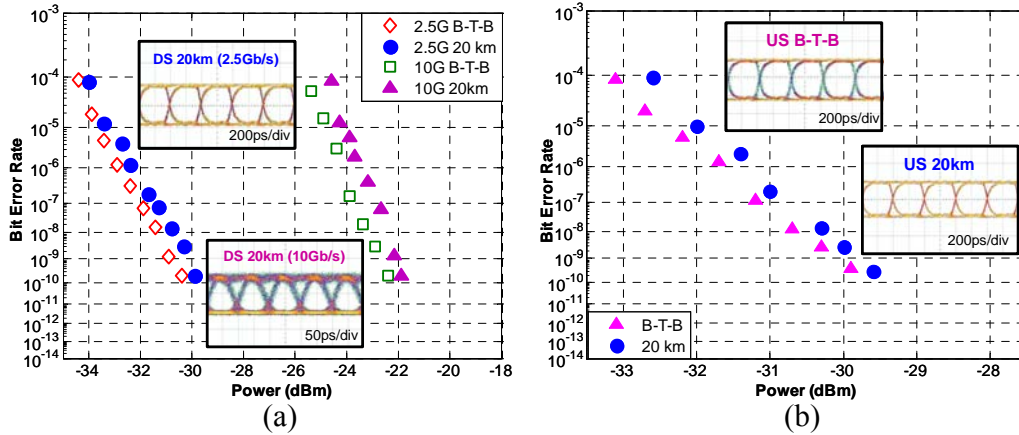
Figure 6.15: Measured BER curves and the corresponding eye diagrams. (a) Downstream B-T-B and after 20 km transmission for 10 Gb/s baseband data and 2.5 Gb/s sub-carrier signals, and (b) 2.5 Gb/s upstream data B-T-B and transmission over 20km SMF-28 fiber.

from residual part of the baseband or SCM signals due to imperfect separation of the interleaver and the imperfect carrier suppression within IM. We believed that the power penalty could be reduced if the modulator was biased at the minimum operation point. The other part from 10 Gb/s downstream data with 6.3 dB extinction ratio (ER) and a DC value was sent to an RSOA and re-modulated at 2.5 Gb/s with a PRBS length of 2^{31} -1 as upstream signals where the modulation condition of RSOA was set to maximize the ER of 7.2 dB of modulated upstream signals. The operation current of the RSOA is 80 mA with 14-dB gain and the PDG is smaller than 1 dB. The upstream re-modulated at ONU passed another 20-km SMF-28 fiber and detected in OLT as shown in Figure 6.15(b). The power penalty caused by upstream transmission fiber is less than 0.2 dB at a BER of 10^{-9}. Compared to reference [76], no delay interferometer (DI) is needed and the bit rate is also upgraded as 10 Gb/s data and 2.5 Gb/s digital video downstream and 2.5 Gb/s data upstream transmission.

6.4.3 Summary

A WDM-PON configuration with centralized lightwaves in the OLT by using only one single-arm $LiNbO_3$ intensity modulator had been experimentally demonstrated. Compared to the previously published schemes, it is a simple way to realize triple-play service without requiring DI, extra interleavers and modulators for cascaded modulation. Because this WDM-PON system employs less number of optical components, it can provide significant improvement on both power budget and system reliability. Using this scheme, 10 Gb/s baseband signals and 2.5 Gb/s sub-carriers downstream transmission over 20-km SMF-28 fiber have been demonstrated. The baseband signals were re-modulated by an RSOA at 2.5 Gb/s for upstream traffic. The power penalties are less than 0.5 dB and 0.2 dB for all downstream and upstream channels after transmission, respectively.
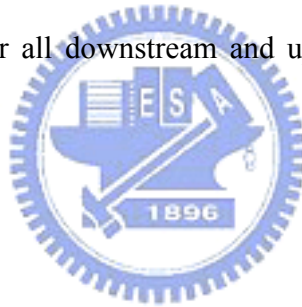
CHAPTER 7

FUTURE DIRECTIONS

The possibility of future networks to meet ever increasing bandwidth requirement is PON technology. WDM-PON system is adapted to next generation optical access network. However, lots of industries, such as Huawei Technologies Co., Ltd., AT&T etc al., are interested in TDM-PON for near future, because of its unsophisticated building. In order to shorten the distance between two destinations, high speed trains had been built up in Europe, Japan and Taiwan. Therefore, delivering super broadband internet access to the fast moving users is another interesting and unsolved issue in the world. In this chapter, 10G/1G hybrid PON and WiMax/ROF transmission in high speed train would be discussed.

7.1 General Architecture for TDM-PON

There are three standardized versions of the PON: Ethernet PON (EPON), Broadband PON (BPON) and Gigabit PON (GPON). All three PONs use a passive
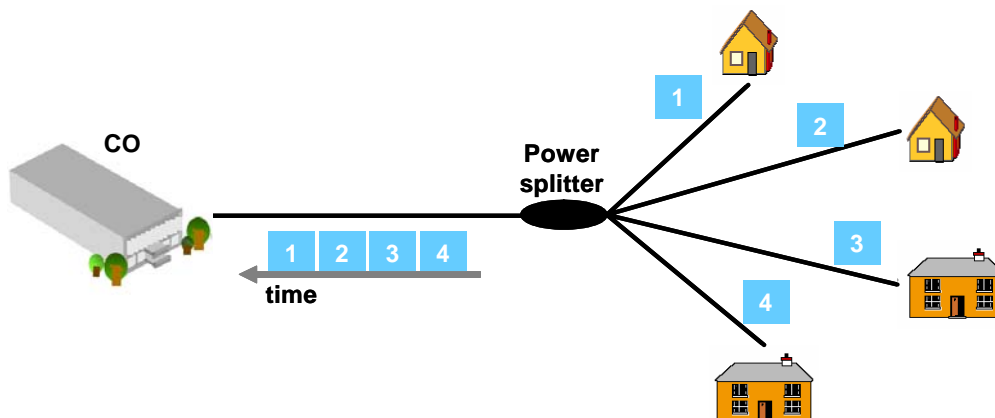
Figure 7.1: General architecture for TDM-PON.

optical $1 \times N$ splitter placed at the remote node (RN) to send signals to subscribers. Therefore, EPON, BPON, and GPON are all TDM-PONs, as presented in Figure 7.1. A signal wavelength containing downstream information is shared by N users. Typically, the upstream transmission from the ONUs to OLT uses a time division multiplexing access, the OLT has a burst mode receiver and each ONU has a burst mode transmitter [77]. Since the optical power is split among the subscribers, the customers have to access the information in a given time slot. To avoid crosstalk between upstream and downstream transmissions, downstream data is operated in the 1550 nm window while upstream traffic is set in 1300 nm window. One important distinction between the three flavors of PON is operational speed. BPON is relatively low speed with 155 Mbps upstream and 622 Mbps downstream operation; EPON supports 1.0 Gbps symmetrical manipulation; and GPON promises 2.5/1.25 Gbps asymmetrical execution. The major merit of the TDM-PON includes:

1) All ONUs can operate on the same wavelength and be absolutely identical component-wise.

2) Allows for a single upstream and a single transceiver in the OLT, resulting in a cost-effective solution.

3) Adequate for broadcasting application services because of its intrinsic attribute.

4) Effectively uses its bandwidth by statistical multiplexing.

7.2 Novel Hybrid 10G/1G Coexisted TDM-PON

In the near future, TDM-PON is good solution for increasing data requirements. Recently, both IEEE 802.3 and FSAN view 10G PON as a next generation access option.

In 10G PON, technical challenges are locating in high speed burst mode receiver of OLT. Currently the commercial maximum burst receiving speed is 1.25 Gbps. There are two ways to deal with this challenge: one way is to achieve technical breakthrough in 10G burst mode clock and data recovery (CDR); another way is to trunk several lower speed channels as upstream channel by imitating 10G Ethernet configuration. Unlike other access networks, high speed TDM-PONs are point-to-multipoint networks capable of delivering services over 20 to 40 kilometers of single-mode fiber and have been intensively discussed to meet the upcoming enormous bandwidth requirement. A simple and cost-effective evolution path from current TDM-PONs to next-generation high speed TDM PONs is highly required without changing the legacies of the current PON infrastructure.

In this section, a novel and efficient 10G bidirectional TDM-PON structure using reflective colorless ONUs to increase bandwidth while reducing system cost, all-optical signal preprocessors for mitigating system impairments and providing intelligent control for data transmitting and receiving management. The carrier-suppressed centralized lightwaves to provide a global clock information and enable instantaneous clock recovery and enforced synchronization for the upstream bursty packets without using traditionally required clock and data recovery (CDR) circuits. The reflective colorless ONU is cost-effective since it contains both amplification and modulation capabilities, and optical carrier is simply provided by the centralized light source at CO, which makes network management and maintenance easier. Such reflective ONU can contain four piped sub-units, and each of them carries 2.5 Gb/s data to realize 10 Gb/s upstream. On the other hand, the burst-mode receiver at CO can be technically challenging since they should

have a wide dynamic range for the different incoming bursty signals from different ONUs, and should also retrieve precise and sufficient clock information to synchronize these upstream packets with extremely short guard times. Such requirements will be even more severe when 10G TDM-PON is considered. Therefore, all-optical signal preprocessors and carrier-suppressed centralized lightwaves are proposed to achieve data rate transparent power equalization in front of the electrical receiving stage, and provide simple detection of continuous and low-jitter clock information, respectively.

7.2.1 Network Architecture and Wavelength Plan

Figure 7.2 shows the proposed hybrid 10G/1G coexisted TDM-PON architecture. In the CO, centralized lightwaves are employed to provide optical carriers for both downstream and upstream simultaneously, which are combined by a WDM coupler and sent to RN with a feeder fiber span. In the RN, a $1 \times N$ optical splitter is used for distributing the whole traffic to each ONU. The 10G/1G transmitter (TX) module contains both 10G and 1G downstream signal at different wavelength bands. In the meantime, 10G upstream traffic is realized by delivering four continuous wave channels at wavelengths $\lambda_1 \sim \lambda_4$ from CO, and modulating them using reflective ONUs. Each 10G ONU contains four reflective transmitters connected with a 1×4 add/drop filter, and can be viewed as a pipe-line upstream module. Thus, 10G upstream can be retrieved by directly modulating the optical carriers of four piped reflective transmitters at $\lambda_1 \sim \lambda_4$ with electrically demultiplexed 2.5 Gb/s patterns. Moreover, using a reflective semiconductor optical amplifier (RSOA) is one of cost-effective solutions to achieve both amplification and modulation functionalities in the ONU.
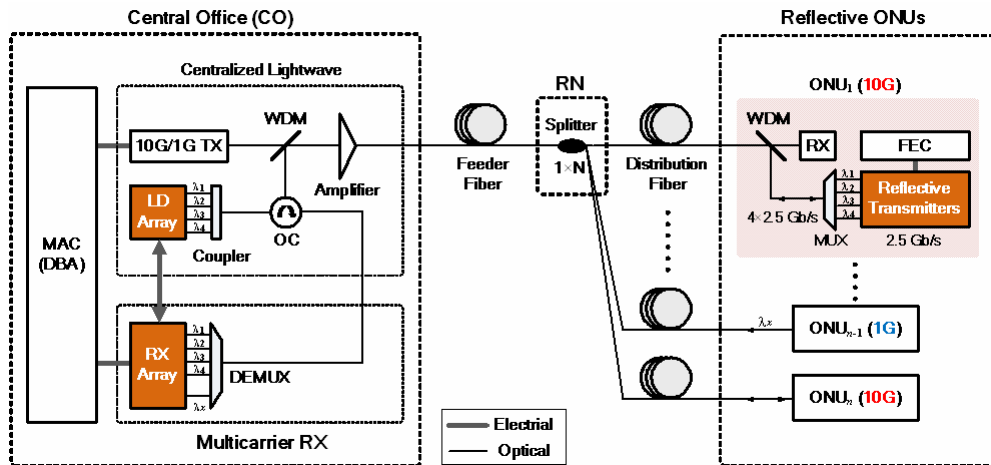
Figure 7.2: Proposed hybrid 10G/1G coexisted TDM-PON architecture using reflective ONUs.

In addition, traditional 1G ONU modules at wavelength λ_x can be seamlessly plugged in this system. As for upstream receiver at CO, four 2.5G ($\lambda_1 \sim \lambda_4$) and one 1G (λ_x) upstream channels are demultiplexed and individually fed into burst-mode receivers. Since the optical carrier for 10G upstream traffic is solely provided by the centralized lightwaves, their wavelength and power level can be easily supervised and adjusted at the CO. Furthermore, a media access controller (MAC) with dynamic bandwidth allocation (DBA) can be equipped at the CO to allow efficient bandwidth sharing of the single-feeder fiber. A forward error correction (FEC) coding can be applied for upstream data modulation to obtain more coding gain and mitigated power budget. Figure 7.3 displays the wavelength plans for (a) the traditional EPON/GPON and (b) the proposed 10G/1G coexisted TDM-PON. In the proposed TDM-PON, only four wavelengths ranging from 1305 to 1315 nm is required for 10G upstream (US), which are entirely and precisely governed by the CO, while a portion of the enhancement band in EPON/GPON from 1540 to 1545 nm is utilized for 10 G downstream (DS). Note that the remained upstream and downstream

wavelength ranges (dash line) are available for existing 1G ONUs in EPON/GPON, which makes coexistence of 10G/1G TDM-PON systems a nature combination.
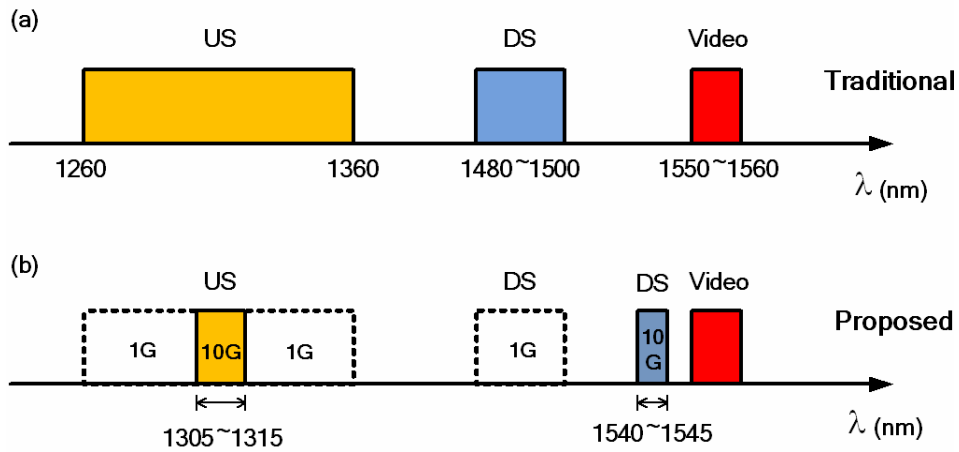
Figure 7.3: Wavelength plans for (a) traditional EPON/GPON and (b) proposed hybrid 10G/1G coexisted TDM-PON reflective ONUs.

7.2.2 Experimental Setup and Results

Figure 7.4 illustrates the configuration of the 10G TDM-PON access system considered in our experiment. For simplicity, C-band components had been used such as RSOA for feasibility demonstration, and employed a single RSOA with four input signals to simulate four piped upstream. In the CO, a single DFB laser (LD_d) at 1557 nm served as the transmitter for downstream, and four laser sources ($LD_{u1\sim u4}$) were used to realize centralized lightwaves for colorless ONU to reduce system cost. These four CW lasers were set to be upstream wavelengths from 1550.00 nm to 1552.4 nm with 100 GHz spacing. The LD_d was fed to a Lithium Niobate intensity modulator to obtain a 10 Gb/s OOK signal for downstream traffic with PRBS of 2^{31}-1 word length. The combined downstream data and four CW sources using a coupler were fed into 15-km SSMF and used a 1 × 4 splitter to share the traffic for more than four ONUs. Another 5-km SSMF was set between RN and ONU to simulate the distribution fiber spans in real market
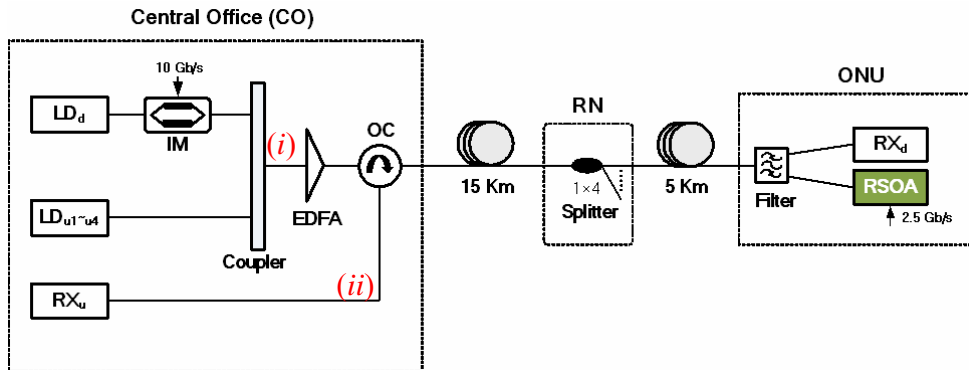
Figure 7.4: Experimental setup for TDM-PON.

system. A thin-film filter has been used to divide downstream signal and four CW sources. These four CW sources were simultaneously injected into an RSOA and then modulated at 2.5 Gb/s with a PRBS length of 2^{31}-1 as four upstream channels with an aggregate capacity of 10 Gb/s.

Figure 7.5(a) illustrates the optical spectrum of the combined downstream signal and four CW sources after optical coupler as inset *(i)* in Figure 7.4. Figure 7.5(b) presents the received optical spectrum for upstream over 20 km transmission as inset *(ii)* in Figure 7.4. Both of spectra were obtained by an optical spectral analyzer (OSA) with a RB = 0.01. It can be seen that good optical signal to noise ratio more than 35 dB for upstream over 20 km transmission has been attained.
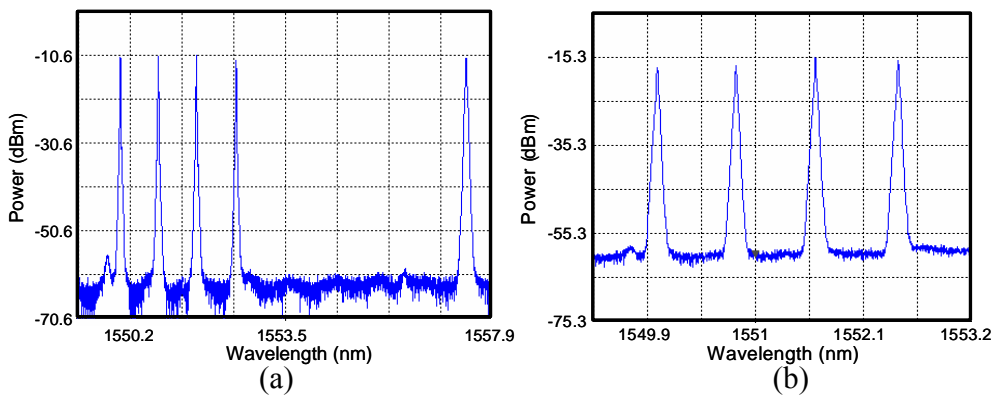
Figure 7.5: Received optical spectra: (a) combined downstream signal and four CW sources as inset (*i*) in Figure 7.4; (b) upstream signal over 20-km SSMF as inset (*ii*) in Figure 7.4

The BER curves and the corresponding eye diagrams for downstream and upstream with back-to-back and over 20-km SSMF are shown in Figure 7.6(a) and (b), respectively. The power penalty caused by downstream and upstream transmission was less than 0.2 dB. The large OSNR, clear eye and negligible receiving power penalty demonstrated the feasibility for this proposed novel TDM-PON architecture. In the future, wavelengths will be switched to *S*-band and *O*-band for downstream and upstream channels in adherence to the EPON/GPON standards.
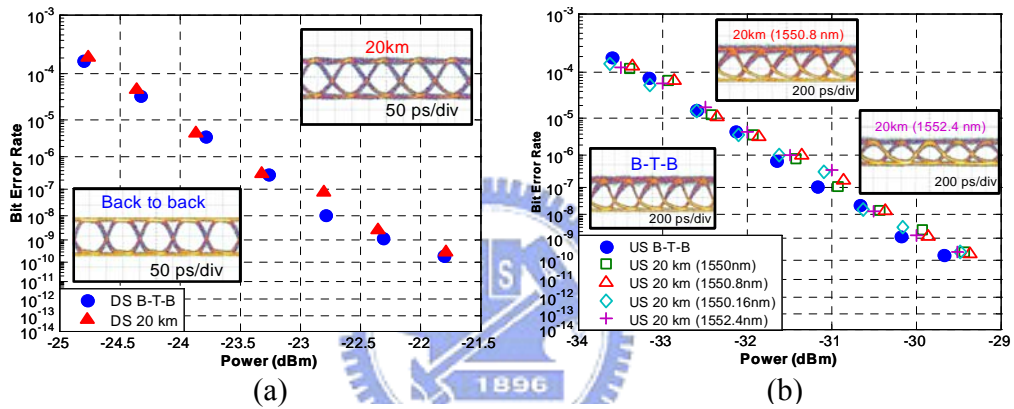
Figure 7.6: BER curves and corresponding eye diagrams: (a) upstream and (b) downstream with B-T-B and over 20 km transmission

7.2.3 10G TDM-PON using Optical Carrier Suppression and Separation Scheme

Based on previous results, a novel and cost-efficient 10G TDM-PON employing clock embedded centralized lightwaves has been proposed to realize instantaneous 10G burst-mode clock recovery while reducing the system cost and enabling easy network management, as shown in Figure 7.7. Downstream traffic is easily achieved by externally modulating the laser diode (LD_d) with 10 Gb/s data sequence, while the upstream traffic is realized by delivering clock embedded wave using OCSS technique. In the CO, a single DFB laser (LD_d) is used as the designated transmitter for downstream service and

86

four DFB lasers (LD$_{u1\sim u4}$) are fed into a DAM to realized OCS and source-free ONUs, the optical spectrum is displayed in Figure 7.8(a). Meanwhile, each wavelength (LD$_{u1\sim u4}$) with internal clock will deliver to ONU and send back to CO as upstream traffic. Therefore, the expensive bust-mode receivers will no longer be required in CO. Figure 7.8(b) presents the received optical spectrum for combined downstream and four CW sources after OCS over 20 km transmission with a RB = 0.01 on an optical spectral analyzer as set inset *(ii)* in Figure 7.7. The received corresponding eye diagrams for back to back and over 20 km transmission of downstream and upstream are shown from Figure 7.8(c) to 7.8(f), respectively. It can be seen that eye diagrams are clear and good OSNR more than 40 dB for downstream and upstream over 20 km SSMF are obtained. By using centralized clock source originated from the OLT or the CO in the proposed architecture, the complex and expensive CDR circuits are not required by conventional burst-mode receivers. Therefore, the simplicity in transmission design has been achieved while reduce the system cost in the TDM-PON. These preliminary test results showed the feasibility for this proposed 10G TDM-PON configuration.
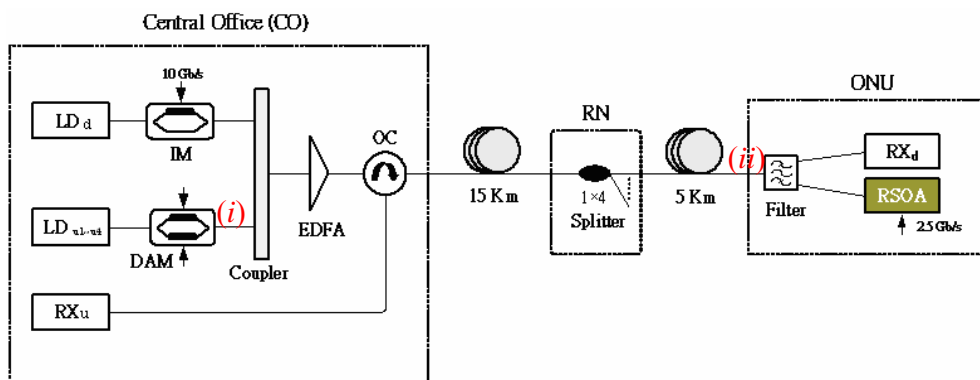
Figure 7.7: Experimental setup for TDM-PON using OCSS scheme.
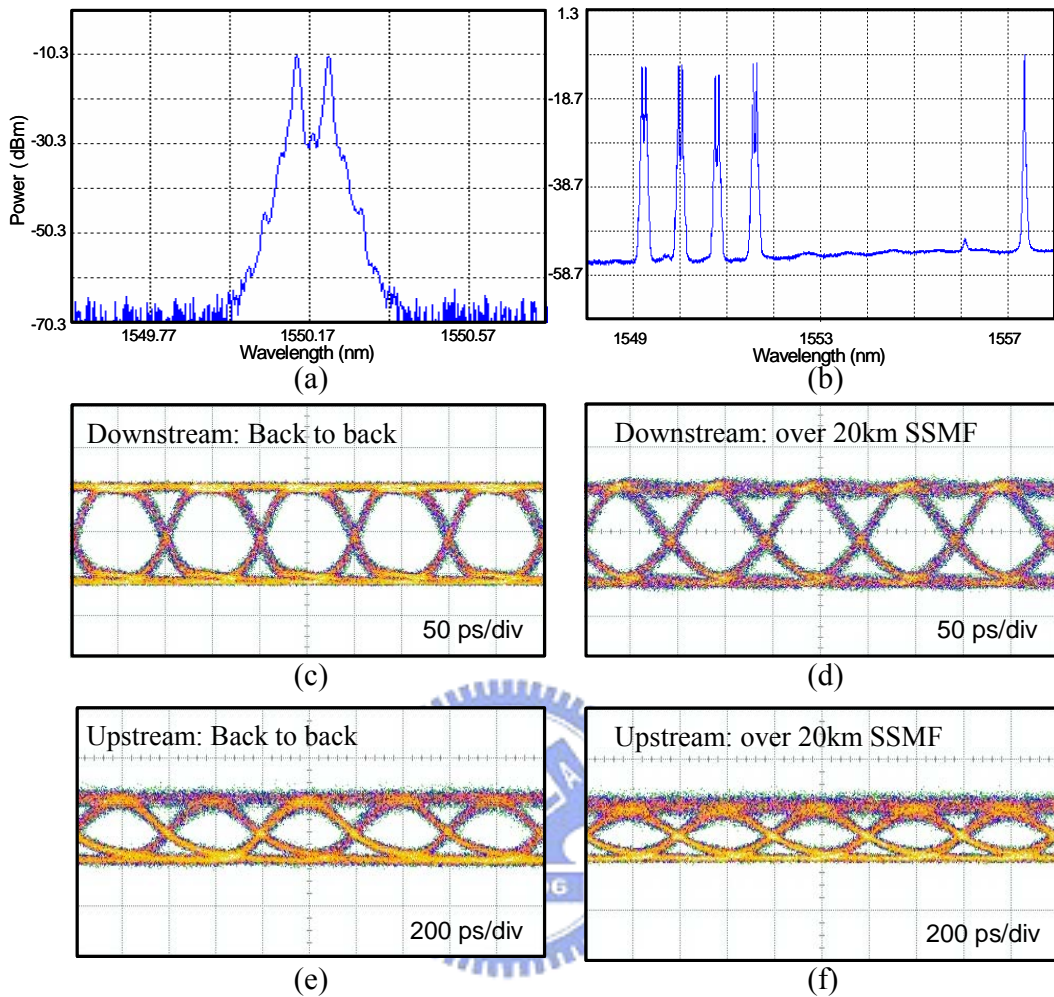
Figure 7.8: Received optical spectra: (a) one of four CW sources after OCS, as inset *(i)* in Figure 7.7. (b) Combined downstream signal and four CW sources over 20 km SSMF, the inset *(ii)* in Figure 7.7.

7.2.4 Summary

This investigation presents and experimentally demonstrates a novel TDM-PON using central office controlled reflective ONUs for reducing system cost, increasing the bandwidth, and making coexistence of 10G/1G PON feasible. 10 Gb/s upstream is achieved by 4 piped 2.5 Gb/s sub-units with negligible power penalty less than 0.2 dB. We believe that this proposed hybrid 10G/1G coexisted scheme is a promising low-cost

solution for the future upgrade of current TDM-PON system. In the future, OCSS technique will be used within the TDM-PON; therefore, no complex and expensive burst-mode receiver would be required. Furthermore, one wavelength with 10 Gb/s upstream would be replaced four wavelengths with 2.5 Gb/s per channel to realize cost-effective 10G TDM-PON system.

7.3 Worldwide Interoperability for Microwave Access (WiMAX)

WiMAX is a new broadband wireless technology which is designed to deliver wireless fidelity (WiFi) connectivity over a wider coverage area. WiMAX is based on the IEEE 802.16 standard, and operates in the 3.5 GHz frequency of the RF spectrum. WiMAX can provide a bandwidth of 70 Mbps over a distance of 50 km. Since WiMAX is a shared technology, the bandwidth supplied to a subscriber may be lower than the channel capacity and will depend on the customer per channel contention ratio [78].
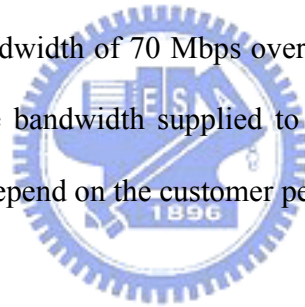
7.4 Mobile WiMAX /Radio over Fiber for Broadband Internet Access in High-Speed Railway System

Delivering super broadband internet access with sufficient level of quality of service to the fast moving users such as high-speed train (~300 km/hr) passengers is an interesting and unresolved issue. Although, the current cellular and satellite technologies can provide limited services to the mobile users, these technologies can not be considered for fast moving train passengers due to their inherent limitations. A direct connection between a train passenger and the ground base station of the cellular network is not possible due to high penetration losses because of the Faraday cage characteristics of the

train. Also, there are tradeoffs among the speed of the train, available bandwidth, and handover issues. On the other hand, the satellite technology is not suitable for real time applications because of its inherent delay, limited bandwidth, and poor coverage in urban and hilly areas and tunnels. In this regards, WiMAX/Radio over fiber (ROF), an integration of wireless and optical systems, could be the powerful solutions for providing high bandwidth internet to fast moving train passengers. Recently, cellular trackside solutions based on RoF have been proposed in [79, 80], which discussed only the architectural aspects and networking perspective of distributing broadband services to the train. Here, three-layer architecture has been proposed to provide both external broadband internet services and internal on-demand entertainment services to the high-speed train passengers using WiMAX/Radio over fiber system.

7.4.1 Proposed Three-Layer ROF Based Transmission System

Figure 7.9 shows the system architecture of the proposed three-layer WiMAX/Radio over fiber based transmission system providing high quality broadband services to the high-speed train. In the first layer, the WiMAX/Radio signal carrying baseband data is distributed to various proxy base stations (PBS) from a central Railway WiMAX/RoF Distribution and Control Center (RDCC). The PBSs are located along the rail tracks and are connected to the RDCC using a ring-based fiber distribution network. The RDCC performs all the expensive signal generation and processing for up-conversion of WiMAX/Radio signal, selection of wavelengths (λ_i) and corresponding intermediate/radio frequency (IF_i/RF_i) using dynamic optical layer handover policy before sending the downstream (DS) signal to the appropriate PBS. The upstream (US)
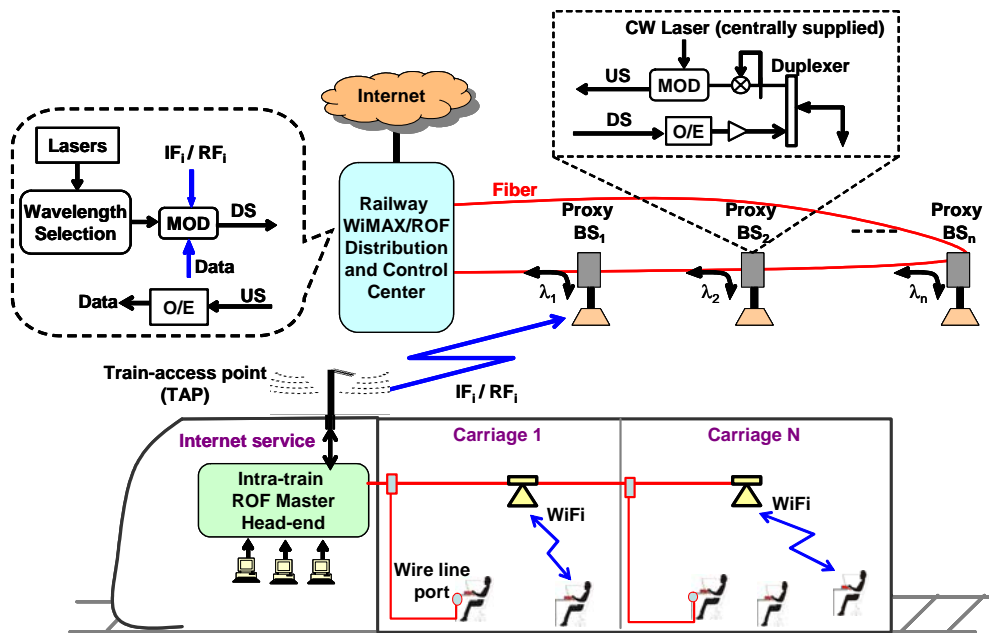
Figure 7.9: Proposed three-layer ROF based transmission system.

signal from the train is down-converted and optically modulated at the PBS before
sending it to the RDCC, where the baseband data is retrieved. The intermediate layer is
the IF/RF wireless communication between the Proxy BS and the moving Train Access
Point (TAP). The TAP is considered as the gateway to the train. It performs up-
conversion and down-conversion of the IF/RF signals to and from the Proxy BS. Finally,
the Intra-train RoF network provides both external broadband internet services and
internal on-demand select services (such as Movie/Video on demand, interactive gaming,
on-train conferences etc.) to the individual passenger using both wire line and wireless
(WiFi) access to each carriage.

7.4.2 Experimental Configuration and Results for WiMAX/radio Over Fiber in High-
    Speed Train
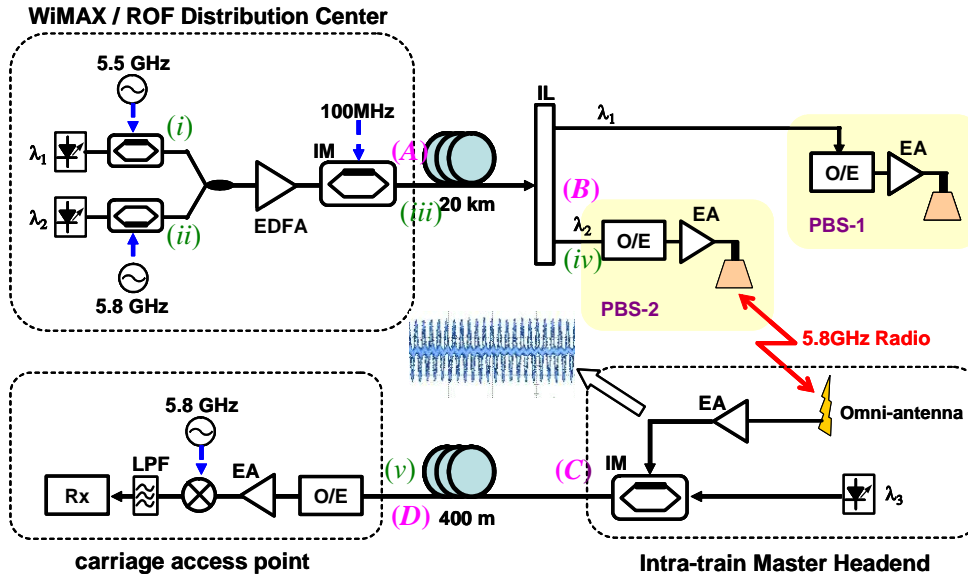
Figure 7.10: Experimental setup of the proposed WiMAX/radio over fiber for high-speed train.

The experimental setup of the proposed WiMAX/RoF based broadband services for high-speed train is shown in Figure 7.11. At the WiMAX/RoF distribution center, two 100 GHz spaced CW lightwaves at wavelength 1550.2 nm (λ_1) and 1551.0 nm (λ_2) are modulated using two LiNbO$_3$ Mach-Zehnder modulator driven by two separate sinusoidal RF clock frequency of 5.5 GHz and 5.8 GHz, respectively. Figure 7.12(a) and 7.12(b) show the corresponding optical spectra as inset (*i*) and (*ii*) in Figure 7.11. After modulation, the generated optical mm-waves are combined, amplified (EDFA) and modulated by an intensity modulator (IM) driven at 100 Mb/s baseband data with pseudorandom bit sequence word length of 2^{31}-1. The output power of the EDFA is set to 6 dBm. Figure 7.11(c) shows the optical spectra of the combined signals after IM as inset (iii) in Figure 7.10. The optical mm-wave channel at wavelength λ_1 and λ_2 are transmitted over 20-km standard single-mode fiber (SMF-28) and separated by a 100-GHz optical interleaver and fed into the respective proxy base station (PBS1 and PBS2).

The optical spectrum after interleaver and route to PBS2 is shown in Figure 7.11(d) as inset (*iv*) in Figure 7.9. At PBS2, a commercial PIN receiver (O/E) is used to recover the 5.8 GHz mm-wave signal with 100-Mb/s baseband data, and boosted by using an electrical amplifier (EA) before broadcast by a commercial dish antenna. The 5.8 GHz ISM/UNII band solid parabolic dish wireless antenna has 32.5dBi of maximum gain and 5^0 of both horizontal and vertical beam width. At the intra-train master head-end, a
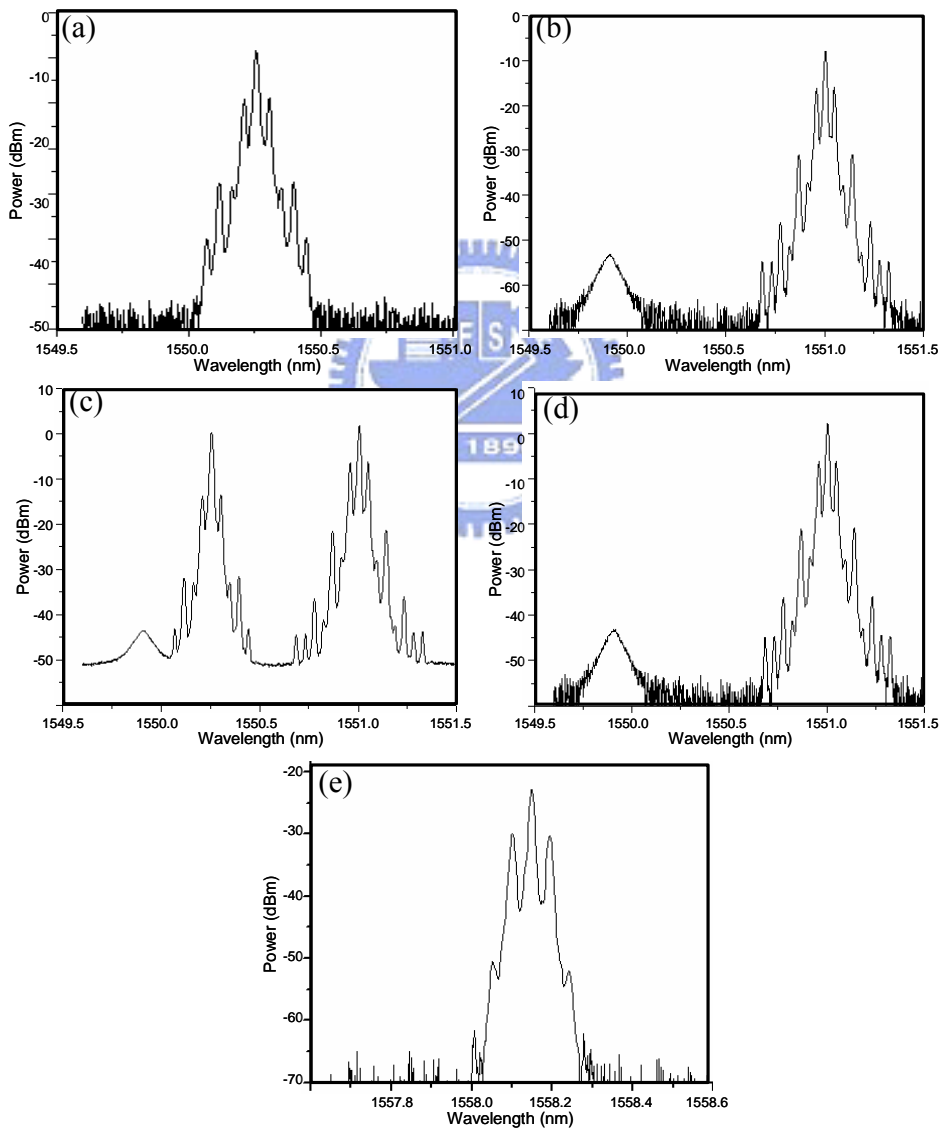
Figure 7.11: Optical spectrum. (a) λ_1 with 5.5 GHz RF clock as inset (*i*), (b) λ_2 with 5.8 GHz RF clock as inset (*ii*), (c) combined signals after IM as inset (*iii*), (d) after interleaver as inset (*iv*), (e) re-modulated signal after 400m SSMF as inset (*v*) in Figure 7.10.

(a) (point (*A*))   (b) (point (*B*))

(c) (point (*D*))   (d) (point (*C*))
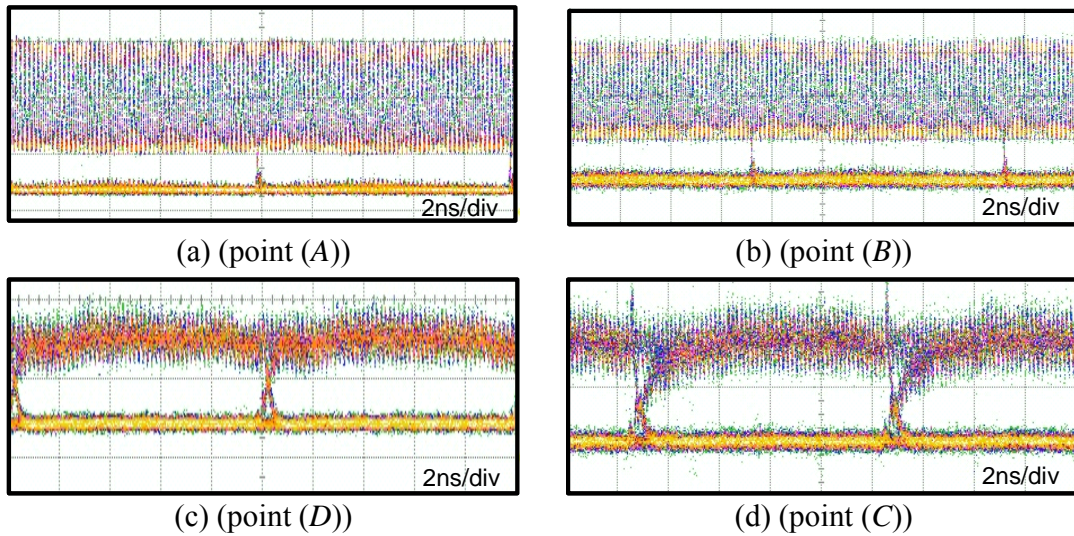
Figure 7.12: Optical eye diagrams at different locations labeled in Figure 7.10.

commercial omni-directional antenna is used to receive the broadcasted 5.8 GHz mm-wave signal. The HyperGain HG2458RD-TM is a triBand rubber duck wireless antenna with only 3-dBi gain. Inset figure of Figure 7.9 shows the received 5.8 GHz mm-wave with 100 Mb/s baseband data after the EA. A CW laser (λ_3) at 1558.15 nm wavelength is directly modulated by the received 5.8 GHz mm-wave signal. Fig. 7.11(d) as inset (*v*) in Figure 7.10 shows the optical spectrum of the re-modulated signal. The re-modulated optical mm-wave signal is transmitted over 400 m of SMF-28 in side the train before received by another commercial receiver (O/E), perform down-conversion to recover 100 Mb/s baseband data. Figure 7.12(a) and (b) show the optical mm-wave before and after 20 km transmission at the railway distribution system as point (*A*) and (*B*) in Figure 7.10. Both the 5.8 GHz mm-wave and 100 Mb/s baseband data exhibit high extinction ratio. Again, Figure 7.12(c) and (d) show the corresponding optical eye before and after 400 m Intra-train RoF system as point (*C*) and (*D*) in Figure 7.10. The re-modulated 5.8 GHz mm-wave and 100 Mb/s baseband exhibit good extinction ratio. The BER

performances of the 100 Mb/s baseband data is shown in Figure 7.13 for both in the railway distribution system (20-km SMF-28) and in the train (400-m SMF-28). Inset of Figure 7.13 also shows the eye diagrams after transmissions. The error free transmission of 100 Mb/s baseband data over 5.8 GHz microwave is observed both in 20-km distribution line and 400-m Intra-train RoF system. However, there are around 2.0 dB of power penalty between the Proxy BS and the Intra-train master head-end. The power penalty could be due to signal quality degradation in the wireless transmission between the narrow beam width dish antenna and the omni-antenna.
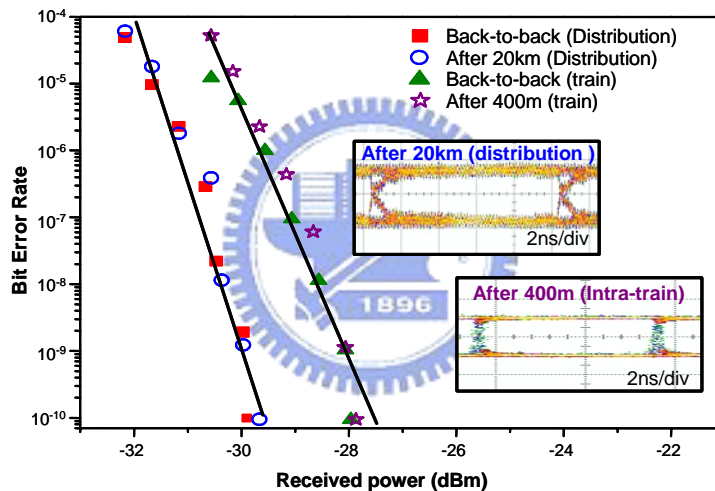
Figure 7.13: BER measurements at railroad distribution RoF system (20-km SMF) and intra-train RoF (400-m SMF)

7.4.3 Summary

Three-layer architecture to provide super broadband internet services in high-speed train systems using WiMAX/Radio signal over fiber is proposed and experimentally demonstrated. The experimental results show the error free transmission of 100 Mb/s baseband data carried by 5.8 GHz microwave WiMAX signal over 20 km distribution

fiber and 400 m Intra-train fiber can be achieved with less than 2 dB power penalty. In the near future, upstream transmission in this proposed architecture will be demonstrated and also the whole configuration will be moved from immobile table to movable train to simulate the real system.

CHAPTER 8

CONCLUSIONS

In this research, the main focus has been on the implementation and applications of novel architectures for reconfigurable broadband optical networks. To achieve this goal, in the first step, a re-circulating loop has been designed and set up to simulate long-distance transmission. Afterward, the research work further moved to metro network to solve the problem of fiber shortage and passive optical network to supply triple-play services.

The first study is long-distance transmission using a re-circulating loop in the networks with 32×4 channels ROADM and dispersion-compensated interleaver pairs. After that, the characteristics of the four-port interleaver had been explored and fully studied the bidirectional transmission by using unidirectional amplification scheme. Not only experimental demonstrated the straight-line, re-circulating loop and high bit rate transmission, but compared with the characteristics in different modulation formats and amplification techniques. Since the bit rate demand is much higher than in the past, PON technique is the effective solution for extensive bandwidth requirements of future services. The cost-effective bidirectional WDM-PON, select-cast WDM-PON and WDM-PON to provide triple-play services had been proposed and investigated.

8.1 Contributions

Primary contributions and experimental results of this dissertation are summarized here:

■ Novel three-port and four-port dispersion-free interleavers with temperature-compensated flat-top passband for bidirectional DWDM transmission systems had been successfully demonstrated.

■ In order to simulate long-distance transmission, one re-circulating loop has been setup.

    1) **Add/Drop applications in fiber ring networks based on a ROADM:**

        ● After 1100 km transmission

            (a) Power penalty for 8 channels are less than 2.25 dB.

            (b) Less than 2 dB sensitivity variations in cascaded transmission traffic.

            (c) Accumulated chromatic dispersion becomes obvious while wavelength detuned ± 11 GHz.

        ● One of the channels was refreshed every 158 km: less than 0.3-dB power penalty between one and seven circulations

        ● This technology can accommodate 32 channels simultaneously.

    2) **Metro add–drop network applications of cascaded dispersion-compensated interleaver**

        ● As the channel wavelengths are set at the center of the interleaver's pass band precisely, there is negligible dispersion introduced by the interleaver,

even for the uncompensated case.

- After 525 km transmission

    (a) Little dispersion induced when wavelengths are at ITU grids.

    (b) A 2.5-dB receiving sensitivity differential was observed when wavelength was detuned by $\pm$ 0.07-nm for the uncompensated pairs.

■ A three-port interelaver was modified to demonstrate a novel four-port interleaver with a 50-GHz channel spacing that enables bidirectional transmission using unidirectional amplification. By rerouting bidirectional transmission to unidirectional amplification, RB is blocked and high OSNR is achieved.

1) **Straight-line bidirectional transmission**

- After 210 km transmission

    (a) Power penalty for eight channels were less than 0.8 dB.

    (b) Less than 0.2 dB penalty differentials for all channels between bidirectional and unidirectional transmission.

    (c) Less than 0.6 dB sensitivity variation in bidirectional data traffic.

2) **Bidirectional recirculating loop transmission**

- No dead zone is need in this proposed transmission scheme.

- After 500 km transmission

    (a) Received OSNR exceeds 30 dB.

    (b) Power penalties for eight channels were less than 2 dB.

3) **Comparison between bidirectional DPSK and OOK signals**

● Over 230 km transmission

  (a) RZ-DPSK: power penalty for all channels is less than 1.1 dB.

  (b) NRZ-DPSK: power penalty for all channels is about 3 dB.

  (c) RZ-DPSK has a data-independent intensity profile and completely
      removes the pattern effects in the fiber.

● It is advantageous to use RZ-DPSK with a dual-stage EDFA in fiber-optic
  transmission.

Bidirectional transmission by using four-port interleaver has been fully studied in
this dissertation. This novel unidirectional amplification technology can
accommodate all optical channels, 32 channels, within the *C*-band with 50 GHz
channel spacing, resulted from this four-port interleaver is designed to cover the
whole *C*-band.
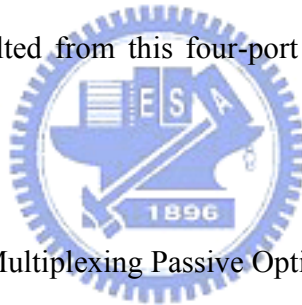
■ Wavelength-division Multiplexing Passive Optical Networks demonstration

  1) Cost-effective bidirectional WDM-PON architecture

    ● To solve the RB problem and reduce the cost in bidirectional WDM-PON
      system.

    ● To provide symmetric 10 Gb/s upstream data and 10 Gb/s downstream
      traffic simultaneously in this bidirectional WDM-PON.

    ● After 100 km transmission

      (a)   Power penalties for all channels were less than 0.7 dB.

      (b)   Penalty differential between bidirection and unidirection was less
            than 0.2 dB.

2) Select-cast services in WDM-PON system

- Using different modulation formats to provide different services in WDM-PON system.

- Novel WDM-PON configuration with centralized lightwave in the OLT to provide multi-services with 10Gb/s OOK and DPSK downstream data and the upstream signals at 1.25 Gb/s.

- After over 20 km transmission

  (a) Power penalty for 10 Gb/s OOK and DPSK downstream was negligible.

  (b) Power penalty for 1.25 Gb/s upstream was less than 0.5 dB at BER equals to 10^{-9}.

3) WDM-PON to provide triple play services

- Using a simple way, no more complex configurations, expensive DI or extra modulators and optical filters are needed, to realize TPS in WDM-PON.

- A WDM-PON configuration with centralized lightwaves in the OLT by using only one single-arm modulator. 10 Gb/s data and 2.5 Gb/s digital video downstream and 2.5 Gb/s data upstream had been demonstrated.

- After over 20 km transmission

  (a)   Power penalty for all downstream data was less than 0.5 dB.

  (b)   Power penalty for all upstream signals was less than 0.2 dB.

These experimental results show that the proposed schemes are desirable solutions for future WDM-PON access networks with low power penalty, cost-effective and power margin improvement.

APPENDIX I

To estimate the influence of the dispersion of refractive index on interleaver design, the dispersion must be included in the simulation model. From:

$$[\Delta n_1(f_0)L_1 - \Delta n_2(f_0)L_2] = m\frac{c}{f_0} \qquad (A1)$$

Given $\Delta n_1(f_0) \equiv \Delta n_{10}$ and $\Delta n_2(f_0) \equiv \Delta n_{20}$ as the difference in the refractive index between the slow and fast axes of the birefringent crystals, m denotes the order of the wave plate, c represents the speed of light and f_0 represents the center frequency.

$$\frac{(\Delta n_{10}L_1 - \Delta n_{20}L_2)f_0}{c} = m \qquad (A2)$$

$$\frac{[\Delta n_1(f_1)L_1 - \Delta n_2(f_1)L_2]f_1}{c} = m+1 \qquad (A3)$$

Subtracting (A2) from (A3) yields

$$\frac{1}{c}\Big[L_1\big(f_1\Delta n_1(f_1) - \Delta n_{10}f_0\big) - L_2\big(f_1\Delta n_2(f_1) - \Delta n_{210}f_0\big)\Big] = 1 \qquad (A4)$$

Using Taylor expansion of $\Delta n(f_1)$ around the center frequency f_0,

$$\frac{1}{c}\left\{\left[L_1f_1\left(\Delta n_{10} + \frac{d\Delta n_{10}}{df}(f_1 - f_0)\right) - \Delta n_{10}f_0\right] - \left[L_2f_1\left(\Delta n_{20} + \frac{d\Delta n_{20}}{df}(f_1 - f_0)\right) - \Delta n_{20}f_0\right]\right\} \cong 1, \quad (A5)$$

Define $FSR \equiv f_1 - f_0$, (A5) can be written as

$$\frac{FSR}{c}\left\{L_1\left[\Delta n_{10} + \frac{d\Delta n_1}{df_1}f_1\right] - L_2\left[\Delta n_{20} + \frac{d\Delta n_2}{df_2}f_2\right]\right\} \cong 1 \qquad (A6)$$

With the group indices Δn_{g10} and Δn_{g20} as:

$$\Delta n_{g0i} = \Delta n_{i0} + \frac{d\Delta n_{i0}}{df_i}f_i; i = 1,2 \qquad (A7)$$

$$FSR = \frac{c}{\left[L_1\Delta n_{g10} - L_2\Delta n_{g20}\right]} \qquad (A8)$$

The crystal length can then be selected using group indices for eliminating the first order error. For typical c-band application, the frequency range of interest is around 4 THz (i.e. from 191.5 THz to 195.5 THz), with center frequency at 193.5 THz. The frequency range corresponds to about 2% of the center frequency. Owing to the small frequency range, the first order approximation is justified and should provide sufficient accuracy.

For a typical Mach-Zehnder interferometer, the transfer function can be written as:

$$
\begin{aligned}
T(f) &= \sin^2\left[\frac{k_{eff}L_{eff}}{2}\right] \\
&\cong \sin^2\left\{\frac{\pi}{c}f\left[L_1\left(\Delta n_{10}+\frac{d\Delta n_{10}}{df}(f-f_0)\right)-L_2\left(\Delta n_{20}+\frac{d\Delta n_{20}}{df}(f-f_0)\right)\right]\right\}
\end{aligned}
\tag{A9}
$$

Inserting (A2) into (A9) yields

$$
\begin{aligned}
T(f) &= \sin^2\left\{\frac{\pi}{c}f\left[L_1\left(\Delta n_{10}+\frac{d\Delta n_{10}}{df}(f-f_0)\right)-L_2\left(\Delta n_{20}+\frac{d\Delta n_{20}}{df}(f-f_0)\right)\right]-m\pi\right\} \\
&= \sin^2\left\{\frac{\pi}{c}\left[L_1\left[\Delta n_{10}(f-f_0)+\frac{d\Delta n_{10}}{df}f(f-f_0)\right]-L_2\left[\Delta n_{20}(f-f_0)+\frac{d\Delta n_{20}}{df}f(f-f_0)\right]\right]\right\}
\end{aligned}
\tag{A10}
$$

After some calculations, we have

$$
= \sin^2\left\{\frac{\pi}{FSR}(f-f_0)+\frac{\pi}{FSR}\frac{(f-f_0)^2}{L_1\Delta n_{g10}-L_2\Delta n_{g20}}\left[L_1\frac{d\Delta n_{10}}{df}-L_2\frac{d\Delta n_{20}}{df}\right]\right\}
\tag{A11}
$$

The following observations can be drawn based on the above equation.

1): A minimum occurs approximately every $(f-f_0)=k\cdot FSR$, and is used as a basis for defining the *FSR* to the first order.

2): there is no first order deviation if group index n_g is selected, i.e. the error term *error* $\propto (f-f_0)$ disappeared.

3): the offset obtained is the second order term, that is

$$\frac{(f-f_0)^2}{L_1 n_{g10} - L_2 n_{g20}} \left[L_1 \frac{d\Delta n_{10}}{df} - L_2 \frac{d\Delta n_{20}}{df} \right]$$

The Sellmeier equation of YVO$_4$ and Rutile can be used to calculate the slope of refractive indices. Moreover, the typical values of the slope of the group index of YVO$_4$ and Rutile are calculated as 1.05×10^{-4} and 1.72×10^{-4}, respectively. Table A1 listed some key parameters for 100 GHz interleavers. Table A1 can be used to estimate the deviation of FSR at the edge of frequency band. Figure A1.1 shows the simulation and measurement results of the center wavelength offset, and reveal that agreement between the measured results and the simulated prediction.

Materials	Group Index Difference @ 193.5THz	Crystal Length (mm)	β (1/°C)	Slope of Group Index Difference (1/THz)
YVO$_4$	0.2139	9.5697	-26.54×10^{-6}	1.05×10^{-4}
Rutile	0.2652	2.0685	-99.06×10^{-6}	1.72×10^{-4}

Table A1: Summary of key parameters for the 100 GHz interleaver.

For C-band application with total bandwidth 4 THz, the frequency offset at 2 THz off the center is about 2.5 GHz. Figure A1.2 shows the simulated results of the center frequency offset with different selected center frequencies. Because the frequency offset increases hyperbolically with frequency range, the effective bandwidth decreases faster at the band edge. The center frequency offset caused by the refractive index dispersion is one inherited design issue due to the material refractive index dispersion. Therefore, different

sets of crystal length are required for C-band and L-band applications to mitigate the center frequency offset.

Measured and Smulated Center Frequency Offset
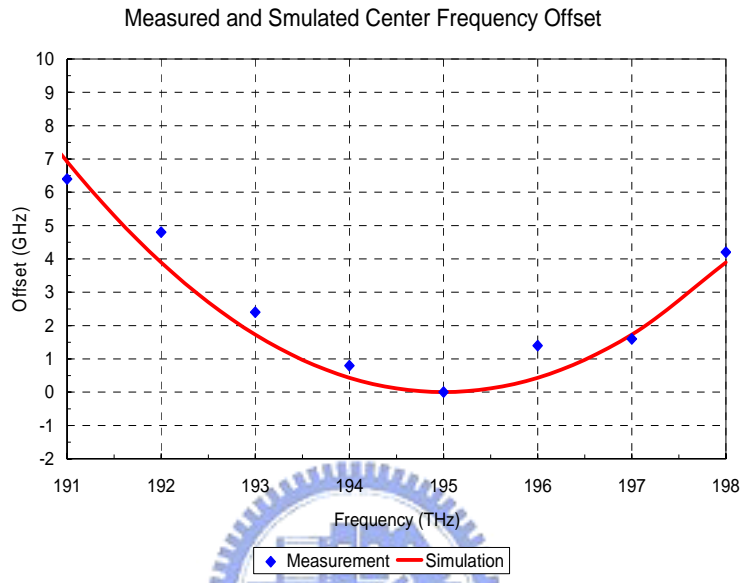
Figure A1.1: Measurement and simulation results of center frequency offset due to dispersion

Smulated Center Frequency Offset
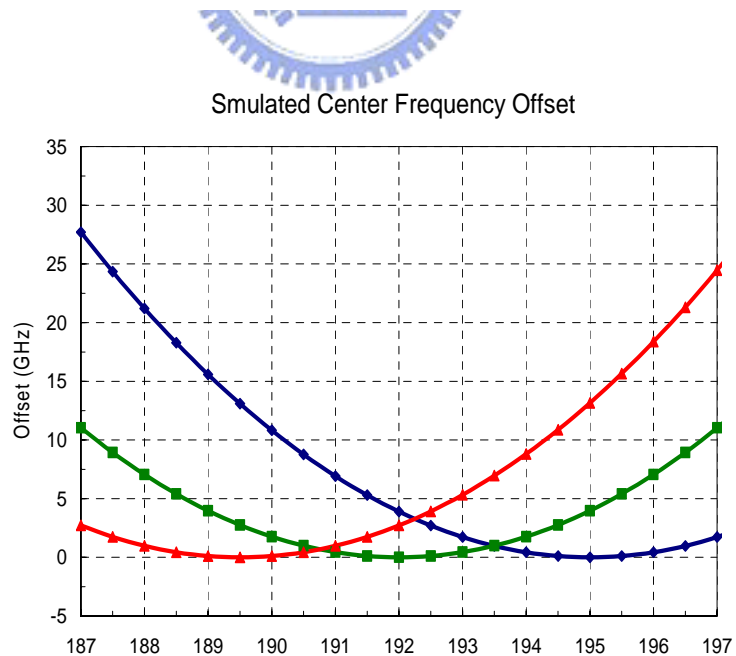
Figure A1.2: Center frequency offset with different selected center frequencies

REFERENCES

[1] S. Y. Kim, S. H. Lee, S. S. Lee and J. S. Lee, "Upgrading WDM networks using ultradense WDM channel groups," *IEEE Photon. Tech. Lett.,* Vol. **16**, No. 8, pp.1966–1968, 2004.

[2] C. Qiao, "Optical buffer switching—A novel paradigm for gigabit WDM optical networks," *Proc. Gigabit Networking Symp.* San Francisco, CA, 1998.

[3] A. E. Willner and S. Hwang, "Transmission of many WDM channels through a cascade of EDFA's in long-distance links and ring networks," *Journal of Lightwave Technology*, Vol. **13**, No. 5, pp. 802–816, 1995.

[4] S. J. B. Yoo, "Wavelength Conversion Technologies for WDM Network Applications", *Journal of Lightwave Technology*, Vol. **14**, No. 6, pp. 955–966, 1996.

[5] B. Mukherjee, "WDM optical communication networks: progress and challenges," *IEEE J. Select. Areas Commun.*, Vol. **18**, pp. 1810–1824, 2000.

[6] L. D. Garrett, M. H. Eiselt, J. M. Wiesenfeld, M. R. Young and R. W. Tkach, "Bidirectional ULH Transmission of 160 Gb/s Full-Duplex Capacity over 5000 km in a Fully Bidirectional Recirculating Loop", *IEEE Photon. Technol. Lett.*, Vol. **16**, No. 7, pp. 1757–1759, 2004.

[7] J. Ko, S. Kim, J. Lee, S. Won, Y. S. Kim and J. Jeong, "Estimation of Performance Degradation of Bidirectional WDM Transmission Systems Due to Rayleigh Backscattering and ASE Noises Using Numerical and Analytical Models," *Journal of Lightwave Technology*, Vol. **21**, No. 4, pp.938–946, 2003.

[8] B. Choi and C. Chae, "An Asymmetric Bidirectional Amplifier With All-Optical Gain Control for Randomly Variable Data Traffic," *IEEE Photon. Technol. Lett.*, Vol. **16**, No. 1, pp. 287–289, 2004.

[9] J. Ko, S. Kim, J. Lee, S. Won, Y. S. Kim and J. Jeong, "Estimation of Performance Degradation of Bidirectional WDM Transmission Systems Due to Rayleigh Backscattering and ASE Noises Using Numerical and Analytical Models," *Journal of Lightwave Technology*, Vol. **21**, No. 4, pp.938–946, 2003.

[10] K. Jinguji and M. Oguma, "Optical Half-Band Filters," *Journal of Lightwave*

Technology, Vol. **18**, No. 2, pp.252–259, 2000.

[11]   S. Cao, J. Chen, J. N. Damask, C. R. Doerr, L. Guiziou, G. Harvey, Y. Hibino, H. Li, S. Suzuki, K.-Y. Wu and P. Xie , "Interleaver technology: comparisons and applications requirements, " *Journal of Lightwave Technology*, Vol. **22**, No. 1, pp. 281–289, 2004.

[12]   K**.** Tai, B. Chang, J. Chen, C. Mao, T. Ducellier, J. Xie, L. Mao, and J. Wheeldon, "Wavelength-Interleaving Bidirectional Circulators," *IEEE Photon. Technol. Lett.,* Vol. **13**, No. 4, pp. 320–322, 2001.

[13]   H. S. Chung, J. S. Han, S. H. Chang, and H. J. Lee, "Bidirectional transmissions of 32 channels x 10Gb/s over metropolitian networks using linear optical amplifiers", *IEEE Photon. Technol. Lett.,* Vol. **16**, No. 4, pp. 1194–1196, 2004.

[14]   J. Yu, A. Buxens, A. Clausen, and P. Jeppesen, "16 x 10 Gb/s WDM Bidirectional Gating in a Semiconductor Optical Amplifier for Optical Cross Connects Exploiting Network Connection Symmetry," *IEEE Photon. Tech. Lett.,* Vol. **12**, pp.702–704, 2000.

[15]   A. H. Gnauck, G. Raybon, S. Chandrasekhar, J. Leuthold, C. Doerr, L. Stulz, A. Agarwal, S. Banerjee, D. Grosz, S. Hunsche, A. Kung, A. Marhelyuk, D. Maywar, M. Movassaghi, X. Liu, C. Xu, X. Wei, and D. M. Gill, "2.5 Tb/s (64 x 42.7 Gb/s) Transmission Over 40 x 100 km NZDSF Using RZ-DPSK Format and All-Raman-Amplified Spans," in *Proc. Optical Fiber Communication (OFC),* pp. FC2-1–FC2-3, 2002.

[16]   W. Huang, C. K. Chang, L. K. Chen, and F. Tong, "An optical network unit for WDM access networks with downstream DPSK and upstream remodulated OOK data using injection-locked FP laser," *IEEE Photon. Technol. Lett.*, Vol. **15**, pp. 1476–1478, 2003.

[17]   C. H. Kim, C. H. Lee, and Y. C. Chung, "Bidirectional WDM selfhealing ring network based on simple bidirectional add/drop amplifier modules," *IEEE Photon. Technol. Lett.*, Vol. **10**, No. 9, pp. 1340–1342, 1998.

[18]   J. M. P. Delavaux, T. Nuyen, O. Mizuhara, S. Granlund, P. Yeates, and A. Yeniay, "WDM repeaterless bi-directional transmission of 73 channels at 10 Gbit/s over 126 km of true wave fiber," in *Proc. Eur. Conf. Optical Communication (ECOC)*, pp. 21–24, 1997.

[19]   S. Radic, S. Chandrasekhar, A. Srivastava, H. Kim, L. Nelson, S. Liang, K. Tai, and N. Copner, "Dense Interleaved Bidirectional Transmission Over 5 X 80 km of Nonzero Dispersion-Shifted Fiber", *IEEE Photon. Technol. Lett.*, Vol. **14**, No. 2, pp. 218–220, 2002.

[20]   Cisco Systems, Inc., "Comparing Metro WDM Systems: Unidirectional vs. Bidirectional Implementations," *White Paper*, 2001.

[21]   C. H. Kim and Y. C. Chung, "2.5 Gb/sx16-channel bidirectional WDM transmission system using bidirectional EDFA based on SIS Etalon filters," *IEEE Photon. Technol. Lett.*, Vol. **11**, pp. 745–747, June 1999.

[22]   M. O. Deventer, "Polarization properties of Rayleigh backscattering in SMF," *Journal of Lightwave Technology*, Vol. **11**, pp. 1895–1899, Dec. 1993.

[23]   M. D. Feuer, "Measurement of OSNR in presence of partially polarized ASE", *IEEE Photon. Tech. Lett.,* Vol. **17**, No. 2, pp.435–437, 2005.

[24]   S. T. Lee and C. J. Chae, "low-cost bidirectional optical amplifier using a single EDFA and a 4-port wavelength interleaver," *LEOS 2000*, 13th Annual Meeting. IEEE, Vol. **1**, pp. 277–278, 2000.

[25]   J. Yu, Y.K. Yeo, O. Akanbi and G.K. Chang, "Bi-ditrctional Transmission of 8 x 20 Gb/s DPSK Signals Over 80km of SMF-28 Fiber Using In-line Semiconductor Optical Amplifier," *Optics Express*, Vol. **12**, pp. 6215–6218, 2004.

[26]   R. Proietti, A. D'Errico, L. Giorgi, N. Calabretta, G. Contestabile, and E. Ciaramella, "16 x 10 Gb/s DPSK Transmission Over 140-km SSMF by Using Two Common SOAs," *IEEE Photon. Technol. Lett.*, Vol. **18**, pp. 1675–1677, 2006.

[27]   V. S. Grigoryan, M. Shin, P. Devgan, J. Lasri, and P. Kumar, "SOA-Based Regenerative Amplification of Phase-Noise-Degraded DPSK Signals: Dynamic Analysis and Demonstration," *Journal of Lightwave Technology*, Vol. **24**, pp. 135–142, 2006.

[28]   Simon X.F. Cao, "Fiber optic dense wavelength division multiplexer with a phase differential method of wavelength separation utilizing a polarization beam splitter and a nonlinear interferometer," *US patent 6,130,971*, 2000.

[29]   K. Y. Wu and J. Y. Liu, "Switchable Wavelength Router," *US patent* 5,912,748, 1999.

[30]   S. Yim and H. F. Taylor, "Spectral slicing optical waveguide filters for dense wavelength division multiplexing," *Optics Communication*, **233**, pp. 113–117, 2004.

[31]   H. F. Taylor: "Tunable spectral slicing filters for dense wavelength-division multiplexing," *Journal of Lightwave Technology*, Vol. **21**, pp. 837–847, 2003.

[32]   D. Di Mola, G. Sanvito, M. Lenzi, and E. Fioravanti: "Flat-band add-drop FIR lattice filter design," *IEEE Journal of Select. Topics Quantum Electron.,* Vol. **5**, pp. 1366–1372, 1999.

[33]   C. R. Doerr, L. W. Stulz, R. Pafchek, and S. Shunk, "Compact and low-loss manner of waveguide grating router passband flattening and demonstration in a 64-channel blocker/multiplexer," *IEEE Photon. Technol. Lett.*, Vol. **14**, pp. 56–58, 2002.

[34]   N. Takato, K. Jinguji, M. Yasu, H. Toba, and M. Kawachi: "Silica-based singlemode waveguides on silicon and their application to guided-wave optical interferometers," *Journal of Lightwave Technology*, Vol. **6**, pp. 1003–1010, 1988.

[35]   T. Chiba, H. Arai, K. Ohira, H. Nonen, H. Okano and H. Uetsuka, "Novel architecture of wavelength interleving filter with Fourier transform-based MZIs," in *Proc. Optical Fiber Communication (OFC),* WB5, 2001.

[36]   B. Lyot, "Optical apparatus with wide field using interference of polarized light," *C. R. Acad. Sci. (Paris),* Vol. **195**, pp. 1593–1597, 1993.

[37]   Y. Öhman, "A New monochromator," *Nature*, Vol. **41**, pp. 291–296, 1938.

[38]   I. Šolc, "Birefringent chain filters," *J. Opt. Soc. Am.*, Vol. **55**, pp. 621–624, 1965.

[39]   J. Chen, "Dispersion-compensating optical digital filters for 40-Gb/s metro add-drop applications," *IEEE Photon. Tech. Lett.,* Vol. **16**, pp.1310–1312, 2004.

[40]   M. Kuznetsov, N. M. Froberg, S. R. Henion, H. G. Rao, J. Korn, K. A. Rauschenbach, E. H. Modiano and V. W. S. Chan, "A Next-Generation Optical Regional Access Network," *IEEE Commun. Mag.*, Vol. **38**, pp. 66–72, 2000.

[41]   P. K. A. Wai, Lixin Xu, L. F. K. Lui, L. Y. Chan, C. C. Lee, H. Y. Tam, M. S. Demokan, " All-optical add-drop node for optical packet-switched networks," *Optics Letters*, Vol. **30**, pp. 1515–1517, 2005.

[42]   C. Riziotis, M. N. Zervas, "Novel Full-Cycle-Coupler-Based Optical Add-Drop Multiplexer and Performance Characteristics at 40-Gb/s WDM Networks," *Journal of Lightwave Technology*, Vol. **21**, pp. 1828–1837, 2003.

[43]   S. Rotolo, A. Tanzi, S. Brunazzi, D. DiMola, L. Cibinetto, M. Lenzi, G. L. Bona, B. J. Offrein, F. Horst, R. Germann, H. W. M. Salemink, P. H. Baechtold, " Integrated Optic Tunable Add-Drop Filters for WDM Ring Networks," *Journal of Lightwave Technology*, Vol. **18**, pp. 569–578, 2000.

[44]   S.   D. Robinson, "How ROADM Technology is Simplifying Network Management," in *Proc. Optical Fiber Communication (OFC)*, NThP2, 2005.

[45]   C. R. Doerr, L. W. Stulz, M. Cappuzzo, E. Laskowski, A. Paunescu, L. Gomez, J. V. Gates, S. Shunk, and A. E. White, "40-Wavelength Add–Drop Filter," *IEEE Photon. Tech. Lett.*, Vol. **11**, No. 11, pp. 1437–1439, 1999.

[46]   C. Pu, L.Y. Lin, E.L. Goldstein and R.W. Tkach, "Client-Configurable Eight-Channel Optical Add/Drop Multiplexer Using Micromachining Technology," *IEEE Photon. Tech. Lett.*, Vol. **12**, No. 12, pp. 1665–1667, 2000.

[47]   N.A. Riza, and S. Yuan, "Reconfigurable Wavelength Add–Drop Filtering Based on a Banyan Network Topology and Ferroelectric Liquid Crystal Fiber-Optic Switches," *Journal of Lightwave Technology*, Vol. **17**, No. 9, pp. 1575–1584, 1999.

[48]   W. Chen, Z. Zhu, Y. Jui (Ray) Chen, J. Sun, B. Grek, and K. Schmidt. "Monolithically Integrated 32 X Four-Channel Client Reconfigurable Optical Add/Drop Multiplexer on Planar Lightwave Circuit," *IEEE Photon. Tech. Lett.*, Vol. **15**, No. 10, pp. 1413–1415, 2003.

[49] M. F. Huang, J. Chen, K. M. Feng, T. Y. Lin, C. Y. Lai, C. C. Wei, S. Chi, Z. Zhu, Y. J. Chen, Y. C. Huang and S. J. Chang, "Add/drop applications in fiber ring networks based on a reconfigurable optical add/drop multiplexer in a re-circulating loop," *Optics Communications,* Vol. **267**, pp. 113–117, 2006.

[50]   E. Almstrom, S. N. Larsson, and H. Carlden, "Cascadability of optical add/drop multiplexers," in *Proc. 24th Eur. Conf.*, Vol. **1**, pp. 589–590, 1998.

[51]   G. Lenz, B. J. Eggleton, C. R. Giles, C. K. Madsen, and R. E. Slusher, "Dispersive properties of optical filters for WDM systems," *IEEE J. Quantum Electron.*, Vol. **34**, No. 8, pp. 1390–1402, 1998.

[52]   K. Tai, Q. Guo, K. Chang, and J. Chen, "4-port interleavers and fully circulating bi-directional circulators," in *Proc. Optical Fiber Communication (OFC)*, pp. MK5/1–MK5/4, 2001,

[53]   K. M. Feng, M. F. Huang, C. C. Wei, C. Y. Lai, T. Y. Lin, J. Chen, and S. Chi, "Metro add–drop network applications of cascaded dispersioncompensated interleaver pairs using a recirculating loop," *IEEE Photon. Tech. Lett.*, Vol. **17**, No. 6, pp. 1349–1351, 2005.

[54]   M. F. Huang, J. Chen, K. M. Feng, C. C. Wei, C. Y. Lai, T. Y. Lin, and S. Chi, "210-km Bidirectional Transmission System With a Novel Four-Port Interleaver to Facilitate Unidirectional Amplification," *IEEE Photon. Technol. Lett.,* Vol. **18**, No. 1, pp. 172–174, 2006.

[55]   M. F. Huang, K. M. Feng, J. Chen, T. Y. Lin, C. C. Wei, , and S. Chi, "Wavelength-Interleaving Bidirectional Transmission System Using Unidirectional Amplification in a 5 x 100 km Recirculating Loop," *IEEE Photon. Tech. Lett.*, Vol. **18**, No. 12, pp. 1326–1328, 2006.

[56]   A. H. Gnauck, S. Chandrasekhar, A. R. Chraplyvy, "Stroboscopic BER Effects in Recirculating-Loop Optical Transmission Experiments," *IEEE Photon. Tech. Lett.*, Vol. **17**, pp.1974–1976, 2005.

[57]   Z. Jia, J. Yu, G. K. Chang, "A Full-Duplex Radio-Over-Fiber System Based on Optical Carrier Suppression and Reuse," *IEEE Photon. Tech. Lett.*, Vol. **18**, pp.1726–1728, 2006.

[58]   C. H Lee, W. V. Sorin, and B. Y. Kim, "Fiber to the Home Using a PON Infrastructure," *Journal of Lightwave Technology*, Vol. **24**, No. 12, pp. 14568–4583, 2006.

[59]   A. Banerjee, Y. Park, F. Clarke, H. Song, S. Yang, G. Kramer, K. Kim, and B. Mukherjee, "Wavelength-division-multiplexed passive optical network (WDM-PON) technologies for broadband access: a review," *Journa of Optical Networking*, Vol. **4**, pp. 737–758, 2005.

[60]   O. Akanbi, J. Yu, and G. K. Chang, "A New Scheme for Bidirectional WDM-PON Using Upstream and Downstream Channels Generated by Optical Carrier Suppression and Separation Technique," *IEEE Photon. Technol. Lett.*, Vol. **18**, pp. 340–342, 2006.

[61]   M. S. Lee, B. T. Lee, B. Y. Yoon and H. S. Chung, "Bidirectional Amplified WDM-PON using a Single LOA," in *Proc. Eur. Conf. Optical Communication (ECOC),* Th 2.3.5, 2005.

[62]   M. F. Huang, J. Yu, J. Chen, G. K. Chang, and S. Chi, "A Coast-Effective WDM-PON Configuration Employing Innovative Bi-directional Amplification," in *Proc. Optical Fiber Communication (OFC)*, Anaheim, LA, USA, OWL3, 2007.

[63]   J. Yu, Z. Jia, T. Wang, and G. K. Chang, "A Novel Radio-Over-Fiber Configuration Using Optical Phase Modulator to Generate an Optical mm-Wave and Centralized Lightwave for Uplink Connection," *IEEE Photon. Technol. Lett.*, Vol. **19**, pp. 140–142, 2007.

[64]   J. Yu, O. Akanbi, Y. Luo, L. Zong, T. Wang, Z. Jia, and G. K. Chang, "Demonstration of a Novel WDM Passive Optical Network Architecture With Source-Free Optical Network Units," *IEEE Photon. Technol. Lett.*, Vol. **19**, pp. 571–573, 2007.

[65]   J. Yu and G.-K. Chang, "A Novel Technique for Optical Label and Payload Generation and Multiplexing Using Optical Carrier Suppression and Separation," *IEEE Photon. Technol. Lett.*, Vol. **16**, pp. 320–322, 2004.

[66]   W. Hung, C.-K. Chan, L.-K. Chen, and F. Tong, "An Optical Network Unit for WDM Access Networks With Downstream DPSK and Upstream Remodulated OOK Data Using Injection-Locked," *IEEE Photon. Technol. Lett.*, Vol. **15**, pp. 1476–1478, 2003.

[67]   G. K. Chang, J. Yu, A. Chowdhury, and Y. K. Yeo, "Optical Carrier Suppression and Separation Label-Switching Techniques," *Journal of Lightwave Technology*, Vol. **23**, No. 10, pp. 3372–3387, 2005.

[68]   Y. Miyamoto, A. Hirano, S. Kuwahara, M. Tomizawa, and Y. Tada, "Novel modulation and detection for bandwidth-reduced RZ formats using duobinary-mode splitting in wideband PSK/ASK conversion," *Journal of Lightwave Technology*, Vol. **20**, no. 12, pp. 2067–2078, 2002.

[69]   N. Chi, B. Carlsson, P. V. Holm-Nielsen, C. Peucheret, and P. Jeppesen, "Dispersion management for two-level optically labeled signals in IP-over-WDM networks," in *Proc. Eur. Conf. Optical Communication (ECOC)*, Copenhagen, Denmark, Paper 5.5.1, 2002.

[70]   D. J. Blumenthal, B. Olsson, G. Rossi, T. E. Dimmick, and L. Rau, "All-optical label swapping networks and technologies," *Journal of Lightwave Technology*, Vol. **18**, No. 12, pp. 2058–2075, 2000.

[71]   S. J. B. Yoo, H. J. Lee, Z. Pan, J. Cao, Y. Zhang, K. Okamoto, and S. Kamei, "Rapidly switching all-optical packet routing system with optical- label swapping incorporating tunable wavelength conversion and a uniform-loss cyclic frequency AWGR," *IEEE Photon. Technol. Lett.*, Vol. **14**, pp. 1211–1213, 2002.

[72]   J. Yu, G. K. Chang, A. Chowdhury, and J. L. Long, "Spectral efficient DWDM optical label/payload generation and transport for next generation internet," *Journal of Lightwave Technology*, Vol. **22**, No. 11, pp. 2469–2482, 2004.

[73]   M. F. Huang, J. Yu, H. C. Chien, A. Chowdhury, Z. Jia, J. Chen, S. Chi (2, 4) and G. K. Chang, "A Novel WDN-PON Using Simultaneously Generated DPSK and OOK Centralized Lightwaves for Future Multi-Services in Access Networks," in *Proc. Eur. Conf. Optical Communication (ECOC)*, Berlin, Germany, Paper 10.6.4, 2007.

[74]   Y. C. Chung, "Challenges toward practical WDM-PON," in *Proc. OECC*, Kaohsiung, Taiwan, R.O.C., 6C4–1, 2006.

[75]   Q. Chang Y. Tian, C. Yan, X. Xu, J. Gao and Y. Su, "A PON System Providing Triple Play Service Based on a Single Dual-Parallel Mach-Zehnder Modulator," in *Proc. Eur. Conf. Optical Communication (ECOC)*, Berlin, Germany, paper 04.4.6, 2007.

[76]   C. A. Chan, M. Attygalle and A. Nirmalathas, "Generation and Separation of Closely Separated Dual baseband Channels for Provisioning of Independent Services in WDM-PON," *IEEE Photon. Technol. Lett.*, Vol. **19**, pp. 1215–1217, 2007.

[77]   J. J. Yoo, H. H. Yun, T. Y. Kim, K. B. Lee, M. Y. Park, B. W. Kim, and B. T. Kim, "A WDM-Ethernet hybrid Passive Optical Network Architecture," in *Proc. International Conference on Advanced Communication Technology (ICACT)*, Vol. **3**. pp. 1754–1757, 2006.

[78]   Corning Inc., "Broadband access networks," *White Paper*, 2001.

[79]   B. Lannoo, D. Colle, M. Pickavet, and P. Demeester, "Radio-over-Fiber-based Solution to Provide Broadband Onternet Access to Train Passenger," *IEEE Comm. Mag.*, Vol. **45**, pp.56–62, 2007.

[80]   F. D. Greve, F. V. Quickenborne, F. D. Turck, I. Moerman, and P. Demeester, "Rapidly Recovering Ethernet Networks for Delivering Broadband Services on the Train," in *Proc. IEEE Conference on Local Computer Networks (LCN)*, pp. 294–302, 2005.

VITA

Ming-Fang Huang

Education:

- National Chio Tung University , Ph.D. in Electro-Optical Engineering
  Thesis: Novel Architectures for Reconfigurable Broadband Optical Networks;
  Advisor: Prof. Sien Chi and Prof. Jyehong Chen
  2003-2007

- National Chiao Tung University, M.Sc. in Electro-Optical Engineering
  Thesis: Wide-band hybrid EDFA/Raman amplifiers with silica-based erbium-doped fiber;
  Advisors: Prof. Sien Chi and Dr. Jeng-Cherng Dung
  2001-2003

- Tamkang University, B.Sc. in Physics
  1997-2001

Honors:

- Reviewer of *Optics Communications*, 2007.

- *Fellowship*, 12 months scholarship by National Science Council (NSC) to pursue advanced research in School of Electrical and Computer Engineering, Georgia Institute of Technology, Taiwan,2006−2007.

- *Fellowship (ranked top 3%)*, Institute of Electro-Optical Engineering, National Chiao Tung University, Taiwan, 2005−2006.

- *First place of student poster section*, Fifth Annual Fitzpatrick Center Symposium Workshop on Global Perspectives in Frontiers of Photonics Computational Imaging, Biophotonics and Nanophotonics, Duke University, USA, 2005.

- *Fellowship (ranked top 3%)*, Institute of Electro-Optical Engineering, National Chiao Tung University, Taiwan, 2003−2004.

- *President's Award (ranked top 3%)*, Institute of Electro-Optical Engineering, National Chiao Tung University, Taiwan, 2003.

- *President's Award (ranked top 3%)*, Department of Physics, Tamkang University, Taiwan, 1998−2001.

Research and Teaching Experience:

- School of Electric and Computing Engineering, Georgia Institute of Technology, Atlanta, GA, USA, Research Assistant, *Optical Networking Research Group*, 2006−present.

- NEC Laboratories American, Inc., Princeton, NJ, USA, Intern, *Broadband and Mobile Networks*, October−December 2007.

- Institute of Electro-Optics Engineering, National Chiao Tung University, Taiwan, Research Assistant, *Optical Communication and Fiber Sensor Research Group*, 2001−2007.

- National Chiao Tung University, Teaching Assistant, *Optoelectronics*, 2005.

Publications:

- **M. F. Huang**, J. Yu, J. Chen, S. Chi, and G. K. Chang, "Cost-effective ROF System with Photonic Frequency Quadrupling to Simultaneously Generate an Optical mm-Wave and Centralized Lightwave," submitted to IEEE Photon. Technol. Lett. (2007).

- J. Yu, **M. F. Huang**, Z. Jia, and G. K. Chang, "A Novel Scheme to Generate Single Sideband Millimeter-wave Signals by Using Low-frequency Local Oscillator signal," submitted to IEEE Photon. Technol. Lett. (2007).

- **M. F. Huang**, J. Yu, H. C. Chien, A. Chowdhury, J. Chen, S. Chi, and G. K. Chang, "Using Single Modulator to Simultaneously Provide Triple-play Services with Centralized Lightwaves in WDM-PON System," revised by Optics Communications (2007).

- **M. F. Huang**, J. Chen, J. Yu, G. K. Chang, and S. Chi, "A Novel Dispersion-free Interleaver for Bi-directional DWDM Transmission Systems," *Journal of Lightwave Technology,* Vol. 25, pp. 3543−3554, 2007.

- **M. F. Huang**, J. Chen, K. M. Feng, T. Y. Lin, C. Y. Lai, C. C. Wei, S. Chi, Z. Zhu, Y. J. Chen, Y. C. Huang and S. J. Chang, "Add/drop applications in fiber ring networks based on a reconfigurable optical add/drop multiplexer in a re-circulating loop," *Optics Communications,* Vol. 267, pp. 113−117, 2006.

- **M. F. Huang**, K. M. Feng, J. Chen, T. Y. Lin, C. C. Wei, and S. Chi, "Wavelength-Interleaving Bidirectional Transmission System Using Unidirectional Amplification in a 5×100 km Recirculating Loop, " *IEEE Photon. Technol. Lett.*, Vol. 18, No. 12, pp. 1326−1328, 2006.

- **M. F. Huang**, J. Chen, K. M. Feng, C. C. Wei, C. Y. Lai, T. Y. Lin, and S. Chi, "210-km Bidirectional Transmission System With a Novel Four-Port Interleaver to Facilitate Unidirectional Amplification," *IEEE Photon. Technol. Lett.*, Vol. 18, No. 1, pp. 172−174, 2006.

- P. C. Peng, K. M. Feng, C.C. Chang, H. Y. Chiou, J. Chen, **M. F. Huang**, H. C. Chien, S. Chi, "Multiwavelength fiber laser using S-band erbium-doped fiber amplifier and semiconductor optical amplifier," *Optics Communications,* Vol. 259, pp. 200−203, 2006.

- Yu. C. Lu, J. Chen, K. M. Feng, P. C. Yeh, T. Y. Huang, W. R. Peng, **M. F. Huang**, and C. C. Wei, "Improved SPM Tolerance and Cost-Effective Phase-Modulation Duobinary TransmissionOver 230-km Standard Single-Mode Fiber Using a Single Mach–Zehnder Modulator," *IEEE Photon. Technol. Lett.*, Vol. 17, No. 12, pp. 2754–2756, 2005.

- C. C. Wei, **M. F. Huang**, and J. Chen," Enhancing the Frequency Response of Cross-Polarization Wavelength Conversion," *IEEE Photon. Technol. Lett.*, Vol. 17, No. 8, pp. 1683−1685, 2005.

- K. M. Feng, **M. F. Huang**, C. C. Wei, C. Y. Lai, J. Chen and S. Chi, "Metro Add/Drop Network Applications of Cascaded Dispersion-Compensated Interleaver Pairs Using a Re-Circulation loop," *IEEE Photon. Technol. Lett.*, Vol. 17, No. 6, pp. 1349−1451, 2005.

Conference Presentations:

- **M. F Huang**, J. Yu, H. C. Chien, A. Chowdhury, J. Chen, S. Chi, and G. K. Chang, "Simple WDM-PON Architecture to Simultaneously Provide Triple-play Services by Using One Single Modulator," The Optical Fiber Communication Conference & Exposition and the National Fiber Optic Engineers Conference (OFC/NFOEC), San Diego, CA, USA, OTuI4, 2008.

- H. C. Chien, **M. F. Huang**, A. Chowdhury, J. Yu, and G. K. Chang, "A Novel Low-Cost 10G TDM-PON Using Clock Embedded Centralized Lightwaves and Conventional Receivers for Instantaneous 10G Burst-Mode Clock Recovery," The Optical Fiber Communication Conference & Exposition and the National Fiber Optic Engineers Conference (OFC/NFOEC), San Diego, CA, USAOWH5, 2008.

- A. Chowdhury, **M. F. Huang**, H. C. Chien, G. Ellinas, and G. K. Chang, "A Self-Survivable WDM-PON Architecture with Centralized Wavelength Monitoring, Protection and Restoration for both Upstream and Downstream," The Optical Fiber Communication Conference & Exposition and the National Fiber Optic Engineers Conference (OFC/NFOEC), San Diego, CA, USA, JThA95, 2008.

- Z. Jia, **M. F. Huang**, R. L. Packham, J. Yu and G. K. Chang, "Testbed Demonstration and Analysis for Delivering Dual Services Simultaneously in a Single Radio-over-Fiber Access Platform," IEEE International Topical Meeting on Microwave Photonics (MWP), Victoria, BC Canada, Th-4.3, 2007.

- **M. F. Huang**, J. Yu, H. C. Chien, A. Chowdhury, Z. Jia, J. Chen, S. Chi and G. K. Chang, "A Novel WDN-PON Using Simultaneously Generated DPSK and OOK Centralized Lightwaves for Future Multi-Services in Access Networks," European Conference on Optical Communication (ECOC), Berlin, Germany, 10.6.4, 2007.

- A. Chowdhury, **M. F. Huang**, H. C. Chien, G. K. Chang, and G. Ellinas, "A Novel Centrally Managed Self-Protected Bi-Directional WDM-PON Architecture using Optical Carrier Suppression, Separation Technique and Wavelength Sharing Scheme," Lasers and Electro-Optics Society (LEOS), Lake Buena Vista, Florida, USA, ThW2, 2007.

- L. Kong, H. C. Chien, A. Chowdhury, **M. F. Huang**, Z. Jia, J. Yu, T. Wang, and G. K. Chang, "A Novel Bidirectional DWDM-PON Using Single Light Source for Simultaneous Download, Upload and Video Selectcast Services," Lasers and Electro-Optics Society (LEOS), Lake Buena Vista, Florida, USA, ThW3, 2007.

- H. C Chien, **M. F Huang**, A. Chowdhury, J. Chen, S. Chi and G. K Chang, " A Novel Hybrid 10G/1G Coexisted TDM-PON Using Central Office Controlled Reflective Transmitters for Low-Cost Upstream 10G Services," Lasers and Electro-Optics Society (LEOS), Lake Buena Vista, Florida, USA, ThW4, 2007.

- **M. F. Huang**, J. Yu, G. K. Chang, J. Chen, S. Chi, "Bi-Directional DPSK Transmission over 230-km SSMF Employing Innovative Bi-Directional Amplification," Conference on Lasers and Electro Optics (CLEO/QELS), Baltimore, MD, USA, 2007.

- **M. F. Huang**, J. Yu, J. Chen, G. K. Chang, and S. Chi, "A Coast-Effective WDM-PON Configuration Employing Innovative Bi-directional Amplification," The Optical Fiber

Communication Conference & Exposition and the National Fiber Optic Engineers Conference (OFC/NFOEC), Anaheim, LA, USA, OWL3, 2007.

- **M. F. Huang**, T. Y. Lin, C. C. Wei, J. Chen, K. M. Feng and S. Chi, "Novel Interleaved Bidirectional Transmission System Using Interleavers to Facilitate Unidirectional Amplification in a Recirculating Loop," International Conference on Communications, Circuits and Systems (ICCCAS), GuiLin, China, 2006.

- T. Y. Lin, **M. F. Huang**, C. C. Wei, J. Chen, K. M. Feng and S. Chi, "Metro Network Applications of Cascaded ROADM Using a Re-circulating Loop," International Conference on Communications, Circuits and Systems (ICCCAS), GuiLin, China, 2006.

- **M. F. Huang,** J. Chen, K. M. Feng, T. Y. Lin, C. C. Wei, C. Y. Lai, S. Chi, Z. Zhu, Y. J. Chen, Y. C. Huang, and S. J. Chang, "Cascaded Reconfigurable Optical Add/Drop Multiplexer (ROADM) in MetroAdd/Drop Network Applications," Conference on Lasers and Electro Optics (CLEO/QELS), Long Beach, LA, USA, 2006.

- **M. F. Huang**, T. Y. Lin, C. C. Wei, K. M. Feng, J. Chen and S. Chi, "Novel Four-Port Interleavers Facilitate Unidirectional Amplification for Wavelength-Interleaving Bidirectional Transmission System," Conference on Lasers and Electro Optics (CLEO/QELS), Long Beach, LA, USA, 2006.

- **M. F. Huang**, C. Y. Lai, J. Chen, K. M. Feng, C. C. Wei, T. Y. Lin, and S. Chi, "Using a Novel Four-Port Interleaver to Enable Unidirectional Amplification in a210-km Bidirectional Transmission System," Lasers and Electro-Optics Society (LEOS), Sydney, Australia, 2005.

- Y. C. Lu, J. Chen, K. M. Feng, P. C. Yeh, T. Y. Huang, W. R. Peng, **M. F. Huang**, and C. C. Wei, "A Cost-Effective Phase-Modulation-Enhanced Duobinary Modulation to Improve SPM Tolerance Using Only One Mach-Zehnder Modulator," European Conference on Optical Communication (ECOC), Glasgow, Scotland, 2005.

- **M. F. Huang**, C. C. Wei, C. Y. Lai, T. Y. Lin, K. M. Feng, J. Chen and S. Chi, "Cascadability Study of Dispersion-Compensated Interleaver Pairs for Metro Add/Drop Applications Using a Re-Circulating Loop," Conference on Lasers and Electro Optics (CLEO/QELS), Baltimore, MD, USA, 2005.

- **M. F. Huang**, C. C. Wei, C. Y. Lai, T. Y. Lin, K. M. Feng, J. Chen and S. Chi, "Cascadability Study of Dispersion-Compensated Interleaver Pairs for Metro Add/Drop Applications Using a Re-Circulating Loop," Fifth Annual Fitzpatrick Center Symposium Workshop on Global Perspectives in Frontiers of Photonics Computational Imaging, Biophotonics and Nanophotonics, Duke University, NC, USA, 2005.

- **M. F. Huang**, T. Y. Lin, C. C. Wei, C. Y. Lai, J. Chen, K. M. Feng, and S. Chi, "A Novel Four-port Interleaver Enables 210 Km Bidirectional Transmission Using Unidirectional Amplification," Optics Photonics Taiwan (OPT), Taiwan, 2005.

- T. Y. Lin, **M. F. Huang**, C. Y. Lai, C. C. Wei, J. Chen, K. M. Feng, S. Chi, Z. Zhu, Y. J. Chen, Y. C. Huang and S. J. Chang, "Cascadability Study of Reconfigurable Optical Add/Drop Multiplexer (ROADM) for Metro Network Applications Using a Re-circulating Loop," Optics Photonics Taiwan (OPT), Taiwan, 2005.

- C. Tsao, Y. C. Lu, J. Chen, K. M. Feng, P. C. Yeh, T. Y. Huang, W. R. Peng, **M. F. Huang**, C. C. Wei, and S. Chi, "A Cost-Effective and Penalty Free Phase-Modulation Duobinary Transmission over 230 km Standard Single-Mode Fiber Using a Single Mach-Zehnder Modulator," Optics Photonics Taiwan (OPT), Taiwan, 2005.

- **M. F. Huang**, T. Y. Lin, C. C. Wei, J. Chen, K. M. Feng, and S. Chi, "A Novel Four-Port Interleaver Used to Enable Unidirectional Amplification for 5×100 Km Bidirectional Transmission Traffics," Optics Photonics Taiwan (OPT), Taiwan, 2005.

- C. C. Wei, **M. F. Huang**, J. Chen and S. Chi, "All-Optical Regeneration of Differential Phase-shift Keying Signals Based on Four- wave Mixing in a Sagnac Loop Mirror," Optics Photonics Taiwan (OPT), Taiwan, 2005.

- **M. F. Huang**, C. C. Wei, C. Y. Lai, K. M. Feng, J. Chen and S. Chi, "Metro Add/Drop Applications of 50-GHz Dispersion- Compensated Interleaver Pairs using a Re-circulating Loop," Optics Photonics Taiwan (OPT), Taiwan, 2004.

- C. C. Wei, **M. F. Huang**, J. Chen and K. M. Feng, "A 300% Rise Time Impronement by Adding A Birefringence Delay Line After Cross Polarization Wavelength Conversion," Optics Photonics Taiwan (OPT), Taiwan, 2004.

- **M. F. Huang**, C. C. Wei, C. Y. Lai, T. Y. Lin, K. M. Feng, J. Chen and S. Chi, "Ring Network Applications of Cascaded Dispersion-Compensated Interleaver Pairs Using a Re-circulation Loop," Symposium on Technologies for High-Capacity Optical Communications (STHCOC), Taiwan, 2004.

- C. C. Wei, **M. F. Huang**, J. Chen and K. M. Feng and S. Chi, "Improving the Frequency Response of Cross Polarization Wavelength Conversion by Adding an Extra Delay Line," Symposium on Technologies for High-Capacity Optical Communications (STHCOC), Taiwan, 2004.

- C. C. Wei, **M. F. Huang**, J. Chen and K. M. Feng and S. Chi, "Study of Bandwidth Improvement of Differential Cross- Polarization Modulation in a Semiconductor Optical Amplifier," Symposium on Technologies for High-Capacity Optical Communications (STHCOC), Taiwan, 2004.